Technical Report Documentation Page

| | | | |
|---|---|---|---|
| 1. Report No.<br>ABC-UTC-2013-C3-UNR02-Final | 2. Government Accession No. | 3. Recipient's Catalog No. | |
| 4. Title and Subtitle<br>**Durable UHPC Columns with High-Strength Steel** | | 5. Report Date<br>April 2019<br>6. Performing Organization Code | |
| 7. Author(s)<br>Mahmoud Aboukifa, Mohamed A. Moustafa (https://orcid.org/0000-0002-1006-7685), Ahmad Itani (https://orcid.org/0000-0002-9813-6314), Negar Naeimi | | 8. Performing Organization Report No. | |
| 9. Performing Organization Name and Address<br>Department of Civil and Environmental Engineering<br>University of Nevada, Reno<br>1664 N. Virgina St., MS 0258<br>Reno, NV 89557 | | 10. Work Unit No. (TRAIS)<br>11. Contract or Grant No.<br>DTRT13-G-UTC41 (for 2013) | |
| 12. Sponsoring Organization Name and Address<br>Accelerated Bridge Construction<br>University Transportation Center<br>Florida International University<br>10555 W. Flagler Street, EC 3680<br>Miami, FL 33174 | | 13. Type of Report and Period Covered<br>Final Report<br>08/2017-05/2019<br>14. Sponsoring Agency Code | |
| 15. Supplementary Notes<br>Visit www.abc-utc.fiu.edu for other ABC reports. | | | |
| 16. Abstract<br>Ultra-High Performance Concrete (UHPC) is a versatile building material as it is characterized by very high compressive strengths reaching 200 MPa (30 ksi), ductile tensile characteristics, and energy absorption. Currently, UHPC is commonly used in small structural applications, such as joints and connections between precast structural elements. However, this material is not widely used in structural elements due to the lack of knowledge of the structural behavior and failure mechanism of these elements. Due to the exceptional mechanical properties of UHPC, compact substructure elements cross-sections can be achieved if properly designed, which make this solution very suitable for accelerated bridge construction (ABC) construction where lighter and easier-to-handle and transport bridge components can be pre-fabricated and shipped to the site. There is also a great potential for application of UHPC in bridge members with high durability requirements in aggressive environmental conditions. To realize new bridge column designs using UHPC, the goal of this project was to use extensive experimental testing to first investigate the confinement behavior of UHPC and study the structural and seismic behavior of UHPC columns subjected to combined axial and lateral loading. Large number of UHPC cylinders with various spiral steel confinement were tested to determine the change in the compression strength and ultimate strain due to confinement effects. However, the main part of the experimental program included four large-scale UHPC column that were tested under axial and quasi-static cyclic lateral loading at the Earthquake Engineering Laboratory at the University of Nevada, Reno. The lateral response of these columns was evaluated for damage progression, failure type, peak strength, and displacement and curvature ductility. The four columns varied in longitudinal and transverse steel reinforcement where conventional Grade 60 and Grade 100 high strength steel were used. The study showed that with proper reinforcement design, the strength of UHPC columns can be almost double that of the conventional concrete columns without compromising on the displacement capacities or curvature ductility. | | | |
| 17. Key Words<br>UHPC columns; confinement; large-scale testing; high strength steel; cyclic loading; seismic behavior; ductility | | 18. Distribution Statement<br>No restrictions. | |
| 19. Security Classification (of this report)<br>Unclassified. | 20. Security Classification (of this page)<br>Unclassified. | 21. No. of Pages<br>130 | 22. Price |

Form DOT F 1700.7 (8-72) Reproduction of completed page authorized

(this page is intentionally left blank)

# Durable UHPC Columns with High-Strength Steel

Final Report

April 2019

**Principal Investigators:** Mohamed Moustafa and Ahmad Itani

Department of Civil and Environmental Engineering
Florida International University

**Authors**
Mahmoud Aboukifa
Mohamed A. Moustafa
Ahmad Itani
Negar Naeimi

**Sponsored by**
Accelerated Bridge Construction University Transportation Center


**A report from**

University of Nevada, Reno

Department of Civil and Environmental Engineering, MS 258

1664 N. Virginia St.

Reno, NV 89557

www.unr.edu/cee

## DISCLAIMER

The contents of this report reflect the views of the authors, who are responsible for the facts and the accuracy of the information presented herein. This document is disseminated in the interest of information exchange. The report is funded, partially or entirely, by a grant from the U.S. Department of Transportation's University Transportation Program. However, the U.S. Government assumes no liability for the contents or use thereof.

## ABSTRACT

Ultra-High Performance Concrete (UHPC) is a versatile building material as it is characterized by very high compressive strengths reaching 200 MPa (30 ksi), ductile tensile characteristics, and energy absorption. Currently, UHPC is commonly used in small structural applications, such as joints and connections between precast structural elements. However, this material is not widely used in structural elements due to the lack of knowledge of the structural behavior and failure mechanism of these elements. Due to the exceptional mechanical properties of UHPC, compact substructure elements cross-sections can be achieved if properly designed, which make this solution very suitable for accelerated bridge construction (ABC) construction where lighter and easier-to-handle and transport bridge components can be pre-fabricated and shipped to the site. There is also a great potential for application of UHPC in bridge members with high durability requirements in aggressive environmental conditions. To realize new bridge column designs using UHPC, the goal of this project was to use extensive experimental testing to first investigate the confinement behavior of UHPC and study the structural and seismic behavior of UHPC columns subjected to combined axial and lateral loading. Large number of UHPC cylinders with various spiral steel confinement were tested to determine the change in the compression strength and ultimate strain due to confinement effects. However, the main part of the experimental program included four large-scale UHPC column that were tested under axial and quasi-static cyclic lateral loading at the Earthquake Engineering Laboratory at the University of Nevada, Reno. The lateral response of these columns was evaluated for damage progression, failure type, peak strength, and displacement and curvature ductility. The four columns varied in longitudinal and transverse steel reinforcement where conventional Grade 60 and Grade 100 high strength steel were used. The study showed that with proper reinforcement design, the strength of UHPC columns can be almost double that of the conventional concrete columns without compromising on the displacement capacities or curvature ductility.

## ACKNOWLEDGMENTS

This project was supported by the Accelerated Bridge Construction University Transportation Center (ABC-UTC at www.abc-utc.fiu.edu) at Florida International University (FIU), as lead institution, and Iowa State University (ISU) and the University of Nevada-Reno (UNR) as partner institutions. The authors would like to acknowledge the ABC-UTC support.

The authors would like to extend special appreciation to the ABC-UTC and the U.S. Department of Transportation Office of the Assistant Secretary for Research and Technology for funding this project. The authors would like to thank the Research Advisory Panel members: Elmer Marx from Alaska DOT and Tareq Masroor from California DOT. The donation of the high strength steel by MMFX® Technologies, a Commercial Metals Company, and partial donation of the UHPC provided by Ductal®, a LafargeHolcim technology, is greatly acknowledged.

**CONTENTS**

## LIST OF FIGURES

## LIST OF TABLES

# Chapter 1. INTRODUCTION

## 1.1. Project Motivation

In the recent decades, Ultra High Performance Concrete (UHPC) has attracted worldwide attention of the industry and academy, due to its significant features, compared to the conventional concrete. UHPC is a cementitious material, reinforced by fiber, which has compressive and tensile strength around 28 ksi and 1.2 ksi, respectively. Strain-hardening behavior of UHPC in tension along with its pre- and post- cracking tensile strength, are of its unique characteristics, associated with the fiber bridging effects. High ductility, energy absorption capacity, considerable shear resistance, self-consolidation, reduced section sizes and low cost of maintenance are other features of UHPC, which make it a desirable candidate in the construction industry, despite its high instant costs. These physical and mechanical outstanding characteristics stems from the particular mix design including: very low water-to-cementitious material ratio (about 0.2) and optimized granular mixture with minimal or no coarse aggregate. The resulting very low porosity of UHPC lead to increased durability, especially for construction in harsh environments. Hence, structures built by UHPC can be much lighter (due to the high strength that lead to smaller cross-sections) and can have longer service life (due to the high durability) than those built by regular concrete. UHPC is currently used in relatively small-scale applications, such as bridge deck joints and connections. However, there is great potential in extending the use of UHPC to larger applications and full structural elements to realize a new generation of resilient and almost maintenance-free structures.

Rapid deterioration of bridge substructures has been one of the major reasons for the increasing number of structurally deficient or functionally obsolete bridges in the past decade. While many of the deteriorating old bridges are originally designed for a 50-year service life, many of the ongoing repairs, retrofits, and new construction aim at extending service life to 75 or 100 years. One approach for protecting and building durable bridge substructures with longer service life is to use very durable materials with very low porosity such as UHPC. If used in substructure elements, UHPC can easily extend the service life of bridge substructures to 100 years where the reinforcement and/or structural steel elements are well protected from corrosion and harsh environments. Due to the exceptional mechanical properties of UHPC, compact substructure elements cross-sections can be achieved if properly designed, which make this solution very suitable for accelerated bridge construction (ABC) construction where lighter and easier-to-handle and transport bridge components can be pre-fabricated and shipped to the site.

Proper reinforcement detailing can increase columns axial capacity and ductility, but also showed that larger longitudinal reinforcement ratios are desired to fully utilize the UHPC superior strength and reduce cross-sections. Meanwhile, for better constructability, codes and standards limit longitudinal reinforcement ratio in bridge columns, for example, to 4%. Thus, considering high-strength steel with UHPC can help optimize cross-sections while maintaining reasonable reinforcement ratio. However, the use of A1035 Grade 100 steel has not been properly investigated, especially when combined with UHPC. Very limited or no previous research properly investigated UHPC sections design optimization for bridge elements and UHPC confinement effects under combined axial and lateral loading. Similarly, extending the use of high-strength steel to further optimize UHPC cross-sections and reduce structural elements sizes has not been studied. Thus, the objective of this study is to fill this gap and

provide the basic knowledge needed to design UHPC sections using high-strength steel for constructing durable and compact pre-fabricated columns for ABC bridges.

## 1.2. Research Objectives and Tasks

The overall objective of this study is to provide the knowledge needed to optimize the design of pre-fabricated bridge substructure elements, mainly columns, using UHPC and high-strength steel. In particular, the purpose of this study is to investigate the effect of longitudinal and transverse reinforcement detailing on the strength and displacement capacity of UHPC columns. The core of this study is an experimental program that consists of UHPC cylinders confinement study and four large-scale column tests under combined axial and lateral quasi-static (cyclic) loading.

This study tested UHPC bridge columns designed using A706 Grade 100 steel and using two different reinforcement ratios to investigate the efficiency of high-strength steel in reducing UHPC columns cross-sections while maintaining strength and displacement design requirements. Another key factor of optimizing columns design under combined axial and lateral loads is understanding the confinement behavior of UHPC along with transverse steel detailing requirements such as minimum hoop spacing. An confinement study was undertaken first on large number of unconfined and confined UHPC cylinders. Moreover, two of the tested UHPC columns had two different transverse reinforcement ratios, i.e. hoop spacing, to study the effect of UHPC core confinement on the flexural capacity of columns. These objectives were accomplished through the following research tasks:

- *Task 1 – Update literature search on structural and seismic performance of UHPC prefabricated bridge components and connections:*

An extensive literature search was conducted to comprehensively summarize the different structural applications of UHPC for bridges or other structures. The search has focused mainly on the structural and seismic response of UHPC structural members (mainly columns) subjected to combined axial and flexural loading.

- *Task 2 – Conduct UHPC confinement tests:*

Most of previous research that studied the compressive behavior of UHPC and developed stress-strain relationships for modeling focused on unconfined UHPC or in other words, tested mainly unconfined UHPC cylinders. For correct estimation of the ultimate strength and displacement design capacity of UHPC columns under combined axial and lateral loading, a better understanding of the effect of confinement on UHPC behavior is crucial. A large number of unconfined and confined UHPC cylinders was sampled, instrumented, and tested under pure compression to properly define UHPC stress-strain relationships. Wire hoops of different spacing were used to provide different confinement cases for UHPC cylinder tests. Common confinement models for conventional concrete, e.g. Mander model, was checked for validity for UHPC.

- *Task 3 – Construct UHPC columns and conduct experimental tests:*

Four Large-scale UHPC columns were tested under axial and quasi-static cyclic lateral loading at the Earthquake Engineering Laboratory at the University of Nevada, Reno. The lateral response

of these columns was evaluated for damage progression, failure type, peak strength, displacement ductility and steel reinforcement strains. This study investigated three test parameters on the structural and seismic response of columns which included: using Grade 100 rebars versus Grade 60 rebars; varying confinement reinforcement, and varying the longitudinal reinforcement ratio.

- *Task 4 – Process and interpret tests results and assess the structural and seismic performance of UHPC columns:*

The data obtained from the experimental tests were processed to interpret and explain the structural and seismic response of UHPC columns with conventional and high-strength steel along with the effect of transverse reinforcement on confinement behavior and column capacity. The knowledge acquired from the confinement study and the column tests provide the foundation for future work that can comprehensively provide design guidelines for high performance durable UHPC columns with high-strength steel.

- *Task 5 – Summarize the investigation and the results in a final report:*

A final report describing the details of different tasks and preliminary design guidelines for UHPC columns with high-strength steel, i.e. this report, was prepared and submitted to the ABC-UTC steering committee for review and comments.

### 1.3. Research Advisory Panel (RAP)

The project work and the developed survey were done in collaboration with the Research Advisory Panel (RAP). The following people participated in the RAP:

- Elmer Marx (Alaska DOT)
- Tareq Masroor (Caltrans)

### 1.4. Report Overview

This report consists of seven chapters. The first chapter provides a brief introduction for the report that includes the study motivation, research objectives and the conducted tasks. Chapter 2 provides a comprehensive summary of existing knowledge on UHPC columns from international codes and guidelines along with previous research. Chapter 3 presents the confinement study on UHPC cylinders. The large-scale column tests are discussed in Chapters 4 through 6. In Chapter 4, the details of the large-scale UHPC column tests in terms of specimens design, construction details, material properties, test setup, and the used loading protocol and the instrumentation plan are presented. Chapter 5 presents the test results and discussion of the UHPC test specimen with Grade 60 longitudinal rebars with respect to its global and local behaviors as it compares to a similar column with normal strength concrete (Group I). Chapter 6 presents the test results and discussion of Group II specimens which used the Grade 100 longitudinal rebars with respect to their global and local behaviors. This chapter also presents a comprehensive comparison between Group I and Group II specimens is provided at the end of this chapter. Chapter 7 presents a brief summary and concluding remarks in addition to some recommendations for future research related to this study.

# Chapter 2. LITERATURE REVIEW

Columns are critical structural components that are designed to carry pure axial loads or combined axial loads and bending moments. The effects of axial loads (mainly compression) can further increase the flexure capacity, which is important to properly quantify when columns are considered as part of lateral load resisting systems, e.g. moment frames in buildings or bridge columns. Previous studies considered testing of UHPC columns under mainly axial loads, and fewer studies considered combined axial and bending. Moreover, the principals of UHPC design has been recently introduced in several international codes and design guidelines but nothing similar is yet available in the United States. Thus, a brief summary of how combined axial and flexure UHPC design is tackled in standards and guidelines along with the different experimental and analytical efforts from previous studies which aimed at response characterization of UHPC is presented in this section. The literature review is divided into several subsections that discuss relevant UHPC columns design guidelines from international codes, confinement of UHPC, behavior of UHPC columns under axial loads, slender columns, effects of different types of hazards, novel UHPC and hybrid column designs, and modeling efforts for UHPC columns.

## 2.1. International Codes and Design Guidelines

In 2006, the Japan Society of Civil Engineers (JSCE) published Recommendations for Design and Construction of Ultra High Strength Fiber Reinforced Concrete Structures (Draft) that builds on the JSCE Standard Specifications for Concrete Structures. The draft recommendations provide design values for materials (e.g. compressive strength, first cracking strength, tensile strength, stress-strain relationships, etc.) and address structural strength design, serviceability, fatigue resistance, structural details, and construction. For flexural design, the use of stress-strain curves rather than an equivalent stress block is recommended. No minimum amount of steel reinforcement is required because the bridging action of the steel fibers provides the strength after cracking. It is noted that the document defaults to the Standard Specifications where information is not available to develop different recommendations for UHPC. It is noted that Uchida et. al. (2006) provided a discussion of the JSCE UHPC design and construction recommendations.

One of most comprehensive design guidelines and/or standards that is concerned with UHPC to date has been developed by the Association Française de Génie Civil (AFGC), i.e. French Association for Civil Engineering. The French standards and design recommendations are composed of three parts. The first part, published in July 2016, is the French standard NF P18-470 (French-standard 2016a) self-supporting document related to UHPFRC specification, performance, production and conformity (this standard has a similar outline as NF EN 206/CN, the French standard for ordinary structural concrete consistent to the European standard). The second part is the French standard NF P18-710 (French standard 2016b), which stands as a national complement to Eurocode 2 for the design of UHPC structures (both buildings and bridges). A third text (NF P18-451) is in final preparation and aims at complementing the standard for execution of concrete structures, NF EN 13670/CN. It is noted that all these documents are based on the French AFGC recommendations on UHPFRC (revised in 2013) and technical feedback of 20 years of UHPFRC projects and realizations. Relevant guidelines related to the design of UHPC columns according to the French standards are presented next.

For UHPC, values of partial factors for material is refined as Table 2-1. These factors shall be 1.0 at serviceability limit state. For preliminary or design studies, and in the absence of tests or an identity card, NF P18-710 (French-Standard 2016b) allows the values given in Table 2-2 to be used for the mechanical characteristics of the UHPC material, compression strength, tensile behavior and Young's modulus along with the shrinkage and creep laws. Poisson's coefficient may be taken as 0.2 for UHPC.

Table 2-1 Partial factors for materials at ultimate limit states (French-Standard 2016b).

| Design situations | $\gamma_c$ (compressed UHPFRC) | $\gamma_{cf}$ (tensioned UHPFRC) | $\gamma_s$ (reinforcing steel) | $\gamma_s$ (prestressing steel) |
|---|---|---|---|---|
| Durable Transient | 1.5 | 1.3 | 1.15 | 1.15 |
| Accidental | 1.2 | 1.05 | 1.0 | 1.0 |

Table 2-2 indicative values for UHPC characteristics (French-Standard 2016b).

| | |
|---|---|
| Young's modulus $E_{cm}$ | 45 - 65 GPa |
| Characteristic compressive strength $f_{ck}$ | 150 - 200 MPa |
| Mean compressive strength $f_{ck}$ | 160 - 230 MPa |
| Characteristic tensile limit of elasticity $f_{ctk,el}$ | 7.0 - 10.0 MPa |
| Mean tensile limit of elasticity $f_{ctk,el}$ | 8.0 - 12.0 MPa |
| Characteristic post-cracking strength $f_{ctfk}$ | 6.0 - 10.0 MPa |
| Mean post-cracking strength $f_{ctfk}$ | 7.0 - 12.0 MPa |
| Global fibre orientation factor $K_{global}$ | 1.25 |
| Local fibre orientation factor $K_{local}$ | 1.75 |
| Linear coefficient of thermal expansion | 11 µm/m/°C |
| Length $L_f$ | 12 - 20 mm |

For non-linear structural analysis, NF P18-710 suggests the compression stress-strain illustrated in Figure 2-1a, which is defined by Equations 1 through 7. The confinement effect brought by fibers in post cracking behavior is considered in term of $f_{ctfm}/K_{global}$ ($K_{global}$ is normally associated with the radial transverse direction).

$$\sigma = f_{cm}\frac{\eta.\frac{\varepsilon}{\varepsilon_{c1,f}}}{\eta - 1 + \left(\frac{\varepsilon}{\varepsilon_{c1,f}}\right)^{\varphi.\eta}} \quad (1)$$

$$\varepsilon_{c1,f} = \left[1 + 4\frac{f_{ctfm}}{K_{global}.f_{cm}}\right]\left[1 + 0.16\frac{k_0}{(f_{cm}^2 + 800)}\right]\frac{f_{cm}^{2/3}}{k_0} \quad (2)$$

$$k_0 = \frac{E_{cm}}{f_{cm}^{1/3}} \quad (3)$$

$$\eta = \frac{k}{k-1} \quad (4)$$

$$k = E_{cm}\frac{\varepsilon_{c1,f}}{f_{cm}} \tag{5}$$

$$\varphi = \begin{cases} 1 & si \quad \varepsilon \le \varepsilon_{c1,f} \\ \dfrac{ln\left(1-\eta+\dfrac{\eta}{0.7}\dfrac{\varepsilon_{cu1,f}}{\varepsilon_{c1,f}}\right)}{\eta.ln\left(\dfrac{\varepsilon_{cu1,f}}{\varepsilon_{c1,f}}\right)} & si \quad \varepsilon > \varepsilon_{c1,f} \end{cases} \tag{6}$$

$$\varepsilon_{cu1,f} = \left[1+15\frac{f_{ctfm}}{K_{global}.f_{cm}}\right]\left[1+\frac{20}{f_{cm}}\right]\left[1+0.16\frac{k_0}{(f_{cm}^2+800)}\right]\frac{f_{cm}^{2/3}}{k_0} \tag{7}$$

In these expressions, $f_{ctfm}$ is the mean value of the post-cracking strength (can be determined based on section 5.5.4 of standard *NF P18-470* (French-Standard 2016a) , and $K_{global}$ is the orientation factor associated with global effect. This standard, however, proposes the constitutive law shown in Figure 2-1b for UHPC sections design in compression at Ultimate Limit State (ULS). The parameters needed to define this curve are as given in Equations 8-10:

$$f_{cd} = \alpha_{cc}\, f_{ck}/\gamma_c \tag{8}$$

$$\varepsilon_{c0d} = f_{cd}/E_{cm} \tag{9}$$

$$\varepsilon_{cud} = \left(1+14\frac{f_{ctm}}{K_{global}.f_{cm}}\right).\varepsilon_{c0d} \tag{10}$$

where, $f_{ctfm}$ is the mean value of the post-cracking strength (can be determined based on section 5.5.4 of standard *NF P18-470*) , $K_{global}$ is the orientation factor associated with global effect ( section 4.4.3 of standard *NF P18-470*), and $f_{cm}$ is the mean value of compression strength (section 5.5.2 of standard *NF P18-470*).

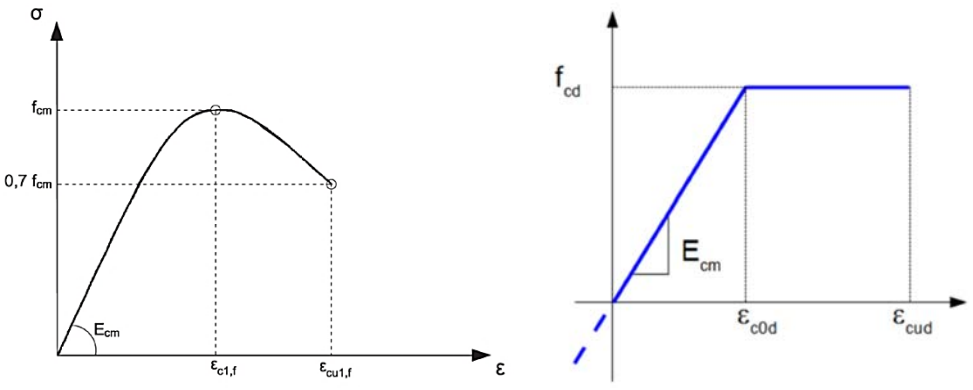


(a) (b)

Figure 2-1 Stress-strain relation of UHPC in compression for: (a) non-linear structural analysis; (b) design at ULS according to French-Standard (2016a).

Standard *NF P18-470* proposes the following options for UHPC sections design in tension at Ultimate Limit State (ULS): (a) either a point-by-point law is chosen which comes

from testing by possibly selecting a simplified description of this piecewise linear law; or (b) a conventional law described in the following sections is chosen, but for which the parameters are determined from test results. In the curves shown in Figure 2-2, $f_{ct,el}$ is the characteristic value of the tensile limit of elasticity, and $f_{ctm,el}$ is its mean value.

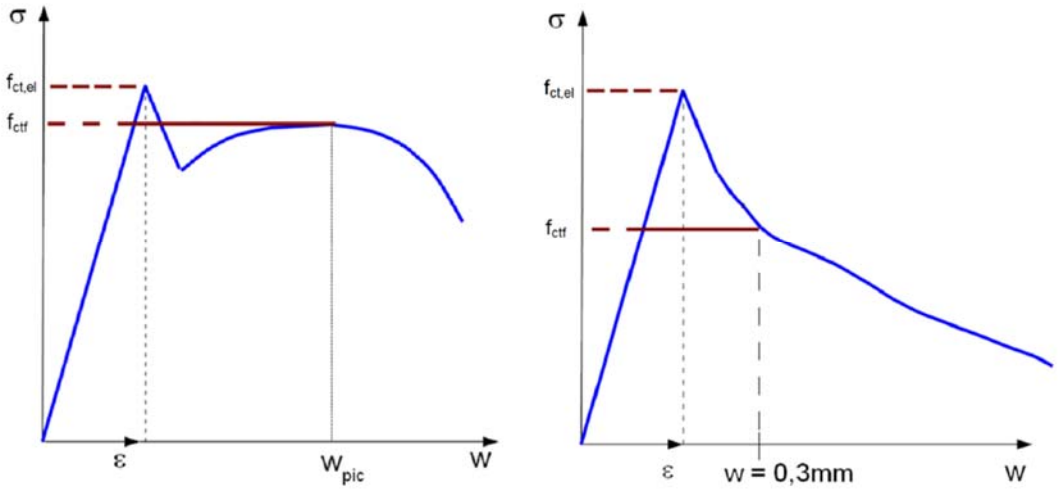


Figure 2-2 Definition of $f_{ctf}$ in case of a local maximum (left) or where there is no local maximum (right) according to French-Standard (2016a).

For the case of Bending with or without axial force in Ultimate Limit State, the compressive strain in the UHPC shall be limited to $\varepsilon_{cud}$ according to the diagram defined in Figure 2-3. The strains in the reinforcing steel and the prestressing steel shall be limited to $\varepsilon_{ud}$. For cross-sections loaded by the compression force (excluding the prestressing force), it is necessary to assume the minimum eccentricity, $e_0 = h/30$ but not less than 20 mm where h is the depth of the section.

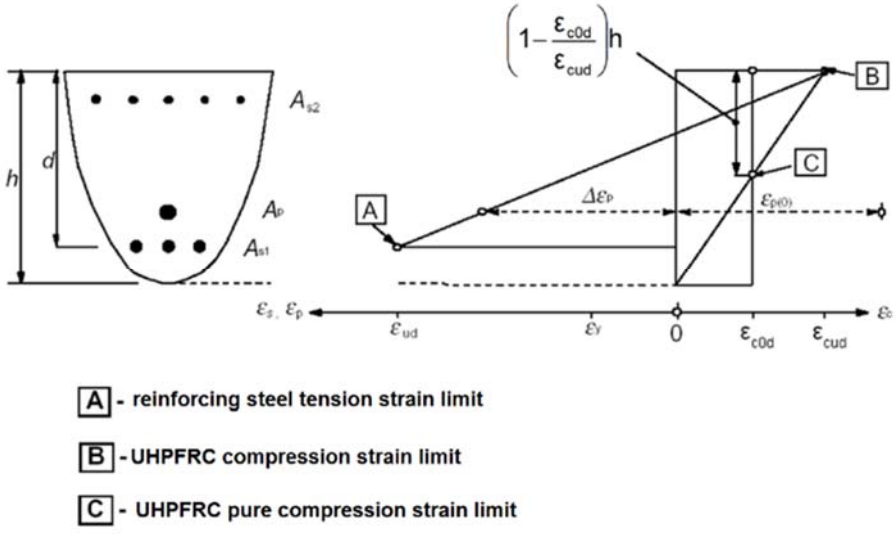


Figure 2-3 Diagram of relative deformations admissible in ultimate limit state (French-Standard 2016a).

## 2.2. Confinement of UHPC

In the recent years, only a handful of published literature addressed compression stress-strain relationships of UHPC cylinders. Hassan et. al. (2012) investigated the effect of steel fibers, modulus of elasticity, stress-strain curve and post peak behavior of UHPC in tension and compression. They obtained the complete compressive stress-strain curve for unconfined specimens using closed-loop controlled testing from Linear Variable Displacement Transducers (LVDTs) feedback. Based on their observations, the BS 1881-121:1983 method was unable to capture the post-peak behavior of UHPC specimens in compression because the strain gauges were detached from the specimens' surface when the concrete spalls after the peak strength. Similarly, they observed that ASTM C469 is inefficient to capture the post-peak behavior of specimens because of the rotation of clamping screws of compressometers after the formation of first cracks. Thus, they recommended the use of compressometers to measure the vertical shortening of the specimen, only in the elastic zone, and LVDTs, placed parallel to the specimen, to measure the movement of machine crosshead, in the post-peak region.

Aghdasi et al. (2016) carried out compression tests on 70.6 mm (2.78 in) cubic specimens cast from their proposed UHPC mixture. They used a pair of LVDTs to determine the deformation for the entire compressive stress-strain curve. Shafieifar et al. (2017) performed compression tests on five 75 mm (3 in) diameter unconfined cylinders and on five, 50 mm and 75 mm (2 and 3 in) cubic specimens, made from the Ductal© UHPC. Based on their observations, Ductal© behaved elastically up to 50% of its compressive strength. They reported the unconfined compression stress-strain curves. Moreover, there is more published work on confinement effect of steel tubes or FRP wraps on the compression behavior of UHPC cylinders (e.g. Zohrevand and Mirmiran 2011). On the other hand, limited studies considered UHPC steel spirals confinement. Yang et al. (2016) conducted compression tests on 3 unconfined and 18 confined UHPC cylinders using steel spirals with yield stress of 60 ksi (414 MPa). Again the tested UHPC material was Ductal© with 2% steel fibers cast into 4 × 8 in (102 × 203 mm) cylindrical molds. Based on their observations, stress-strain behavior of confined specimens could be categorized into three different parts. The initial linear part was following by the nonlinear inelastic hardening region, and then by the gradual load decrease or the sudden load drop after the peak strength, while the unconfined UHPC response was relatively linear up to the peak strength, following by a sudden load drop. They found steel reinforcement more efficient than FRP for confinement of UHPC, except for very large confinement ratios, where FRP is more effective. Moreover, for the same confinement ratio, steel-confined UHPC was found to have a larger ultimate strain than FRP-confined UHPC.

## 2.3. UHPC Axial Columns

Several studies investigated the behavior of UHPC columns. Kimura et. al. (2007) investigated the effect of 1) volumetric ratio of steel fibers, 2) lateral reinforcement ratio, and 3) axial loading type of reinforced UHPC columns with varying axial load under cyclic loading. They used NSK (Nagashima et al. 1995) model for stress-strain relationship of concrete, developed for HSC, in which the effect of steel fibers is not taken into account. Furthermore, they considered NZS equations for assessment of maximum flexural strength of RC columns, which is suitable for concrete with the maximum strength of 200 MPa and without steel fibers. The results of their tests summarized as follows: (1) UHPC columns exhibited very good flexural strength and load

carrying capacity up to drift angel of 3% even under varying high axial loading condition; (2) For UHPC with strength of 200 MPa, the maximum flexural strength under varying axial load was about 1.47 times of Ultra High Performance Columns without steel fibers; (3) The NSK and NZS equations are appropriate for calculation of maximum flexural strength of UHPC with maximum strength of 200 MPa, while ACI and AIJ equations overestimate the strength by 15 to 20% (Table 2-3); (4) Addition of steel fibers results in reduction of column damage, crack dispersion, and decreasing crack width. In Table 2-3, unit 600 is 198 MPa plain concrete without any steel fibers, and unit 601, 602, and 603 are 207 MPa UHPC with 1% steel fibers. Moreover, Illich et. al. (2014) studied the load-carrying behavior of full-scale pre-tensioned columns of UHPC under the same eccentric compression loads at the both ends. They used their special method of loading control to be able to record post-peak behavior of columns.

Table 2-3 Comparison of measured to calculated maximum strength (Kimura et al. 2007).

| Unit | ${}_{ex}Q_{mu}$[kN] | NSK eq. | ACI318 | NZS3101 | AIJ eq. |
|---|---|---|---|---|---|
| 600 | 507 | 0.97 | 0.80 | 1.05 | 0.85 |
| 601 | 750 | 1.34 | 1.14 | 1.50 | 1.21 |
| 602 | 685 | 1.22 | 1.04 | 1.37 | 1.11 |
| 603 | 788 | 1.41 | 1.19 | 1.58 | 1.28 |

*Shear force due to P-Δ effect is included

Hosinieh et al. (2015) examined the influence of UHPC and transverse reinforcement detailing on strength, ductility, and failure mechanisms of six large-scale specimens, designed based on Canadian CSA A23.3-14 code, under pure axial load. They observed that for a particular transverse reinforcement configuration, reduction of space of transverse reinforcements results in enhancement of columns post-peak ductility with moderate increase in column capacity under axial loads. For a particular spacing of transverse reinforcement, their configurations did not have a significant effect on column strength whereas toughness (area under the load-strain curve) enhanced. Compared to the same experiments, carried out on HSC columns, UHPC columns have higher load carrying capacity (Figure 2-4a). The influence of UHPC on post-peak ductility was more apparent in low confined and less important in highly confined columns. This means UHPC and transverse reinforcement have hybrid role in enhancement of post peak behavior. The authors also used two literature proposed confinement models for HSC; however, they need to be modified for UHPC. They observed good agreement between the experimental and numerical results from Aoude's FRP confinement model (2008), and their own proposed model for unconfined UHPC (Figure 2-4b). In Figure 2-4a, CRC stands for Compact Reinforced Composite, a UHPC mixed developed in Denmark. C3-80 column has the reinforcement configuration type of C3 with 80 mm hoop spacing, and CS8 is a HSC column with similar size and configuration to C3-80. In Figure 2-4b, HSC1 and HSC2 are confinement models proposed respectively by Razvi and Saatcioglu (1999) and Légeron and Paultre (2003), and FRC1 is fiber-reinforced concrete confinement model proposed by Aoude (2008).

Shin et. al. (2017) investigated the axial load response of UHPC column with compressive strengths of 163 and 181 MPa. They used UHPC of 1.5 % steel fibers. They tested nine UHPC columns with different ratio of 0.9-9.9% transverse reinforcement and two different configurations. They studied the applicability of the existing equations in predicting behavior of UHPC columns.

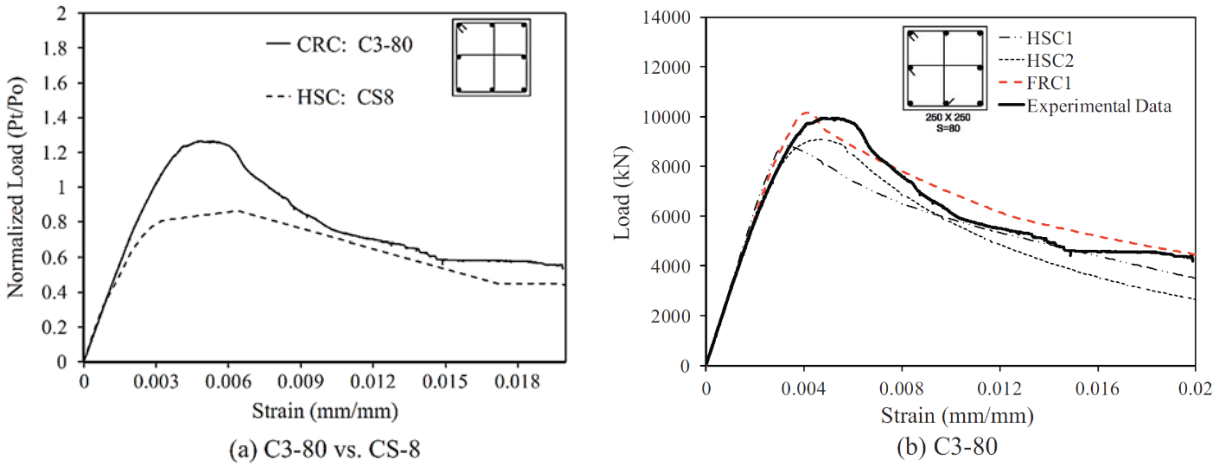


Figure 2-4 Comparison of: (a) normalized load-strain response for UHPC vs. HSC columns; and (b) experimental and analytical load-strain curves predicted using HSC models after Hosinieh et al. (2015).

## 2.4. Slender UHPC Columns

In addition to studying axial capacity of UHPC columns, few studies considered buckling of UHPC columns associated with the likely UHPC smaller sections compared to conventional concrete. Schmidt and Heimann (2011) and Heiman et al. (2013) investigated the reliability of slender UHPC structural members to assess the likelihood of their buckling and decrease in safety level, and compared the results of probabilistic analysis of HSC columns of high rise buildings with the conservative design provisions of Eurocode 1 and 2. Based on their study, there is a considerable safety deficit in Eurocode 2, Part 1-1 (buildings). The safety elements become ineffective when buckling occurs prior to steel yield or concrete strength. The reliability of UHPC members must be considered and the effects of shrinkage have to be taken into account in a probabilistic model of UHPC.

Another study was made by Hung and Hu (2018) to experimentally investigate the behavior of ten slender high-strength concrete of 100 MPa compressive strength and steel fiber contents ranging from 0% to 1.5% under concentric axial loads. They found that inclusion of 1.5% fibers enhanced the post-peak behavior as it became more ductile and it controlled the cover spalling preventing the longitudinal rebars from buckling. Hung and Hu (2018) experimentally investigated the behavior of ten slender high-strength concrete (100 MPa compressive strength) columns under concentric axial loads and compared their capacities to the ACI 318 equations. The experimented variables were (1) the stirrup spacing (h/2 & h/4), (2) the cross ties (presence or absence) and (3) the amount of steel fibers (0, 0.75, & 1.5%). The columns dimensions were 200 × 200 × 1200 mm (buckling Ratio = 40, According to ACI 318). It was found that all of the transversely reinforced columns without fibers exhibited a brittle post-peak behavior with an abrupt loss in their strength after reaching peak strength because of large region of concrete spalling and crushing. Inclusion of 1.5% fibers enhanced the post-peak behavior as it became more ductile and it controlled the cover spalling preventing the longitudinal rebars from buckling. Finally, the ACI 318 equations overestimated the strength of HSC slender columns with 6% and 12%.

Hung et al. (2018) experimentally investigated the behavior of eight slender UHPC (100 MPa compressive strength) columns under eccentric axial loads and compared their capacities to the ACI 318 equations. The experimented variables were (1) the stirrup spacing (h/2 & h/4), (2) the cross ties (presence or absence) and (3) the amount of steel fibers (0, 0.75, & 1.5%). The columns dimensions were 200 × 200 × 1200 mm (buckling Ratio = 40, According to ACI 318). It was found that using the cross ties improved the brittle post-peak behavior of the columns without fibers and using of the fibers with 0.75% or more enhanced the strength retention and ductility by postponing the crushing and spalling. Finally, the ACI-318 magnified Moment approach generated acceptable estimations for the total moment demand of the tested slender UHPC columns with accuracy ratios between 0.94 and 1.04 but slightly underestimated the actual total moment demand of the columns with fibers and overestimation of the columns without fibers. (Knowledge gap, comparing nominal values to actual values and they are almost the same)

Schmidt and Curbach (2017) experimentally and analytically addressed the design optimization of UHPC columns to increase buckling stability by changing the cross section and shape of the column in both longitudinal and transverse directions by using the same amount of material used in their corresponding rectangular shaped columns. The experimental program consisted of two groups of 14 columns without longitudinal or transverse reinforcement and with compressive strength ranging from 120-160 MPa; the first group of 4 square columns and 4 triangular columns with the same amount of materials and of 130-135 slenderness ratio and hinged-hinged end conditions to investigate the effect of changing the X-section on increasing the buckling stability, while the second group consisted of 3 rectangular columns and 3 optimized rectangular columns of equally UHPC volumes with smaller cross-sections at the points of inflection of the column buckling profile and bigger X-sections elsewhere along the column, the columns are of 99-100 slenderness ratio and fixed-fixed end conditions. The authors concluded that the variation of the geometry and the shape of the column have a large potential to increase the stability.

Redaelli et al. (2014) experimentally evaluated the contribution of fibers to the structural response of the columns under bending with normal force, and to assessing to which extent fibers could replace longitudinal or transversal reinforcement. Two preliminary test series on full scale columns with or without ordinary reinforcement were carried out. The first test series experimentally investigated the behavior of nine UHPC columns (slenderness ratio= 42) without transverse reinforcement under axial load and imposed end rotation, the experimented variables are 3 different longitudinal reinforcement configurations (unreinforced, reinforced & prestressed), with 3 different applied axial load ratios (30%, 50% and 70%). The second test series experimentally investigated the behavior of nine more slender columns (slenderness ratio= 83) with circular X-section made of HSC columns and reinforced alternatively with: only fibers; only ordinary longitudinal and transversal reinforcement; both fibers and reinforcement and the Columns were tested under an eccentrically applied compressive force, the experimented variables are concrete type (HSFRC with 2% fibers, HSC); the initial eccentricity (30 to 60 mm); the presence of longitudinal and transversal reinforcement; steel quality (ordinary or high strength steel). The authors concluded that Despite the relatively ductile behavior in compression of HSFRC and UHPFRC, columns without ordinary reinforcement subjected to high compressive forces fail in an extremely brittle way, while columns with longitudinal reinforcement and without any transversal reinforcement promotes longitudinal cracking which cannot be controlled by fibers alone, thus leading to early spalling of concrete cover and a

reduction of column strength and finally, When fibers are added (> 2.0% in vol.) to columns with longitudinal and transversal reinforcement, cover spalling is prevented.

Aarup et al. (2004) tested a wide range of CRC columns with compressive strengths ranging from 120 to 145 MPa that had slenderness varying from 1.11 to 12.76 (the column dimensions ranged from 80×80mm cross-section with a height of 4.2m to 200×200mm cross-section with a height of 2.7m), a reinforcement ratio ranging from 0 to 8.8% and steel fiber ratio of 2, 4 or 6%. A total of 77 tests were carried out – 61 columns (57 centrally loaded & 4 eccentrically loaded) were tested in ambient conditions and 16 columns were tested in standard fire conditions. Only some of the columns were tested to failure while the others are tested until the reached their expected capacity. The test results showed good correlation between test results and expected bearing capacities calculated according to design guides established based on earlier CRC investigations. The fire resistance tests demonstrated that the slender columns were very sensitive to thermal stresses and changes in stiffness due to high temperatures. Thus, very slender columns failed early in the tests even though temperatures at the reinforcement were low. Failure was always ductile and there was no spalling.

## 2.5. UHPC Columns Behavior under Different Hazards

Some studies considered also the behavior of UHPC columns under different types of lateral or dynamic loads along with hazards such as earthquakes, fire, or blast as briefly summarized below.

### *2.5.1. Earthquakes*

Sugano et al. (2007) studied a series of tests of columns and frames of UHPC buildings under seismic loading to provide guidelines for design and construction. Based on their investigations UHPC is basically a brittle material which can be confined using high or ultra-high strength lateral reinforcements. In this case, the UHPC columns can tolerate very high axial compression forces. The flexural behavior of UHPC columns also can be well assessed when taking the tensile resistance of UFC and confinement by lateral reinforcements into considerations. Steel-fibers in UHPC mixture significantly enhanced the shear resistance of columns and frames. On the other hand, Joe and Moustafa (2016) conducted a preliminary analytical study to investigate the design implications of using UHPC for seismic bridge piers in lieu of conventional concrete. They showed that up to 40% reduction in the columns cross-section can be obtained if UHPC is used to achieve same plastic moment capacity and ductility as conventional concrete piers under seismic loading.

Chao et al. (2016) studied seismic response of UHPC beams and columns with relatively higher amount of longitudinal reinforcement (> 2.5%) used for moment frame beams compared to what is acceptable for conventional RC beams. Based on their research, UHPC columns have higher strength and drift capacity before significant damages, compared to RC columns. In UHPC columns failure phenomena such as: concrete spalling and crushing, bar buckling and hoop failure are reduced. At moderate drift of 1.0 to 2.0 %, minor damages happens. UHPC column had no strength degradation till 2.5 % drift and could maintain its peak strength approximately close to 4 % drift. The researchers also showed that the ACI 318 requirements can be relaxed if UHPC columns and beams are designed. Particularly, the confinement requirements and amount of transverse reinforcement can be reduced for high strength concrete (>10 ksi) columns.

Wang et al. (2016) established a finite element model, using Kent-Park model, to study the seismic performance of a pier of UHPC and high-strength steel. Concrete 02 by OpenSees platform is used as the constitutive model while the modified Kent-Park model is used for the skeleton curve. Based on their parametric studies, the following requirements were suggested to be considered for desirable seismic performance of UHPC: (1) Axial load ratio to be less than 0.4; (2) To have a drift ratio less than 1%, for a UHPC pier under minor axial load ratio and medium amount of transverse reinforcement, less than 2% longitudinal reinforcement to be used; (3) For small axial load ratio, the increase of transverse reinforcement can reduce residual drift ratio while does not have any effect on ductility and energy dissipation of UHPC columns; (4) For short piers with high axial load ratio, the maximum ground acceleration capacity is a little insecure using inelastic response spectra, based on the nonlinear dynamic time history analysis.

### *2.5.2. Blast*

Aoude et al. (2015) presented the results of a study examining the blast load performance of UHPC columns. Li et al (2015) carried out field blast tests on the four columns of their own developed UHPC, and compared the results with the numerical model. They note that UHPC have superior blast resistant features. In the later study, the authors used the material model type 10 in LS-DYNA, which can be defined by user based on the uniaxial compression test on UHPC, to model the UHPC behavior in compression. Similarly, Zhang et al. (2017) also used LS-DYNA to study the behavior of UHPC filled double skin steel tube (UHPCFDST) columns under blast loading. They derived pressure-impulse diagrams for UHPCFDST columns in terms of residual axial load-carrying capacity after blast load, and examined the effect of axial load ratio, steel tube thickness, column dimension and concrete strength on pressure-impulse diagrams.

Zhang et al. (2015) evaluated the residual behavior of UHPC infilled double-skin steel tubular columns after close-in blast loading. They carried out eight blast tests on three square and five circular columns with two different axial load levels. Then, they applied static axial compressive loads on the specimens until failure to investigate their residual capacity. Based on their observations, the axial load capacity of both undamaged circular and square columns were the same with negligible difference, which was probably due to better confinement status for circular ones. However, the flexural capacity of square columns was larger than circular ones. The columns with applied axial load of about 25% of their axial capacity, had larger flexural capacity while less ductility, compared to the load free columns. The UHPC infilled double-skin steel tubular columns could retain 60% of their axial load capacity after blast load. Localized buckling of outer steel tubes at mid span/ or column ends were observed. The columns with smaller permanent displacement had larger peak residual axial capacity. Besides, columns with no axial load, were more ductile than those with axial load during blast tests.

Xu et al. (2016) tested four 0.2m×0.2m×2.5m reinforced UHPC columns under different designed explosions with same standoff distance of 1.5m, and compared their efficiency with four same sized and same reinforced HSC columns. Based on their investigations, use of UHPC rather than HSC can reduce the maximum and residual displacements and enhance the blast resistance of columns. Moreover, the axially loaded specimens have smaller deflections because of the influence of boundary conditions, which outweighs the P-delta effect.

### *2.5.3. Fire*

Unlike all the outstanding mechanical features of UHPC, its particular material properties and slenderness of structural elements leads to its sensitivity against fire. High packing density

causes the high pore pressure, which results in concrete spalling when the remained water is evaporated. Zehfuss and Siemon (2015) showed that it is possible to prevent explosive spalling using polypropylene fibers. They evaluated the load bearing capacity of UHPC columns in expose of fire, and simulated it using finite element method.

## 2.6. Novel Hybrid Column designs using UHPC

The previously mentioned studies considered mainly columns entirely constructed using UHPC. However, numerous other studies considered UHPC as one component of novel and innovative new columns designs (e.g. Xiangguo et al. 2013; Markowski and Lohaus 2017). Two popular hybrid columns are UHPC-filled steel tubes and Fiber Reinforced polymer (FRP) tubes. Other designs include UHPC cores in conventional concrete and segmental UHPC columns.

### *2.6.1. UHPC-filled Steel Tubes*

Liew and Xiong (2012) tested 18 steel tubes infilled with ultra-high strength concrete, 4 steel tubes infilled with normal strength concrete, and 5 hollow steel tubes. Although tubes filled with UHPC had higher load-carrying capacity, they were brittle after the peak load. Their ductility, however, could be improved by applying the load only on the concrete core, adding steel fibers into the concrete core or increasing the steel contribution ratio. Based on their study, on average, Eurocode 4 underestimate the strength of UHPC filled composite stub columns by 14.6%, ignoring confinement effect of fibers, and by 3.5% considering confinement effect of fibers. They recommended use of at least 0.3-1.0% steel fibers. Dexin (2012) examined the structural behavior of Concrete filled steel tubes CFSTs with ultra-high strength concrete (UHSC) and high strength steel (HSS) under static loading, to assess the preload effect on the overall buckling resistance of CFST columns under concentric compression, and extend current design codes to UHSC, HSS and preload effect. N.V. Tue et al. (2014) studied load bearing behavior of three different stub columns of confined NSC, HSC, and UHPC in steel tubes. Based on their observations, UHPC, compared to the two other groups of concrete, has higher stiffness, upper level of service load, and a rather intense shrinkage, which leads to closing of the gap between concrete core and steel tube only beyond the service level. Besides, smaller section area can be chosen if UHPC is used as concrete core in the stub columns. Guler et al. (2013) conducted some experiments on circular UHPC-filled steel tube columns under monotonic axial compression. They investigated the concrete contribution ratio, strength enhancement index and ductility index, in relation to the diameter-to-thickness ratio of the columns. Liew et al. (2014) investigated the behavior of tubular columns in-filled with UHPC at ambient and elevated temperature. Empelmann et al. (2016) investigated the behavior of compact thin-walled reinforced UHPC columns with circular hollow sections under centric and eccentric normal force.

Recently, Hoang and Fehling (2017a) presented a review of past experimental studies on UHPC-filled steel tubes under axial loading on entire section and on concrete core. They investigated the behavior of circular UHPC filled steel tube columns under concentric loading on concrete core using a finite element model in ATENA-3D (Hoang and Fehling 2017b). They carried out a parametric study to assess the effect of concrete compressive strength, steel tube thickness, and steel yield strength on compressive behavior. Hoang and Fehling (2017c) also studied the effect of confinement factor and the diameter to thickness ratio on strength and ductility in circular steel tube confined concrete columns infilled with UHPC.

### *2.6.2. FRP-filled Steel Tubes*

Zohrevand (2012) developed a hybrid system of UHPC-filled fiber reinforced polymer (FRP) tubes and provided a comprehensive experimental investigation using different fiber types and thickness under uniaxial compression. Zohrevand and Mirmiran (2012, 2013a, 2013b) studied he confinement behavior of UHPC due to FRP tubes and experimentally evaluated its cyclic behavior within twice length of the plastic hinge in columns under a constant axial load and reverse cyclic lateral load. Based on their observations, such a system has significantly higher flexural strength and initial stiffness, lower residual drift, and relatively similar energy dissipation compared to the reinforced concrete. Guler et al. (2013) and Guler (2014) investigated the behavior of axially loaded UHPC short circular columns wrapped with CFRP, GFRP, and AFRP sheets. They developed a three dimensional finite element model to predict the axial stress-strain relationship and ultimate strength of FRP-wrapped UHPC columns. They evaluated the validity of four confinement models and three codes (ACI-440, CSA-S806-02, and ISIS CANADA) in comparison with the experimental results from six unconfined and 36 different types of the FRP-wrapped UHPC columns under monotonic axial compression. Girgin et al. (2015) pursued a design oriented combined model to predict the ultimate strength and strain for axially loaded 7 to 190 MPa FRP-confined circular short columns. Ridha (2017) numerically and experimentally investigated the performance of square FRP tubular columns in filled with UHPC under axial-flexural (P-M) loading. They tested eight specimens: four with FRP tubes under initial load eccentricity 0, 10, 85 and 95 mm, three reference columns without FRP tube under initial load eccentricities 0, 10, 85 mm, and one with FRP tube under pure bending.

### *2.6.3. Other Designs*

Hudoba and Mikus (2013) compared load carrying capacity of a column of conventional reinforced concrete with four different groups of hybrid columns: solid steel core, smooth 70-mm diameter UHPC core, corrugated 72-mm diameter UHPC core, and 78-mm diameter UHPC core in corrugated steel tube, which all had same steel reinforcement. Zhang et al. (2016) examined behavior of UHPC infilled double-skin tube columns under close-in blast loading. Popa et al. (2016) investigated the differences in economy and section between design of a 40 story building by two types of columns: simple section (regular columns made of regular concrete class C35/45) and compound section (columns with the core made of UHPC class C130 and an outer shell of RC also class C34/45). They used an equivalent strength and modulus of elasticity to calculate the pre-dimensions for compound sections in Ultimate Limit State (ULS). They analyzed the 40-story building in SAP2000 and processed the data for each column independently. As a conclusion, the reduction of the transversal section was between 32.18% and 62.13% for the columns belonging to the first 30 stories. Ichikawa et al. (2016) tested two different details of UHPC segments, they proposed for plastic hinge region in conventional reinforced concrete columns, under orbital bilateral cyclic loading. They investigated the failure modes, dissipated energy, and equivalent viscous damping.

Using UHPC for column repairs and retrofits can also be considered a hybrid column design. Massicotte et al. (2013) presented a seismic strengthening technique using UHPC jackets to prevent splitting failure mode (lap-splice failure, concrete cover spalling, and longitudinal buckling) in splice regions which does not have adequate reinforcement details. They tested their proposed technique on four large-scale rectangular bridge piers with the 2:1 cross sectional ratio. For unconfined $24d_b$ long lap splices, they captured drift ductility ratio up to 8 without any strength reduction for bars up to 45mm in diameter. The longitudinal bar buckling was also

eliminated for 300 mm stirrup spacing. Based on their claim, UHPC with 3% fiber content is sufficient for elimination of failure when using reinforcement diameter up to 45 mm. Li et al. (2017) developed a technique to repair conventional reinforced concrete columns damaged in earthquake, using HPC. They evaluated the efficiency of their proposed technique by comparing load-carrying capacities, displacement ductility, stiffness, and energy dissipation. They recommended 1.5 times of the width or height as the repair height of HPC for damaged columns.

## 2.7. Modeling of UHPC Columns

Davila (2007) discussed analytical modeling for UHPC and the evolution in design codes and their philosophical bases. Caldwell (2011) used the stress-strain relation illustrated in Figure 2-5a for UHPC modeling to numerically study the incurrence of plastic hinges and inspect the resultant behavior of NSC and UHPC columns under severe and short duration dynamic loads. Using a similar constitutive model (Figure 2-5b), Astarlioglu and Krauthammer (2014) numerically compared the response of a reinforced UHPC column with the same size and same reinforced NSC column under four levels of idealized loads. They analyzed 16 columns (four axial load cases for each blast load level and four blast load configurations). They observed that the difference of UHPC and NSC in peak displacement, when the load is small enough that does not lead to failure, was relatively small. On average, displacement in UHPC columns was respectively 27% and 30% smaller than NSC columns for simply supported and fixed boundary conditions.

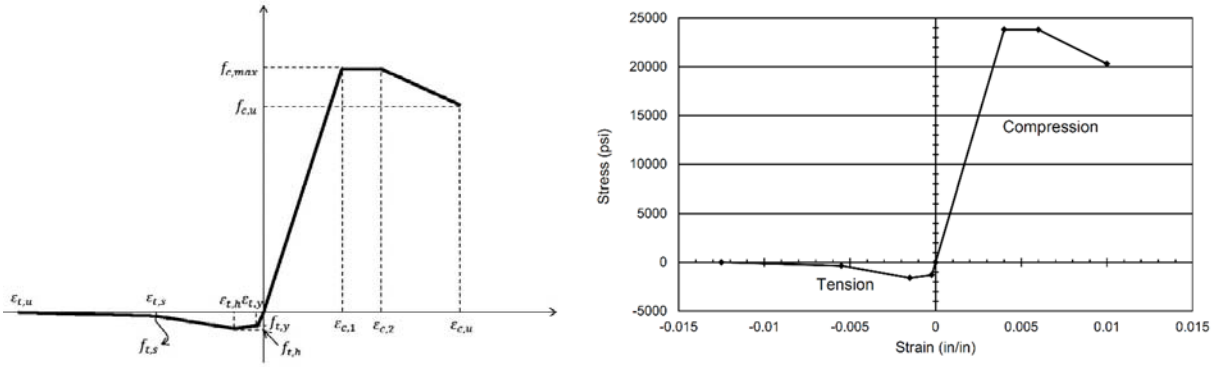


(a) (b)

Figure 2-5 Stress-strain curve used for UHPC modeling: (a) Caldwell (2011) and (b) Astarlioglu and Krauthammer (2014).

# Chapter 3. UHPC CONFINEMENT STUDY

## 3.1. Material and mix design

In this study, the Ductal© JS1000 commercial UHPC was used. Ductal© is composed of the premix, which is a proprietary blend of cement, silica sand, silica flour and silica fume, super plasticizer, and 2% steel fibers. In Table 3-1, the UHPC mix by Ductal© is presented. Based on the reported data, steel fibers have 399 ksi (2750 MPa) yield stress, 0.5 in (13 mm) length, and 0.008 in (0.2 mm) diameter. For the purpose of this study, one batch of Ductal© UHPC was mixed following rigorous mixing and sampling procedures. Materials were accurately weighed and placed in a high shear mixer (Imer Mortarman 360 mixer). The premix, superplasticizer and water (or ice when needed) were initially mixed for about 15-20 min until a good consistency is reached. Next, the steel fibers were added slowly to the paste and mixed for an additional 10-15 min. As soon as mixing was completed, the casting and sampling of test specimens was completed. The UHPC was scooped into the plastic molds and was not rodded to avoid fibers segregation. The UHPC cylinders were just hit by a hammer on the side to allow the trapped air to exit. Cylinders were field cured to represent actual performance of UHPC in a structural scale. Note that the UHPC paste and ambient temperature were measured and controlled to be in the allowable range during the mixing and casting. Moreover, the static and dynamic flow tests were conducted to control the quality of the UHPC paste.

Table 3-1 UHPC mixture by Ductal© (based on number of premix bags).

| | $kg/m^3$ | $lb/yd^3$ | Percentage by weight |
|---|---|---|---|
| Premix (kg) | 2,195 | 3,700 | 87.4 |
| Water (or ice if needed) | 130 | 219.1 | 5.2 |
| Superplasticizer (Premia 150) | 30 | 50.6 | 1.2 |
| Steel fiber (2% volume) | 156 | 263 | 6.2 |

## 3.2. Test specimens

In total, 6 unconfined and 16 confined specimens were cast from one batch into the 3×6 in (76×152 mm) plastic cylindrical molds and demolded after at least 10 days of casting. Specimens were tested between 123 and 127 days after casting. Age of the specimens at the test day, volumetric ratio of steel spirals, and number of specimens for each group of specimens are summarized in Table 3-2. Confined cylinders were reinforced by steel spirals of three different pitch sizes: 1, 0.5, and 0.25 in (25, 13 and 6 mm). The volumetric ratio of the wires (ρ) in confined cylinders were 1.91%, 3.82% and 7.63%, respectively. Spiral wires were of low carbon steel with 70 ksi (483 MPa) tensile strength and 0.135 in (3.44 mm) diameter. Figure 3-1 shows how the spirals used for confining the UHPC cylinders were made and installed in the cylinders. Figure 3-2 shows the fresh UHPC after filling the cylinders. To prepare the specimens for the uniaxial compression test, the top end of the confined and unconfined specimens were firstly cut using a saw machine. Next, both ends were ground using a HC-2980 grinding machine as also illustrated in Figure 3-2.

Based on the Ductal© Operating Procedures for cylinders end-grinding, using a concrete saw, approximately 10-12 mm of top of the cylinders shall be finished end, and the ultimate

length of the cylinders must be 150 mm ± 1 mm. Note that the cylinders' molds are typically 75 mm × 165 mm but the molds used in this study were shorter with the height approximately equal to 150 mm. Accordingly, the finished height of the specimens were less than 150 mm. Hence, the effect of specimens' height on the compressive strength is investigated as discussed in a following section. The height of the specimens were calculated as the average of four lengths measured in two perpendicular directions at the cross section. The diameter of UHPC specimens was measured at three locations along the height: top, mid-height and bottom. At each height level, the diameter was measured in two perpendicular directions. Thus, the diameter of each cylinder is the average of six measured diameter at different locations at height and cross section. The average diameter was used to calculate the cross section area of the cylinders, which was used for stress calculations. The strain was then calculated from the average displacement captured from three LVDTs (novotechniks) divided by the average specimen height as shown in next section.

Table 3-2 Summary of the varied confinement tests parameters and age of testing.

| Specimen Group | ρ (%) | # of specimens | Specimen Number (Age in days) |
|---|---|---|---|
| Plain UHPC | 0 | 6 | No. 1 (123), No. 2 (123), No. 9 (126), No. 10 (126), No. 18 (127), No. 19 (127) |
| 1-in confined UHPC | 1.91 | 5 | No. 3 (123), No. 4 (123), No. 11 (126), No. 12 (126), No. 20 (127) |
| 0.5-in confined UHPC | 3.82 | 6 | No. 5 (126), No. 6 (126), No. 13 (126), No. 14 (126), No. 21 (127), No. 22 (127) |
| 0.25-in confined UHPC | 7.63 | 5 | No. 7 (126), No. 8 (126), No. 15 (127), No. 16 (127), No. 23 (127) |

Figure 3-1 Assembling the spirals used for the UHPC confinement study.

Figure 3-2 Fresh UHPC after filling the cylinders (left) and process of grinding the cylinders ends for straight and smooth surface for compression testing (right).

### 3.3. Instrumentation and test set-up

All the specimens were tested under uniaxial compression loading using a Tinius-Olsen 300 kip (1334 kN) compression testing machine (shown in Figure 3-3) under force control. The loading rate was constantly maintained at approximately 15 kip/min (67 kN/min). Three different novotechnik devices were placed around the perimeter with 120º angle in between as illustrated in Figure 3-3 to measure the axial shortening of the specimens. The axial load and the vertical displacement were both measured at sampling rate of 256 Hz.

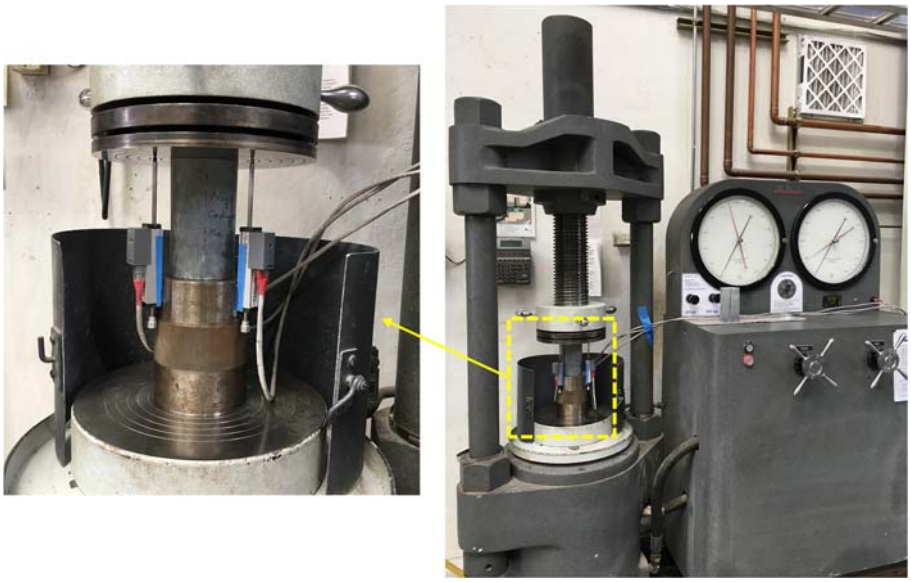

Figure 3-3 Tinius-Olsen testing machine used for UHPC cylinders compression tests and the novotechniks arrangement for displacement/strain measurements (one is behind the specimen).

### 3.4. Test results and discussion

Unconfined UHPC, also referred to as plain UHPC herein, cylinders typically failed by the gradual widening of multiple cracks in the vertical direction. In case of confined cylinders, the steel spirals stopped the progression and widening of the vertical cracks and prevented explosive failure of the specimens. The mode of failure for confined cylinders was a combination of small vertical cracks and spalling or crushing of UHPC in between the spirals. The typical failure mode of each group of UHPC specimens is illustrated in Figure 3-4.

To evaluate the ductility of the specimens, the ultimate strain was determined and compared for each group as shown in Table 3-3. The ultimate strain was defined as the strain at which the UHPC peak strength has already decreased by 20% (Yang et al. 2016). Based on the results, the ultimate strains were equal to 0.0076, 0.0095 and 0.0103 for 1-in, 0.5-in and 0.25-in confined cylinders, respectively. The increased strains reflect higher ductility which consistently increased by the increase of confinement ratio. It is noted that for plain UHPC specimens a sudden drop typically occurred after peak strength is reached and accordingly, an accurate post-peak behavior or ultimate strain values were not determined.

(a) (b) (c) (d)

Figure 3-4 Typical failure mode of (a) unconfined (plain) UHPC, (b) 1-in confined UHPC, (c) 0.5-in confined UHPC and (d) 0.25-in confined UHPC cylinders.

Table 3-3 Summary of UHPC confinement test results.

| Specimen Group | confinement ratio $f'_l/f'_{co}$ | *Modulus of Elasticity, E ksi (GPa)* | *Peak strength ksi (MPa)* | $\varepsilon_p$ | $\varepsilon_{p,cc}/\varepsilon_{p,c}$ | $\varepsilon_{cu}$ | confinement effectiveness $f'_{cc}/f'_{co}$ |
|---|---|---|---|---|---|---|---|
| Plain | - | 6,585 (45.4) | 29.90 (206) | 0.0049 | 1.00 | - | 1.00 |
| 1-in confined | 0.019 | 6,507 (44.9) | 28.26 (195) | 0.0050 | 1.04 | 0.0076 | 0.95 |
| 0.5-in confined | 0.042 | 7,479 (51.6) | 30.85 (213) | 0.0058 | 1.20 | 0.0095 | 1.03 |
| 0.25-in confined | 0.088 | 7,396 (51.0) | 31.68 (218) | 0.0066 | 1.37 | 0.0103 | 1.06 |

In Table 3-3, the confinement effectiveness is defined as the ratio of compressive strength of confined UHPC ($f'_{cc}$) to the unconfined compressive strength ($f'_{co}$). The confinement ratio is defined as the ratio of the effective lateral confining pressure ($f'_l$) to the unconfined compressive strength of plain UHPC ($f'_{co}$) using the following equation adopted from Mander et al. (1988).

$$f_l' = \frac{1}{2} k_e \rho_s f_{yh}$$

where $f_{yh}$ = yield strength of transverse steel; ρ = volumetric ratio of transverse confining steel to the confined concrete core; and $k_e$ = confinement effectiveness coefficient, which in turn, is calculated as follows.

$$k_e = \frac{1 - \frac{s'}{2d_s}}{1 - \rho_{cc}}$$

where $d_s$ = center-to-center diameter of spiral; s′ = clear spacing between spiral wires (pitch) and ρcc = ratio of area of longitudinal steel to area of UHPC, which is zero for this study. The overall results indicates that confinement enhances the peak strength by about 6% (for 0.25-in confined UHPC) but increases the corresponding strain at peak strength by about 37%.

Moreover, Figure 3-5 shows a relation between the degree of out-of-planeness or distortion of cylinders versus the compression strength. Out-of-degree planeness of cylinders after grinding must be under 1 degree; otherwise, the specimen must be reground (Graybeal 2006). Based on Figure 3-5, all cylinders had out-of-planeness in the range of 0-0.5º, which had an insignificant impact on the compressive strength. As previously mentioned, the UHPC specimens were cast in 3×6 in (76×152 mm) cylinders but became shorter than what Ductal© suggests in the manual of Operating Procedures for Cylinders End-Grinding after grinding. Thus, the effect of height on the compressive strength of UHPC cylinders is investigated and summarized in Figure 3-6. Based on this figure, the height of specimen did not seem to have a trend that can affect the test results.

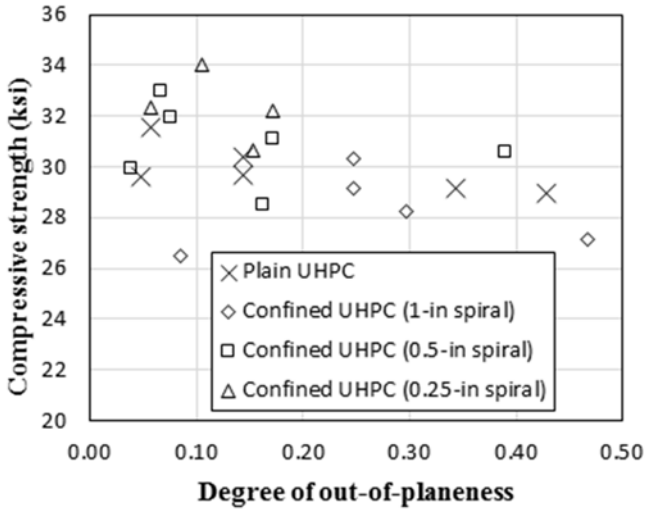


Figure 3-5 Compressive strength as varies with cylinders end planeness of cylinders.

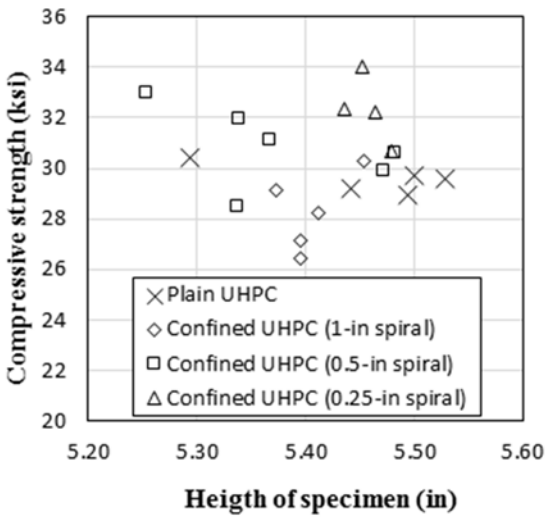


Figure 3-6 Compressive strength as varies with height of cylinders.

The obtained stress-strain curves of plain UHPC, 1-in confined, 05-in confined, and 0.25-in confined UHPC cylinders are presented in Figures 3-7 (a) through (d), respectively. As shown in Figure 3-7a, the unconfined cylinders behave almost linearly until the peak strength which is followed by a sudden load drop that corresponds to an explosive failure. The confined cylinders show a smoother behavior as the peak strength is approached. The behavior of 1-in, 0.5-in and 0.25-in confined cylinders is also found to be almost linear up to 80%, 70%, and 60% of the peak strength, respectively (Figure 3-7).

Similar to what Yang et al. (2016) observed, the confined stress-strain curves can be categorized to three different phases. The first phase is the elastic phase in which the transverse reinforcements are not yet active and the UHPC core mainly tolerate the load. In the second phase, small cracks and dilation of the UHPC core begin to occur, which in turn, activate the transverse reinforcements. Finally, in the last phase, UHPC reach its strength limit and a gradual load decrease starts. The shape of the curves in the second and third phases are apparently dependent on the volumetric ratio of the steel spirals. The higher the volumetric ratio of the steel spiral, the more energy dissipates through plastic deformations. This is exactly what is desirable for bridge columns designed for severe seismic loading. Therefore, confinement of UHPC columns can be beneficial as it is in conventional concrete columns to boost the ductility and strength of a cross-section.

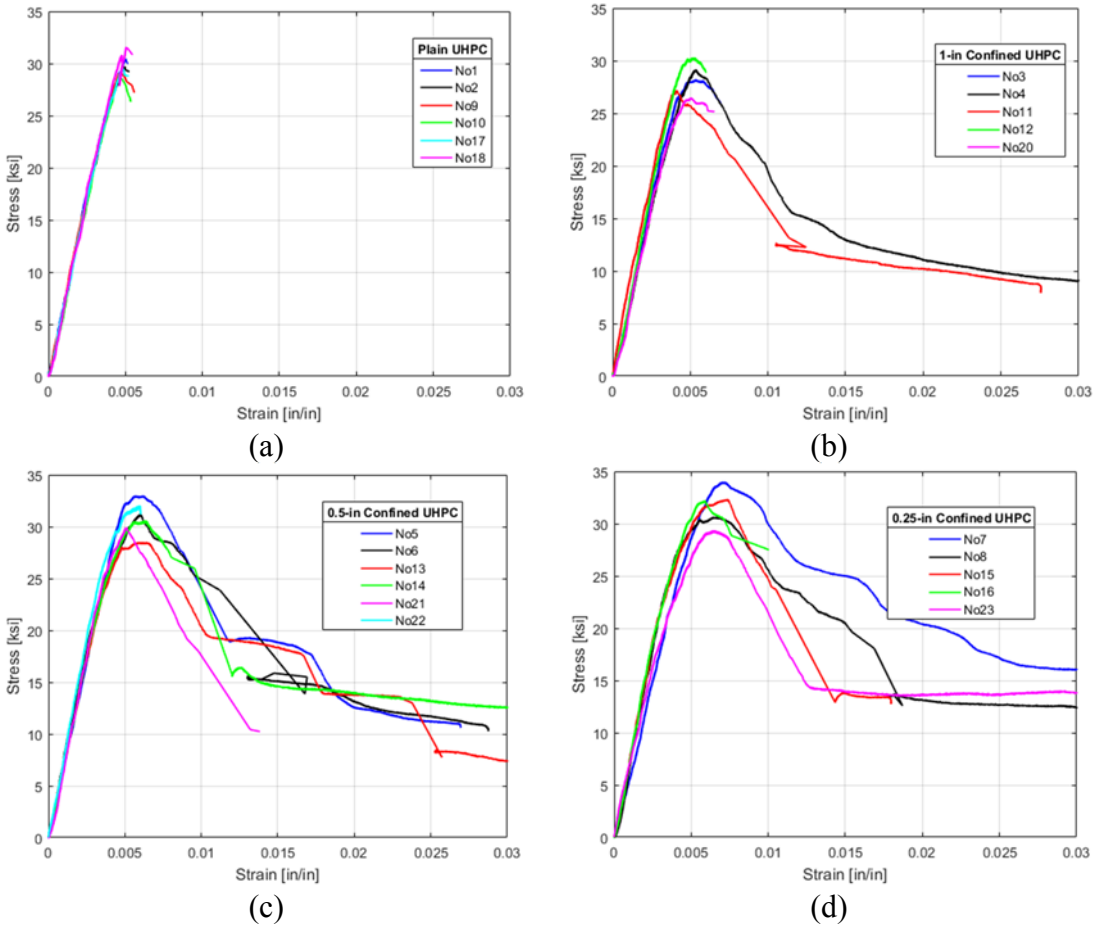


Figure 3-7 Stress-Strain response of (a) unconfined (plain) UHPC, (b) 1-in confined UHPC, (c) 0.5-in confined UHPC and (d) 0.25-in confined UHPC cylinders

## 3.5. Concluding Remarks

This chapter presented the experimental tests on uniaxial compression behavior of unconfined UHPC and UHPC cylinders confined by steel spirals. The obtained and presented results include the stress-strain curves, modulus of elasticity, peak strength, and ultimate strain. Based on the test results, steel spirals improved the overall behavior of UHPC cylinders in term of strength and ductility. However, the ductility enhancement was more significant. The confinement effect of steel spirals is rendered in the stress-strain curves where the more confined UHPC cylinders showed higher plastic deformations. The obtained confined stress-strain curves could be categorized into three different zones: linear-elastic, nonlinear hardening, and softening phases, whereas the plain UHPC specimens demonstrated only an almost linear behavior up to the peak strength followed by a sudden drop.

Peak strength and ductility of confined specimens, compared to the unconfined ones, were quantitatively investigated by two parameters: confinement effectiveness ratio and ultimate strain. For the most confined specimens, i.e. 0.25-in confined cylinders, the confinement effectiveness ratio and ultimate strain were determined to be 1.06 and 1.03%, respectively. The results presented herein can be further used to inform finite element models of confined UHPC components. However, to have more statistically significant conclusions, more cylinders and tests need to be conducted, which motivated another experimental program that is currently undergoing.

# Chapter 4. LARGE SCALE UHPC COLUMN TESTING

This chapter presents the experimental testing program used to investigate the behavior of UHPC columns subjected to combined axial and lateral loading. Four large-scale UHPC columns were tested under axial and quasi-static cyclic lateral loading at the Earthquake Engineering Laboratory at the University of Nevada, Reno. The experimental program presented herein is discussed in terms of: the specimens design and their construction stages; the properties of the materials used to construct the specimens; the test setup; the loading procedure used in the test; and the instrumentation plan used to investigate the behavior and quantify the column deformations and the rebars strains.

## 4.1. Specimens Design and Construction

The specimens' dimensions as shown in Figure 4-1 which was the same for all four columns. Although testing was mainly comparative, yet the dimensions of the scaled-columns could be considered a 1/5 scale of the normal strength concrete (NSC) column used in the California department of transportation Academy Bridge. The height and diameter of the UHPC columns were 58 in. and 10 in., respectively. The test matrix is shown in Table 4-1. The test matrix consists of two groups. The first group consists of an analytically investigated NSC column and an experimentally tested UHPC column reinforced with Grade 60 longitudinal reinforcement, this group was intended to mainly investigate the difference in the damage behavior and flexural capacity between the UHPC and NSC column. It is noted that the NSC column was not tested because the structural and seismic response of conventional columns can be accurately captured using current modeling and analytical methods. The second group consisted of three UHPC columns reinforced with Grade 100 high strength steel (HSS) longitudinal rebars of different longitudinal and transverse steel ratios. The variation within this group aimed to investigate the difference in behavior between the Grade 100 and Grade 60 reinforced UHPC columns and to investigate the effect of confinement effect and longitudinal steel ratio. The footing was designed to be capacity protected and consisted of two parts: an UHPC inner part connected to the UHPC column to ensure the continuity of UHPC in the plastic hinge region, and a NSC footing. The plan dimensions were 2×2 $ft^2$ for UHPC and external dimensions of 5×5 $ft^2$ for NSC and both parts were 14 in. deep as illustrated in Figure 4-1.

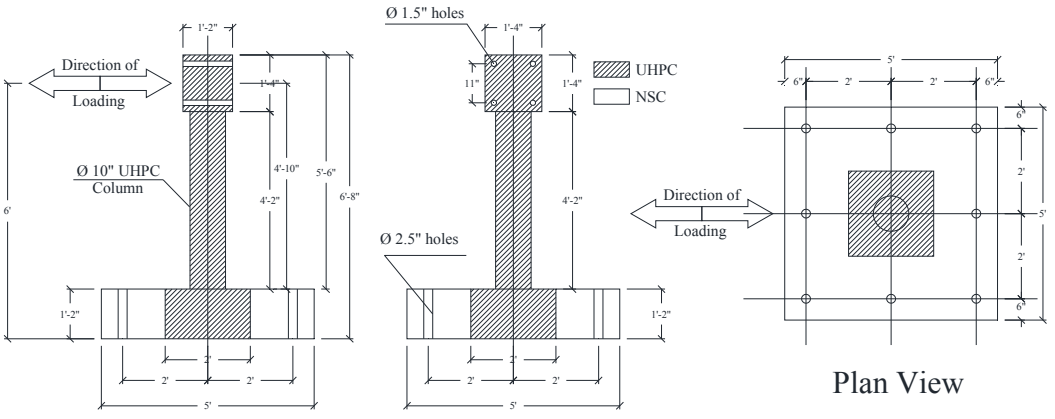


Figure 4-1 UHPC specimen dimensions.

The construction stages of the specimen consisted of the following: (1) casting the NSC outer part of the footing and roughening the inner surface of the footing as shown in Figure 4-2; (2) casting the UHPC inner part of the footing as shown in Figure 4-3; (3) casting of the UHPC column as shown in Figure 4-4 along with an UHPC column head (Figure 4-5). It is noted that the joint type between each two consecutive casting stages was a cold joint which means that each casting stage was done after the previous cast hardened.

Table 4-1 UHPC columns test matrix.

| Specimen | | Longitudinal Reinforcement | | Transverse Reinforcement | | Tested Variable | Type of Testing |
|---|---|---|---|---|---|---|---|
| | | # | $\%A_g$ | # | $\%A_g$ | | |
| Group I (Gr. 60) | S0 | 6#5 | 2.37% | #3@2in | 1.1% | NSC | Analytical |
| | S1 | 6#5 | 2.37% | #3@2in | 1.1% | UHPC vs NSC | Experimental |
| Group II (Gr. 100)* | S2 | 6#5 | 2.37% | #3@2in | 1.1% | Gr 100 vs Gr 60 | Experimental |
| | S3 | 6#5 | 2.37% | #3@4in | 0.55% | Low confinement | Experimental |
| | S4 | 6#4 | 1.53% | #3@2in | 1.1% | Low long. steel ratio | Experimental |

* Gr. 100 is for the longitudinal reinforcement only in Group II specimens.

Figure 4-2 Casting of NSC footing and roughening of the inner surface of the footing.

Figure 4-3 Casting of UHPC footing.

Figure 4-4 Casting of UHPC column.

Figure 4-5 Casting of UHPC column head.

## 4.2. Material Properties

In this section, the material characteristics of the UHPC, the reinforcing bars of grades 60 and 100 are presented and discussed with regards to the material preparation, sampling, and mechanical strength (compression for concrete materials, and tension for steel).

### *4.2.1. Ultra High Performance Concrete*

A commercial proprietary UHPC mix was used in this study, similar to the confinement study presented in Chapter 3, which is the Ductal® JS1000 mix design. Lafarge commonly delivers UHPC in three different parts: (1) a premix which is a proprietary blend of cement, silica sand, silica flour and silica fume (Figure 4-6a); (2) steel fibers (Figure 4-6b); (3) Superplasticizer (Figure 4-6c). The Ductal® mix components and mix ratios are given again here for convenience and shown in Tables 4-2 and 4-3, respectively. Steel fibers with 2% volume were used for all the mixes. The mechanical properties of the sued steel fibers are given in Table 4-4. The mixer used to mix the components of the UHPC is a high shear mixer type that is available at UNR: Imer 750 which has a capacity of 5.12 $ft^3$ (0.145 $m^3$) for single batch and is shown in Figure 4-7. For all mixes, the mixer was used only up to half of its capacity for each batch to ensure good quality of the mix.


Figure 4-6 Ductal® UHPC mixture components: (a) dry Ductal® premix; (b) steel fibers; and (c) superplasticizer.


Figure 4-7 UHPC high shear mixer at UNR (Imer 750).

Table 4-2 UHPC mixture by Ductal® (based on number of premix bags).

| Number of bags per batch | 5 | 6 | 7 | 8 | 9 |
|---|---|---|---|---|---|
| Premix (lb) | 250 | 300 | 350 | 400 | 450 |
| Water or ice (lb) | 14.37 | 17.24 | 20.12 | 22.99 | 25.86 |
| Superplasticizer (lb) | 3.43 | 4.11 | 4.80 | 5.48 | 6.17 |
| Steel fiber (lb) | 17.77 | 21.32 | 24.88 | 28.43 | 31.99 |
| Volume / Batch ($ft^3$) | 1.82 | 2.19 | 2.55 | 2.92 | 3.285 |

Table 4-3 UHPC mixture by Ductal®.

| | $kg/m^3$ | $lb/yd^3$ | Percentage by weight (%) |
|---|---|---|---|
| Premix | 2195 | 3700 | 87.6 |
| Superplasticizer (Premia 150) | 30 | 50.6 | 1.2 |
| Steel Fiber (2.0% volume) | 156 | 263 | 6.2 |
| Water (or ice) | 130 | 219.1 | 5 |

Table 4-4 Typical mechanical properties of steel fibers used for Ductal®.

| | SI units | US units |
|---|---|---|
| Tensile Strength | 399 MPa | 3750 ksi |
| Length | 13 mm | 0.5 in |
| Diameter | 0.2 mm | 0.008 in |

During UHPC mixing, to control the temperature of the UHPC mixture given that mixing took place in Reno in the summer with temperatures greater than 20°C, ice was added as a part of the water weight. When the daytime temperatures exceeded 25°C (77°F), 100% ice substitution of water was used to increase the working time of the mix. The mixing procedure as demonstrated in Figure 4-8 consists of 3 stages: (1) the premix is added to the mixer and left for about 1 minute mixing; (2) the liquid including the superplasticizer and the water or the substituted ice is added to the premix and mixing continues for almost 12-15 minutes until the UHPC paste is formed; (3) the steel fibers are added gradually to the mix and mixing continues for 3-5 minutes until they become well distributed inside the UHPC paste.

For the test specimens, every UHPC footing used two batches while each column used only one batch. It is worth noting that the UHPC was poured for each member from the same place to prevent the formation of a cold joint between two separate flows, and no vibrators were used to prevent any fiber segregation of the mix. During the casting of two UHPC batches, if the UHPC of the first batch started to form a crust on the surface, a wooden piece was used to break this crust before casting the second batch to ensure continuity between the pours and allow for the fibers to bridge between the two casts, which is important to prevent any cold joints inside the member.

For each UHPC batch static and dynamic slump (flow characteristics) were measured to check values are within the allowable ranges. A flow table and brass cone, as shown in Figure 4-9, that satisfies (ASTM C 230) are used for these tests. The actual dynamic slump tests for most

of the batches were in the range of 8.5 ins to 9 ins, noting that the allowable slump must be in the range of 7 ins to 10 ins (180 mm to 250 mm) after 20 shocks on the impact flow table.

Figure 4-8 UHPC mixing procedure.

Figure 4-9 UHPC slump testing.

For compressive strength evaluation, 3x6 in cylinder samples were taken from each batch and were tested at 14 days and at the column test day. Similar to the confinement study, The surface of the UHPC cylinders was prepared by making a rough cut by a saw machine to remove the weak surface crust formed on the top of the cylinder then grinding the surface to get smooth flat surfaces at the two ends for accurate strength evaluation (see Figure 4-10 for illustration of the process). A summary of the measured compressive strength of the materials is presented in Table 4-5. The reported material strengths are the average of a minimum of three cylinders tested for every material at each stage of construction. For compression testing, a force-controlled universal testing machine with capacity of 500 kips was used and the applied loading rate was in the range of 10-15 kip/min (25 psi/sec). The test setup for compression tests is shown in Figure

4-11 and a sample of the tested cylinders, where the damage can be illustrated, is shown in Figure 4-12.

Figure 4-10 UHPC cylinders preparation.


Figure 4-11 UHPC compression test setup.

Figure 4-12 UHPC cylinder damage and mode of failure under compression tests.

Table 4-5 UHPC compressive strength for large-scale test specimens.

| Specimen | Element | Measured at | Strength (ksi) |
|---|---|---|---|
| S1 | Inner Footing | 14 days | 25.18 |
| | | Test day | 31.38 |
| | Column | 14 days | 24.62 |
| | | Test day | 29.64 |
| S2 | Inner Footing | 14 days | 26.94 |
| | | Test day | 32.99 |
| | Column | 14 days | 25.62 |
| | | Test day | 31.17 |
| S3 | Inner Footing | 14 days | 15.15 |
| | | Test day | 17.54 |
| | Column | 14 days | 28.06 |
| | | Test day | 33.28 |
| S4 | Inner Footing | 14 days | 22.91 |
| | | Test day | 27.18 |
| | Column | 14 days | 29.44 |
| | | Test day | 30.95 |

### *4.2.2. Reinforcing steel*

The Grade 60 longitudinal steel reinforcement used in this study was conforming to the ASTM A706 Grade 60 specifications (ASTM 2009) and #5 rebars were used. The measured yield and ultimate tensile strength of the longitudinal reinforcing steel bars were 70.4 ksi and 101.2 ksi, respectively. The yielding strain was 0.23% and the ultimate elongation was 19%.

The HSS longitudinal steel reinforcement used was nominally Grade 100 rebars, MMFX rebars conforming to ASTM A1035 Grade 100 specifications. The MMFX HSS used included both #4 and #5 rebars and is shown in Figure 4-13. To know the actual tensile properties of the rebars, direct tension tests were made using displacement-controlled testing machines. The tested rebar samples were 17 samples of #4 rebars and 6 samples of #5 rebars representing all received batches of the rebars. The samples were tested using an Instron universal testing machine and an MTS machine for the #4 and #5 rebars, respectively. The Instron machine capacity is 56 kips (250 kN) and stroke of 0.3 in/min, wich was not sufficient to test the #5 HSS rebars. Thus, the MTS machine with a capacity of 250 kips (1,100 kN) and stroke of 0.3 in/min was used. For direct tension tests, displacements were recorded using laser and conventional extensometer as shown in Figures 4-14 and 4-15 for #4 and #5 testing, respectively. A summary of the test results is shown in Table 4-6 and the average stress-strain curves for #4 and #5 rebars are shown in Figures 4-16 and 4-17, respectively.

Figure 4-13 High strength steel rebars (#4 and #5).


Figure 4-14 Direct tension tests on #4 rebars samples.

Figure 4-15 Direct tension tests on #5 rebars samples.

Table 4-6 Mechanical properties of HSS tested coupons.

| Diameter bar | Yield Strength (ksi) | Ultimate Strength (ksi) | Young's Modulus (ksi) | Ultimate Strain (%) |
|---|---|---|---|---|
| #4 | 124 | 167.25 | 26,000 | 12.6 |
| #5 | 128 | 162 | 26,000 | 15.4 |

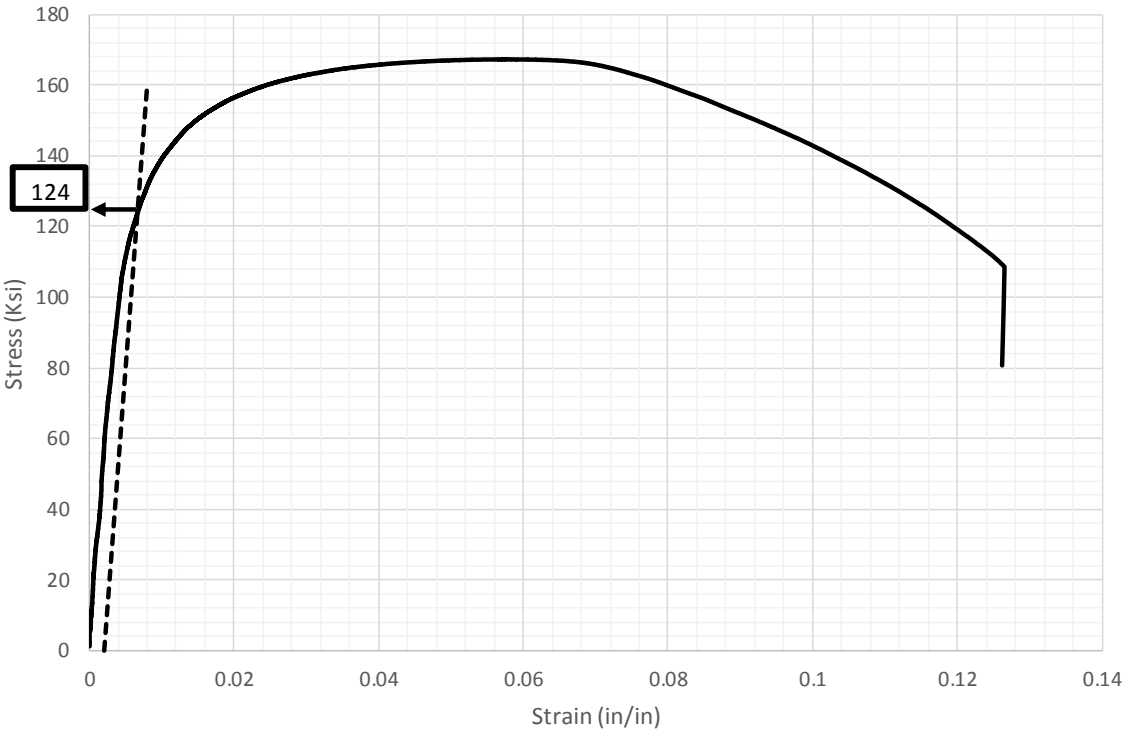


Figure 4-16 Tensile stress-strain curve of #4 HSS rebars.

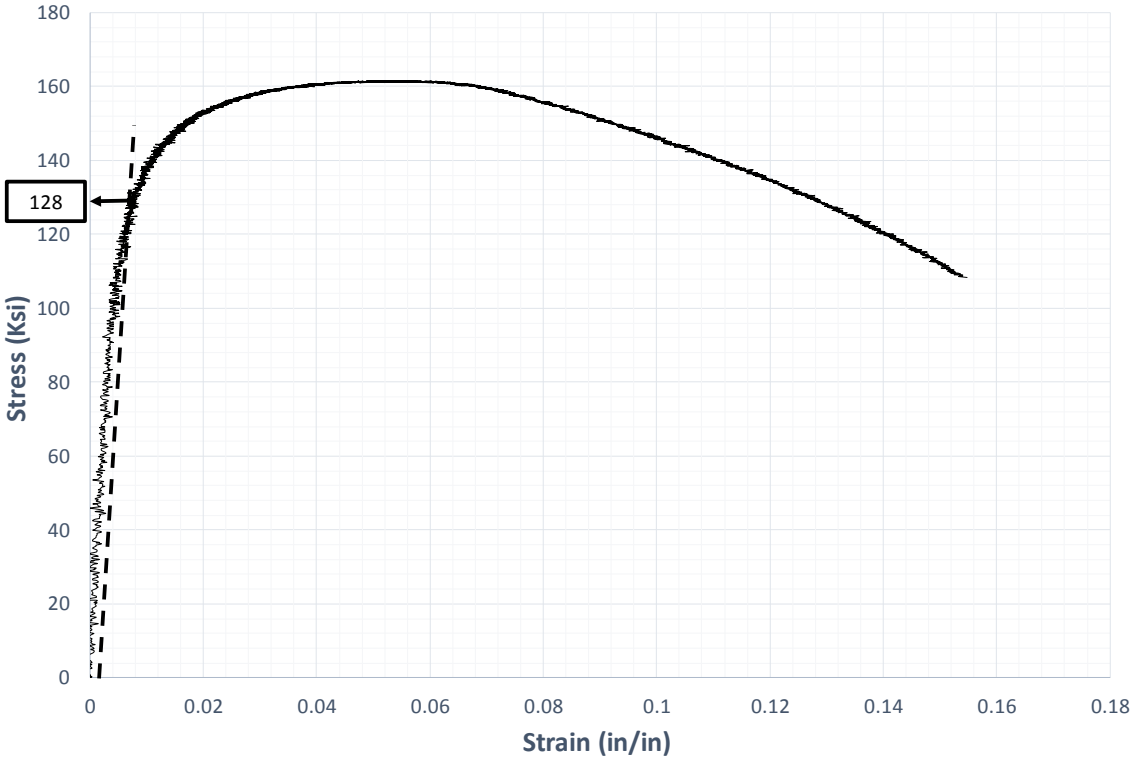


Figure 4-17 Tensile stress-strain curve of #5 HSS rebars.

## 4.3. Test Setup and Loading Protocol

The columns were tested in a cantilever configuration setup as shown in Figure 4-18. Assuming an average column concrete strength of 30 ksi, the axial load index, which is the ratio of the axial load to the product of column gross section area and the specified compressive strength of the concrete column, was kept constant at 5% during the test. The axial load was applied to the top of the column through two center-hole rams placed on a load spreader beam perpendicular to the lateral load direction to apply approximately 120-kip axial load to the column. The cyclic loading was applied through a servo-hydraulic actuator with displacement-controlled loading. The selected loading protocol was adopted from FEMA 461 (FEMA 2007) where every applied cycle is a ratio of the column displacement at which the longitudinal reinforcing bars yield as shown in Figure 4-19. The loading also applied two main full cycles for each drift ratio, as summarized in Table 4-7, and after reaching the yield displacement, a small cycle with half the yield displacement was applied after each two complete main cycles to capture the stiffness degradation with increasing the drift ratio. Two displacement rates of 0.25 mm/sec (0.01 in./sec) and 1.27 mm/sec (0.05 in/sec) were used, with the former used for drift ratios up to 3% and the latter used for larger drift ratios.

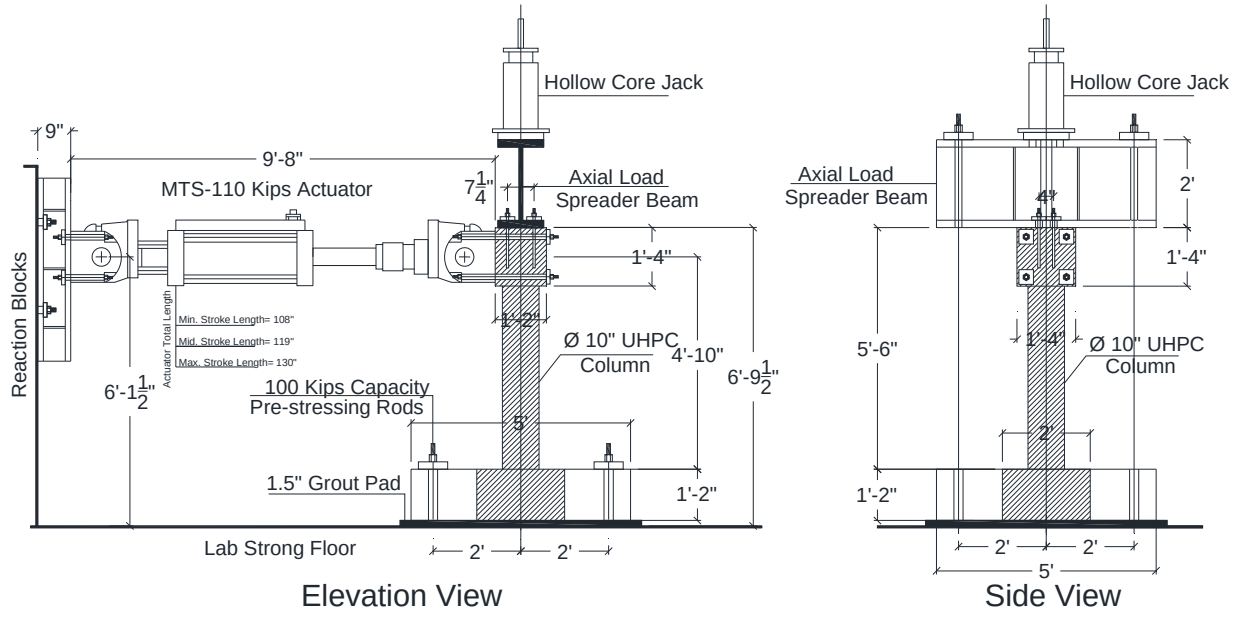


Figure 4-18 Test Setup for UHPC column under combined axial and bending at UNR.

## 4.4. Instrumentation Plan

As shown in Figure 4-20, the specimen was instrumented with 21 reinforcement strain gages to capture the longitudinal and transverse bars strains in the column plastic hinge region. The strain gages were named according to their position and their height level. Five levels of strain gauges were assigned to the strain gages labels. Three string pots were attached to the column head to capture the column top displacement. Ten displacement Transducers were attached to the column plastic hinge region as shown in Figure 4-20 to capture the column curvature at the different drift ratios.

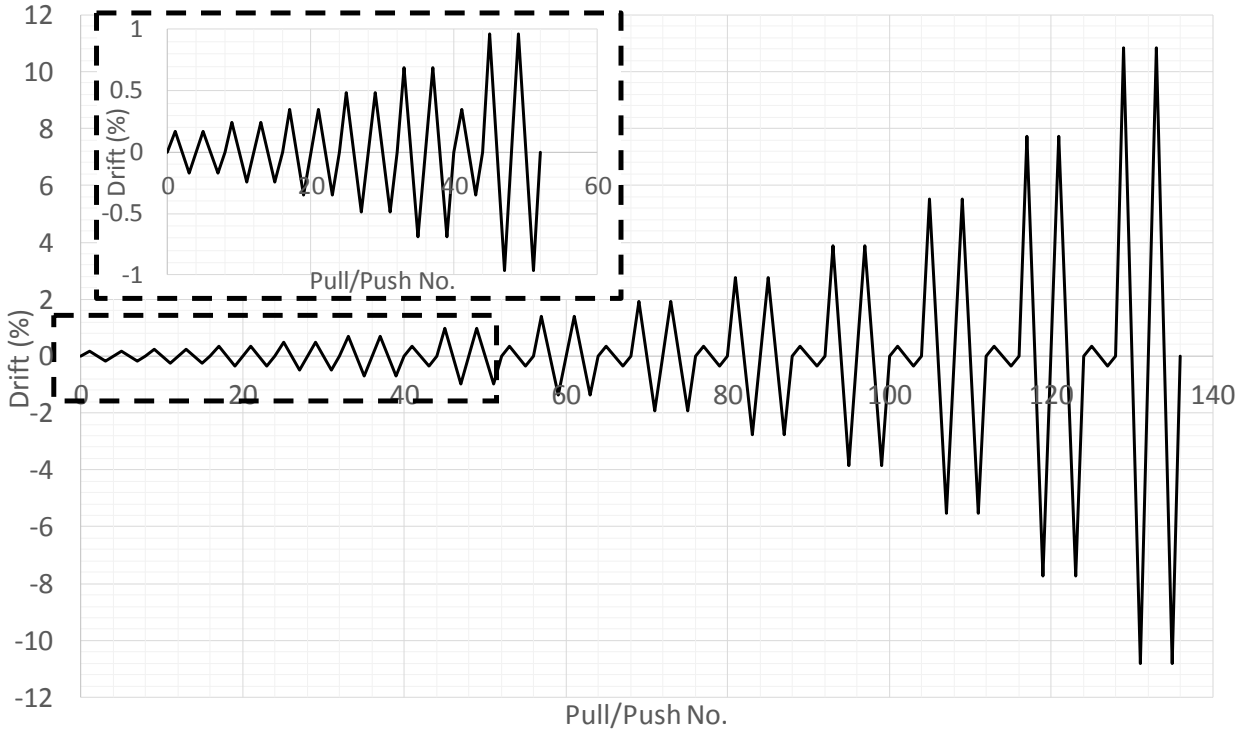


Figure 4-19 Cyclic loading protocol for lateral loading of UHPC columns.

Table 4-7 Specifications of the cyclic loading protocol used for lateral loading of UHPC columns

| Run # | % of Yield Displacement | Displacement (in) | Drift (%) | Displacement Rate |
|---|---|---|---|---|
| 1 | 25 | 0.1 | 0.17 | 0.01 in/sec |
| 2 | 35 | 0.14 | 0.24 | |
| 3 | 50 | 0.2 | 0.34 | |
| 4 | 70 | 0.28 | 0.48 | |
| 5 | 100 | 0.4 | 0.69 | |
| 6 | 140 | 0.56 | 0.97 | |
| 7 | 200 | 0.8 | 1.38 | |
| 8 | 280 | 1.12 | 1.93 | |
| 9 | 400 | 1.6 | 2.76 | |
| 10 | 560 | 2.24 | 3.86 | 0.05 in/sec |
| 11 | 800 | 3.2 | 5.52 | |
| 12 | 1,120 | 4.48 | 7.72 | |
| 13 | 1,570 | 6.28 | 10.83 | |

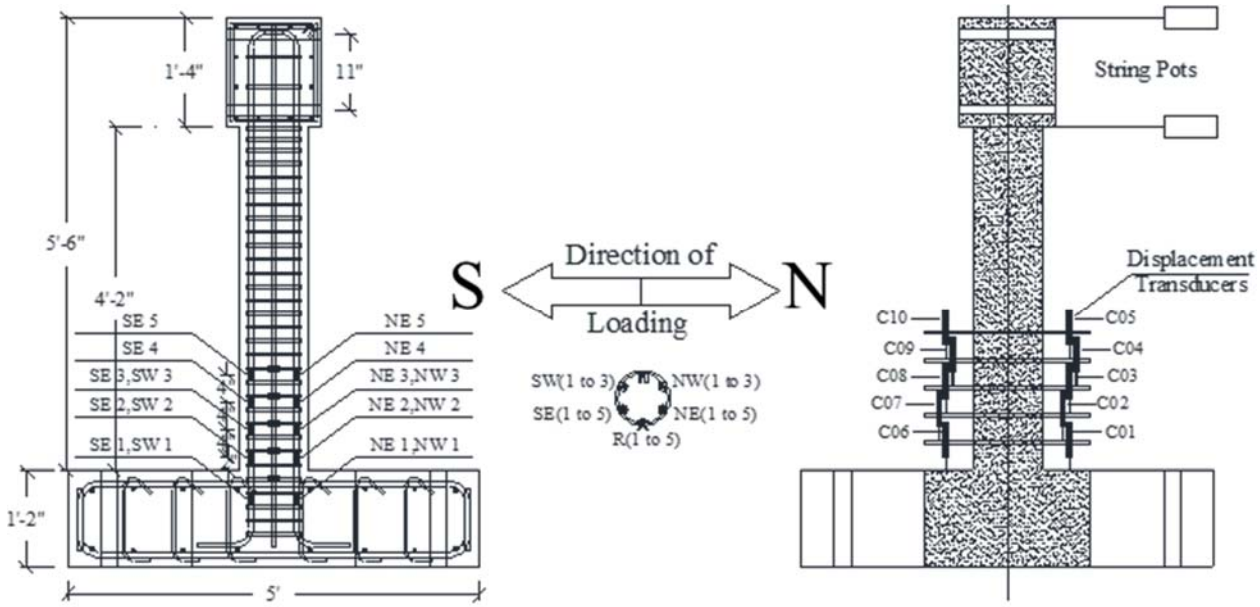


Figure 4-20 Schematic of different instrumentation types and layout as sued for UHPC columns tests under combined axial and lateral cyclic loading.

# Chapter 5. TEST RESULTS AND DISCUSSION OF GROUP I SPECIMENS

This chapter presents the experimental test results of specimen S1 of Group I with respect to the global and the local behavior perspectives. The chapter also provides a comparison of the UHPC specimen S1 with a hypothetical NSC specimen (S0) to show the effect of using UHPC instead of NSC on the column strength. The response of the NSC column S0 was determined using analytical methods as explained in this chapter.

## 5.1. Column Global Behavior

### *5.1.1. Plastic Hinge Damage and Mode of Failure*

The observed mode of failure for the UHPC column (S1) was the fracture of reinforcing bars without any spalling of UHPC. However, crushing of UHPC in compression was observed as well. The test was stopped after the rupture of the four outer-most rebars in the north and south directions of the column and before the rupture of the two middle rebars for test setup stability purposes. Figure 5-1 shows an overview of the deformed column during the test under the maximum applied drift.

Figure 5-1 Overview of Column Model Under Maximum Drift.

The first bar ruptured at the second cycle of almost 8% drift ratio while the other three bars ruptured at almost 11% drift ratio cycles. There was no evidence of rebar buckling. Furthermore, no concrete spalling or reinforcement exposure was observed until the end of the test. No cracks were observed until reaching 1% drift ratio. The onset of UHPC crushing in compression was observed at 2.76% drift ratio and the first significant crack started to appear at a level of 2 in above the footing at 4% drift ratio with 0.03 in crack width. A wide crack appeared at the column-footing interface at drift ratio 8% with almost 0.1 in crack width. Figures

5-2 through 5-10 show the progression of the damage at the plastic hinge region of the column at selected different drift ratios. It should be noted that the cracks were marked on the south direction for the odd numbers of the run when the column was in the push direction (tension side is at south direction), while the cracks were marked on the north direction for the even numbers of the runs when the column was in the pull direction (tension side is at the north direction). It is also worth noting that the cracks were marked at the peaks of the second cycle of each run number.


**(a) South-East Face** **(b) South-West Face**

**(c) North-East Face** **(d) North-West Face**

Figure 5-2 Damage Observed at Second Cycle of 0.69% Drift, (Specimen S1).

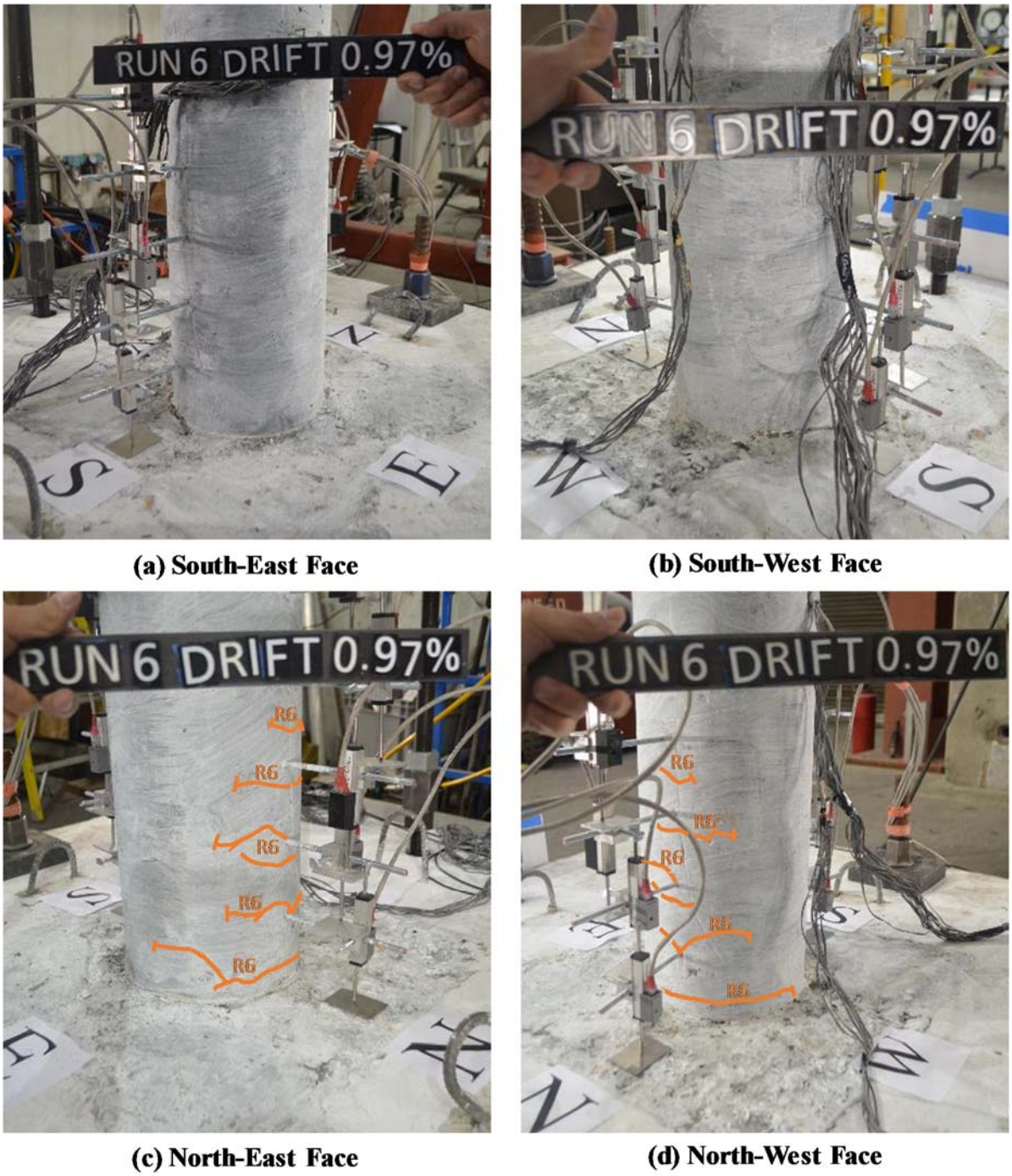


Figure 5-3 Damage Observed at Second Cycle of 0.97% Drift, (Specimen S1).

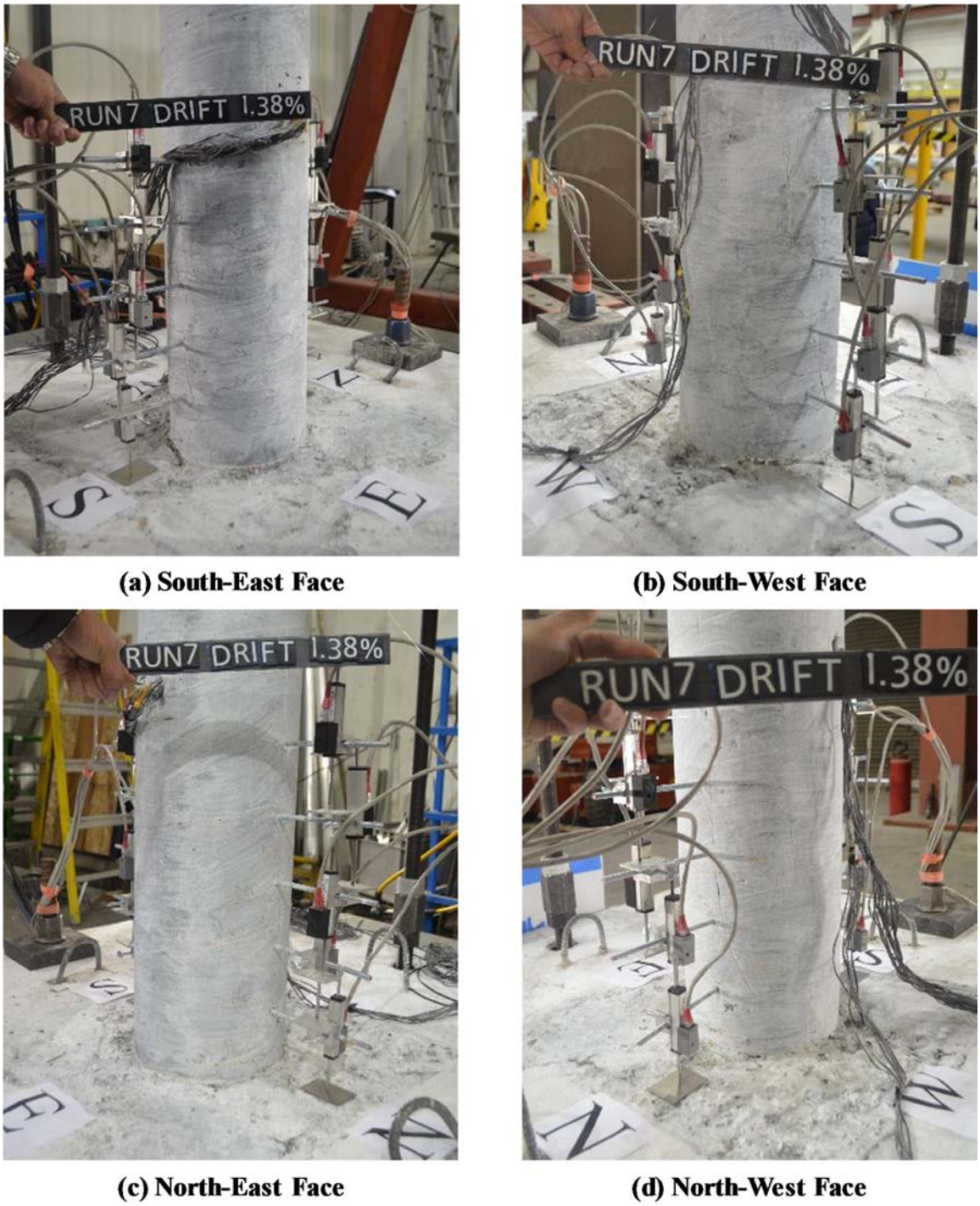


**(a) South-East Face** **(b) South-West Face**

**(c) North-East Face** **(d) North-West Face**

Figure 5-4 Damage Observed at Second Cycle of 1.38% Drift, (Specimen S1).


(a) South-East Face


(b) South-West Face


(c) North-East Face


(d) North-West Face

Figure 5-5 Damage Observed at Second Cycle of 1.93% Drift, (Specimen S1).

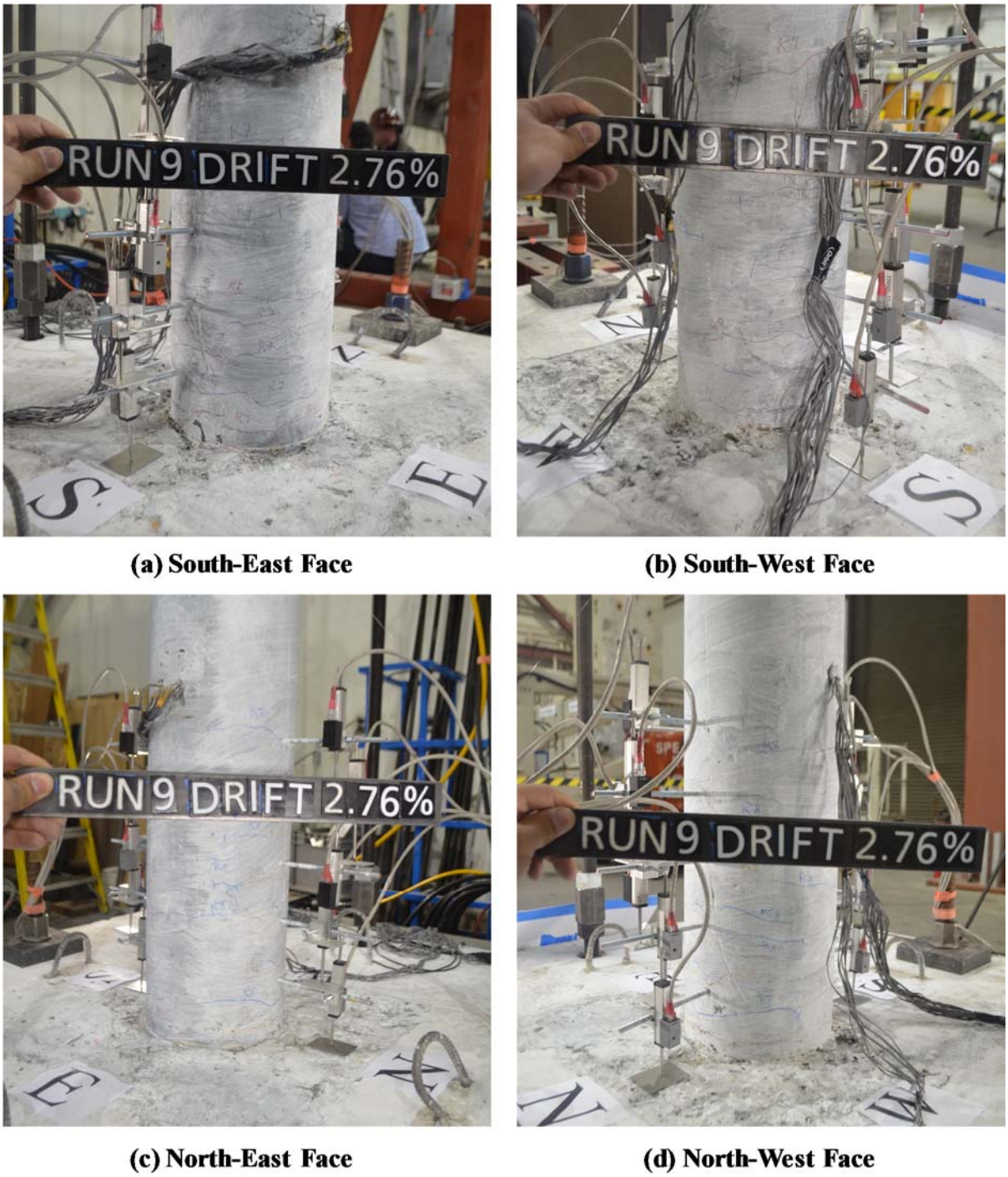


**(a) South-East Face** **(b) South-West Face**

**(c) North-East Face** **(d) North-West Face**

Figure 5-6 Damage Observed at Second Cycle of 2.76% Drift, (Specimen S1).

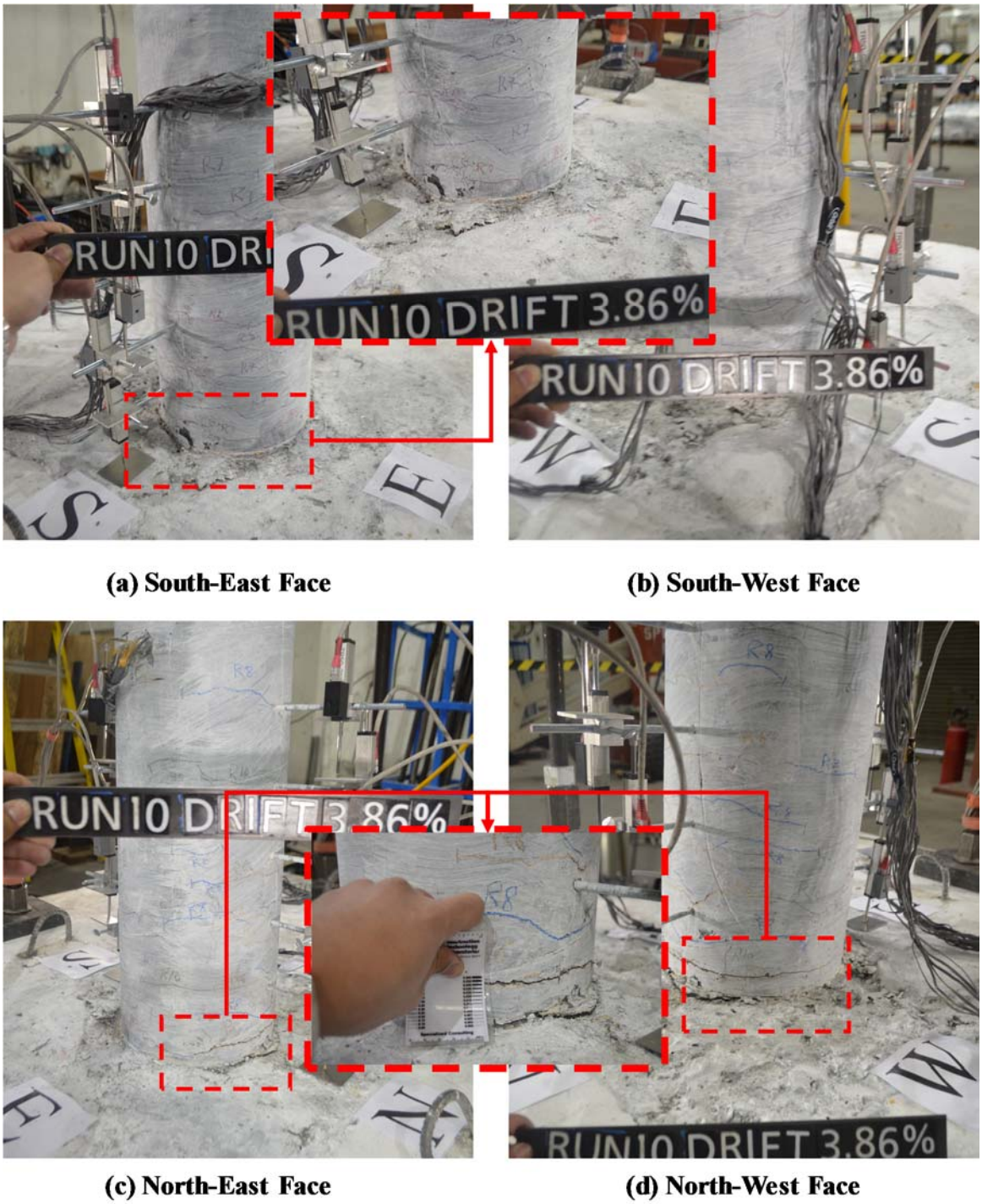


(a) South-East Face (b) South-West Face

(c) North-East Face (d) North-West Face

Figure 5-7 Damage Observed at Second Cycle of 3.86% Drift, (Specimen S1).

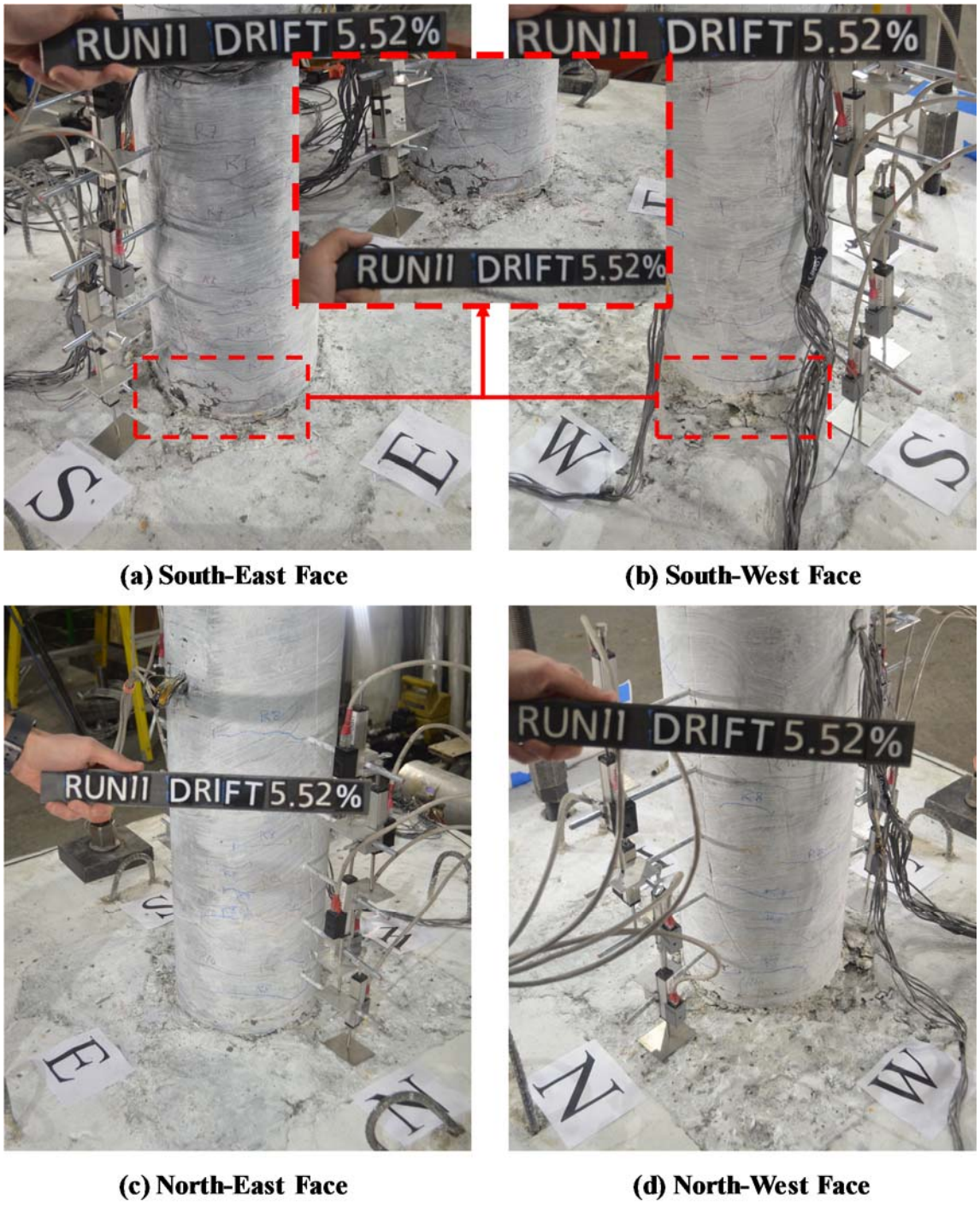


(a) South-East Face (b) South-West Face

(c) North-East Face (d) North-West Face

Figure 5-8 Damage Observed at Second Cycle of 5.52% Drift, (Specimen S1).

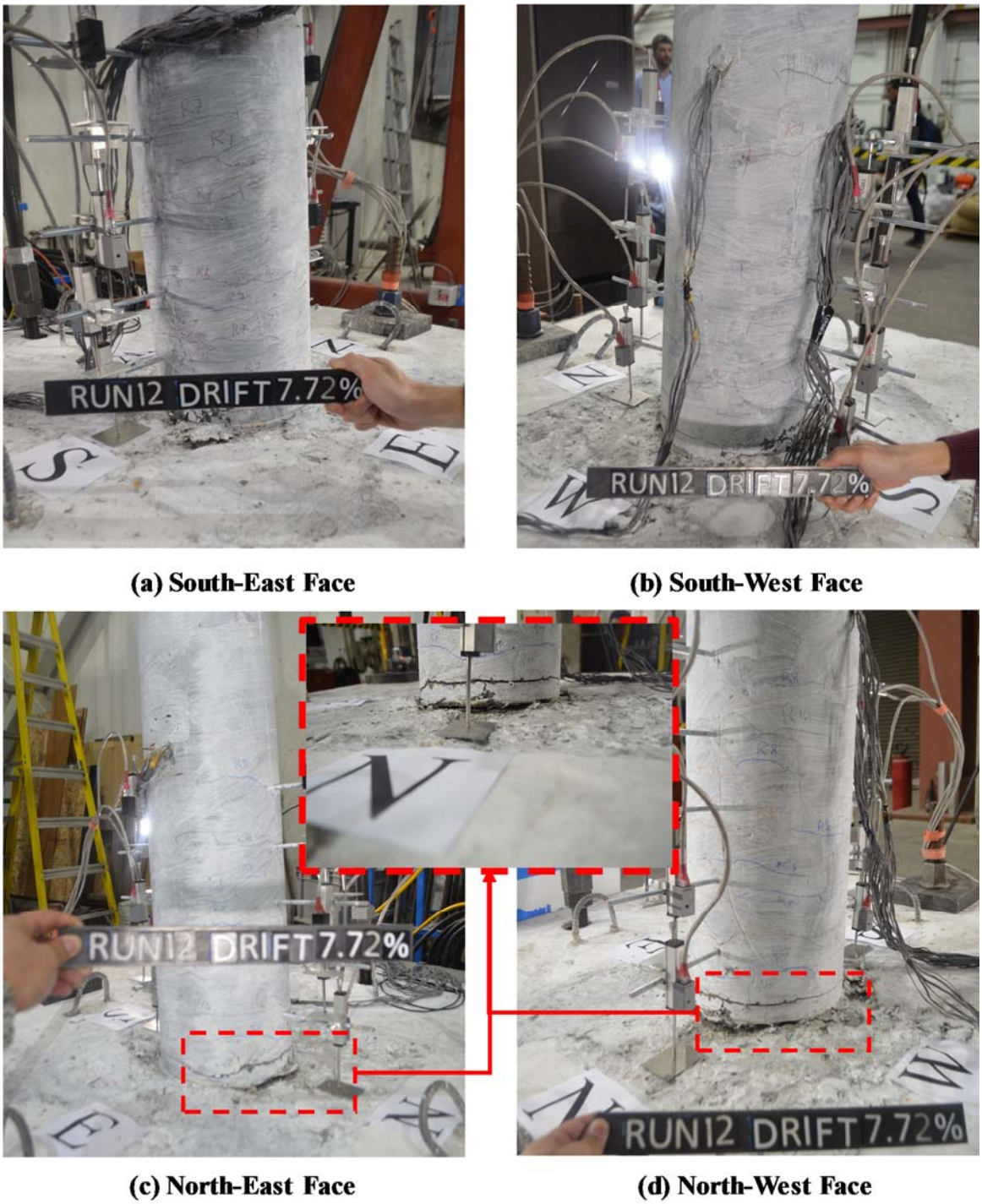


(a) South-East Face (b) South-West Face

(c) North-East Face (d) North-West Face

Figure 5-9 Damage Observed at Second Cycle of 7.72% Drift, (Specimen S1).

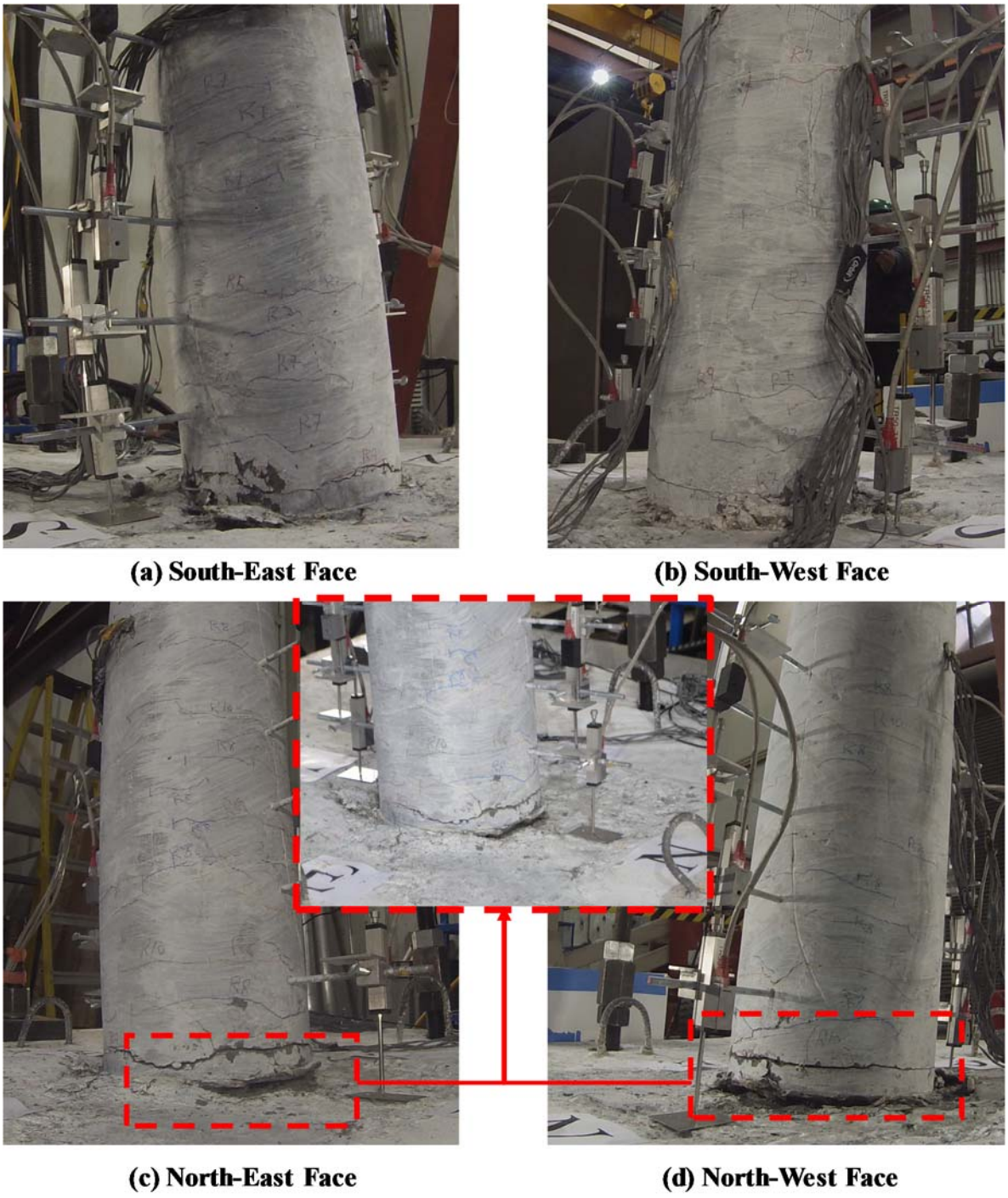


Figure 5-10 Damage Observed at Second Cycle of 10.83% Drift, (Specimen S1).

### *5.1.2. Force-Drift Relationship*

The hysteretic behavior of the UHPC column as shown from the global force-drift relationship is presented in Figure 5-11. The positive values on the plot indicate pushing the column towards north direction. The force shown in this plot was recorded directly from the load cell used for the MTS actuator used to apply the lateral displacement to the column. The column displacement was calculated by taking the average of the data from three string potentiometers attached to the

column head which represent the actual column displacements. The asymmetric response observed in the figure was a result of reinforcement misalignment during construction. Figure 5-12 shows the distorted pattern of the six longitudinal rebars which was discovered after the test when the column was fully separated from the footing and the actual cross-section was inspected. From Figure 5-11, it is shown that the peak strength was reached and maintained at drift ratios 5.5% and 7.7% for the pull and push directions, respectively. The maximum reported lateral loads were 16.1 kips and 22 kips for the push and pull directions, respectively.

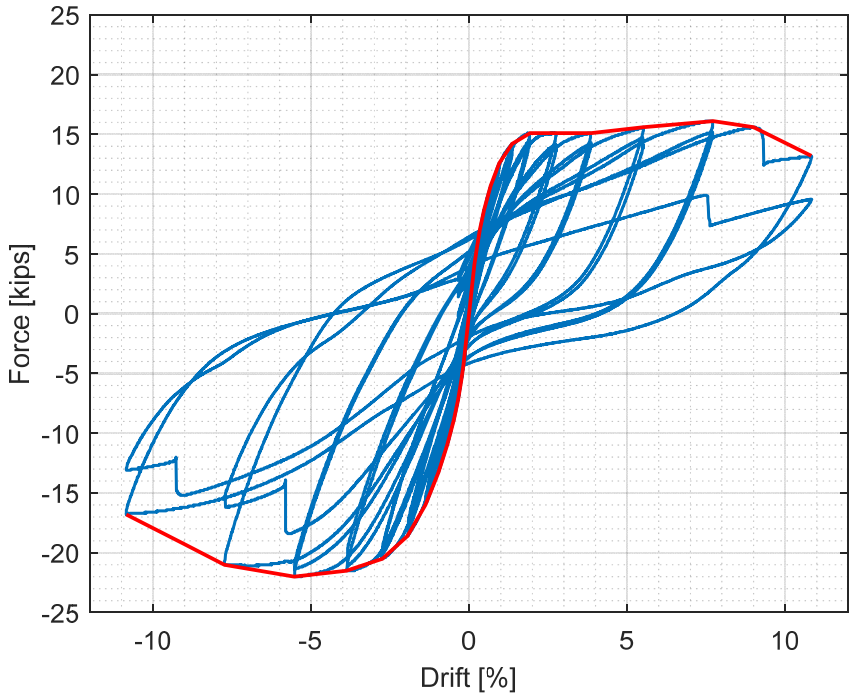


Figure 5-11 Global force-drift relationship for specimen S1.

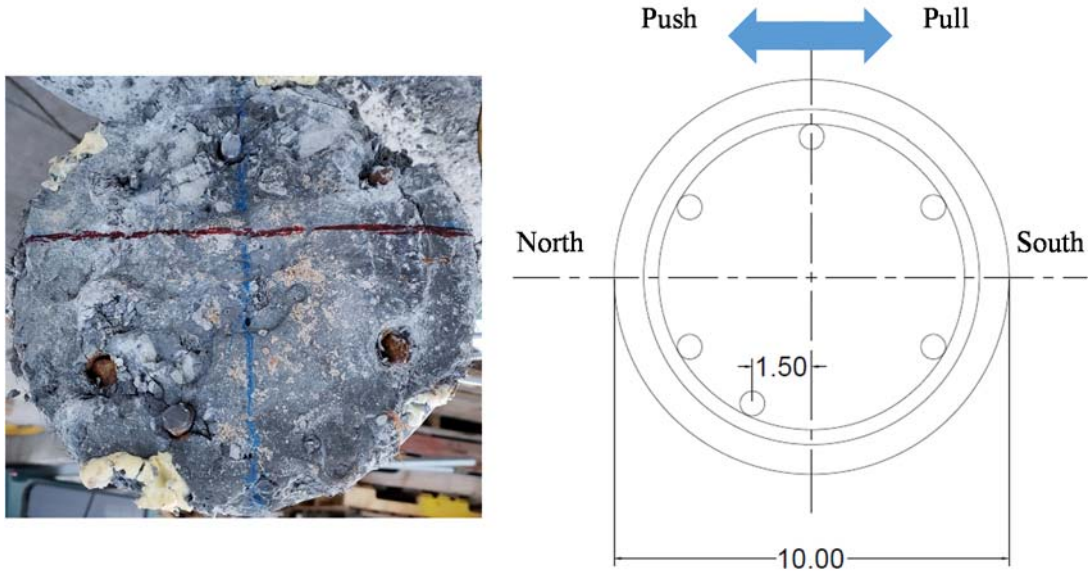


Figure 5-12 The as-built S1 UHPC column cross-section (full column was separated from the footing after testing).

The first bar yielding was observed on the south-east rebar at drift ratios of 0.92% at the first cycle of the 0.97% drift ratio run which can be observed from Figure 5-13 that gives the strain history of the rebars at level 2 above the footing level (see Figure 4-20 in previous section for instrumentation level). The first bar ruptured was observed on the north-west rebar at drift ratio of 7.7% at the second cycle of the 7.72% drift ratio run which can be implied from the sudden drop of the strain at level 3, at 6-in above the footing level, as shown in Figure 5-14 and the sudden drop of the measured force in the force history relation showed in Figure 5-15.

The measured displacement ductility was almost 8.4 which meets and exceed the AASHTO (2014) requirements for maximum displacement ductility demand of 5. It is also seen from Figure 5-11 that the column has more than 65% reserved displacement capacity, which allows UHPC columns to be used in high seismic regions. The envelopes of the hysteresis curves in the positive and negative displacement regions and their idealized elasto-plastic idealization are shown in Figure 5-16. The plastic segment was obtained by preservation of energy, i.e. maintaining the same areas under the envelope and the idealized curve. The recorded drift history with the projected first bar yielding and the rebar rupture sequence are shown in Figure 5-17.

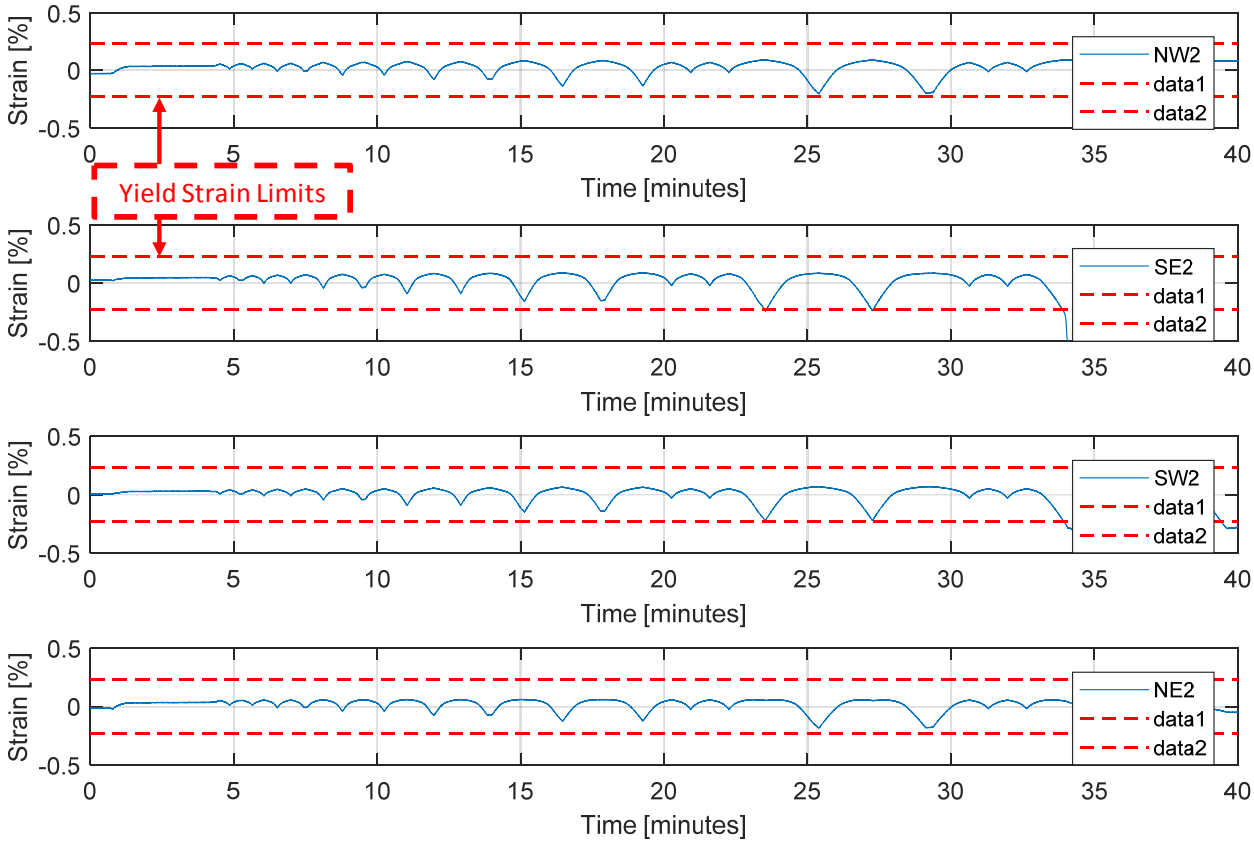


Figure 5-13 Rebars Strain History at Level 2 to Imply Yielding, (Specimen S1).

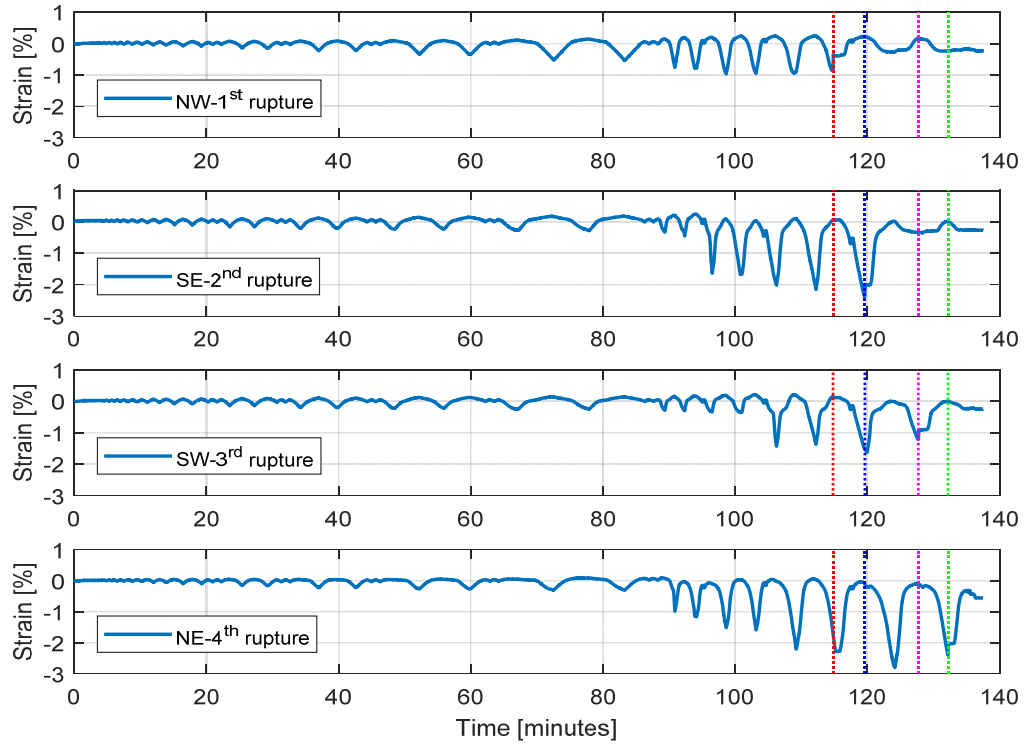


Figure 5-14 Rebars strain history at level 3 to imply bar rupture for UHPC specimen S1.

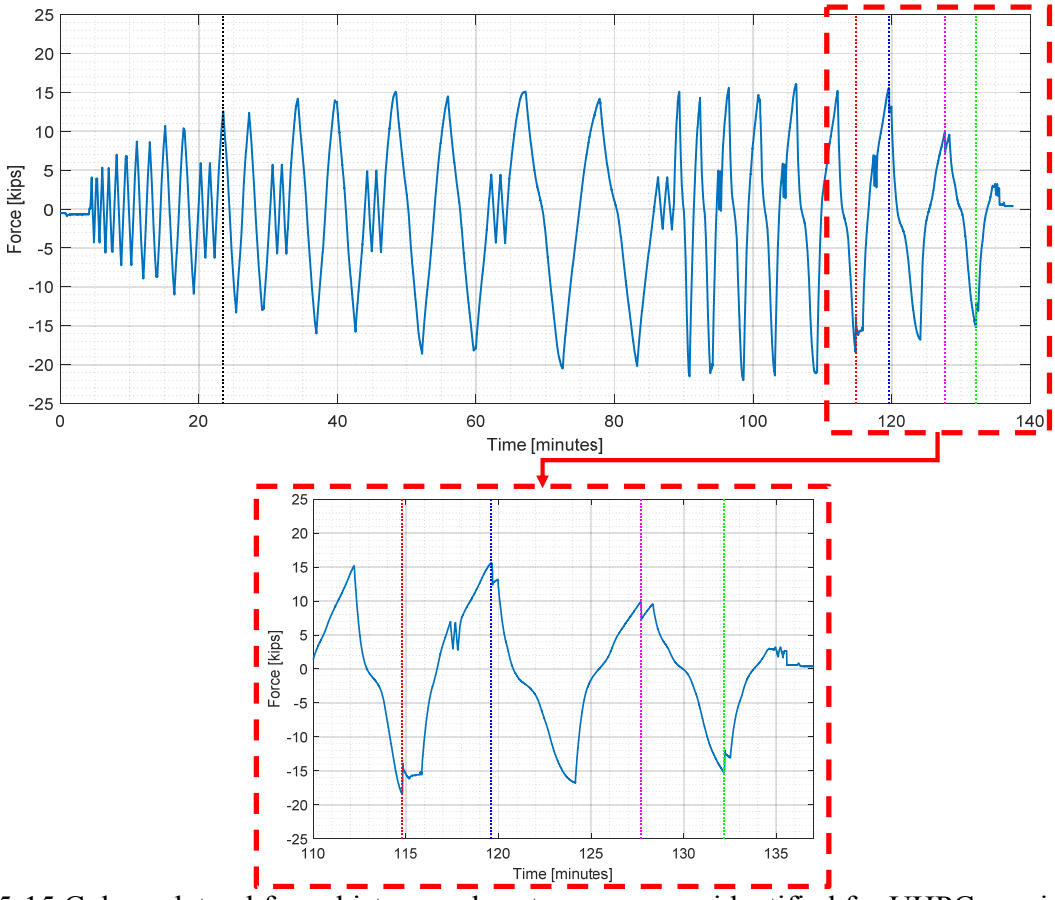


Figure 5-15 Column lateral force history and rupture sequence identified for UHPC specimen S1.

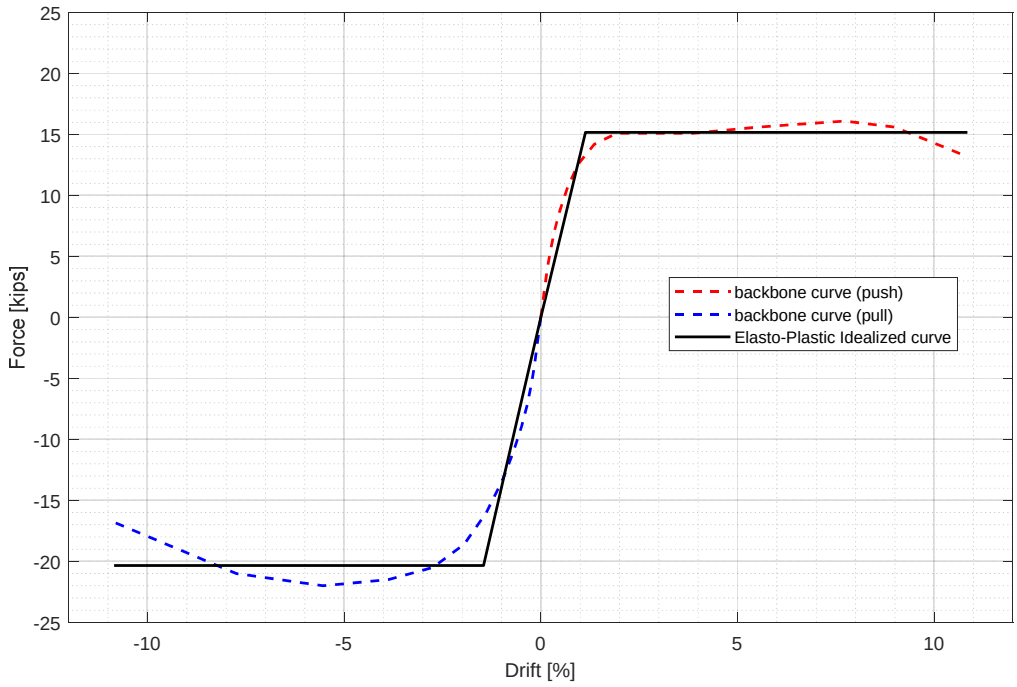


Figure 5-16 Envelope of force-drift relationship and elasto-plastic idealization for specimen S1.

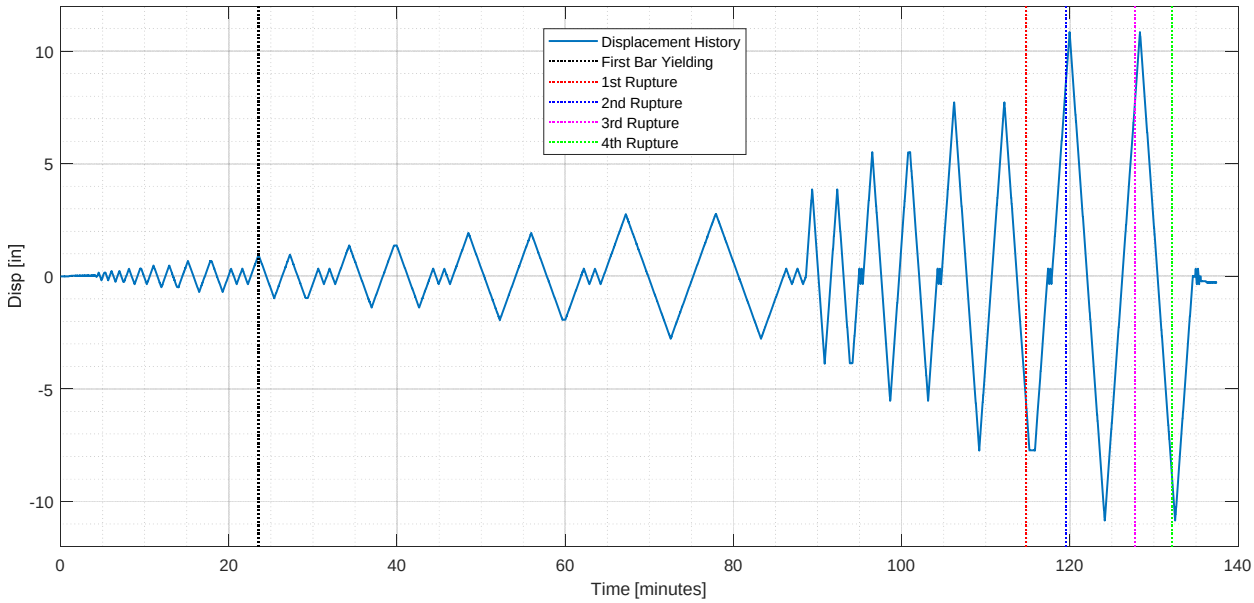


Figure 5-17 Recorded drift history with rupture sequence identified for specimen S1.

### *5.1.3. Stiffness Degradation*

The stiffness degradation of the UHPC column was investigated at different drift ratios. As shown in Figure 5-18, the column exhibited good stiffness degradation behavior. It was observed that the column lost 50% of its initial stiffness after reaching 2% drift ratio. It is also noted that the column initial stiffness was 7.35 kN/mm (42 kips/in.) which corresponds to an initial stiffness of almost 0.7 $E_cI_g$ after the first run based on the UHPC modulus of elasticity recommended by Graybeal (2007) which is equal to 1,460 times the square root of $f'_c$ in ksi.

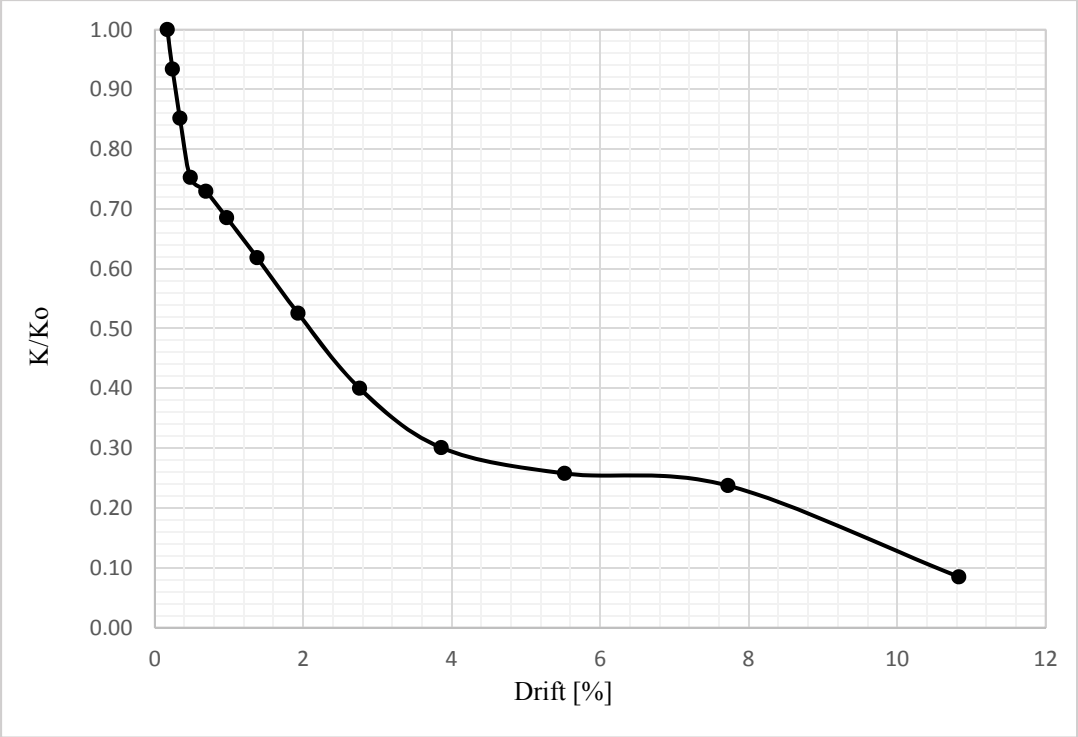


Figure 5-18 Stiffness degradation of UHPC specimen S1 as related to drift ratio.

## 5.2. Column Local Behavior

### *5.2.1. Strains*

The longitudinal reinforcement strain profiles at the plastic hinge region are shown in Figure 5-19. The strains values reported in the figure are the maximum absolute strains of the two complete cycles at each drift ratio. A sample of the strain gage profiles is reported and shown at 0.97, 1.93 and 3.86% drift ratios. It can be seen that the reinforcing bar strains were well distributed in the plastic hinge region of the column-footing interface. The Transverse reinforcement strain profiles at the plastic hinge region is shown in Figure 5-20. A sample of the strain gage profiles is reported and shown at 0.97, 1.93, 3.86, 5.52, 7.72 and 10.83% drift ratios. It is noted that the strain gauge at level 1 (2 in below footing level) have stopped working after the 3.86% drift run. It is observed that none of the stirrups yielded and the recorded strains were very small which didn't exceed 0.1% strain and this returns to the fact that no cover spalling happened to the column at the plastic hinge region and the UHPC itself provides a good confinement without engaging the stirrups.

### *5.2.2. Curvature Profiles*

The curvature profiles at the plastic hinge region reported at different drift levels are shown in Figures 5-21 and 5-22. Curvatures were measured indirectly by using displacement transducers mounted on both loading sides of the columns as illustrated before in Figure 5-20. Curvatures at each level were computed as the ratio of the section rotations of that level to the vertical distance of the transducers, where in turn, the rotations were the ratio of the summation of the relative displacements to the horizontal distance between the transducers in the same level. The curvature

was measured at five levels. The curvature of the column at the base was the highest mainly because of yield penetration at the column-footing interface.

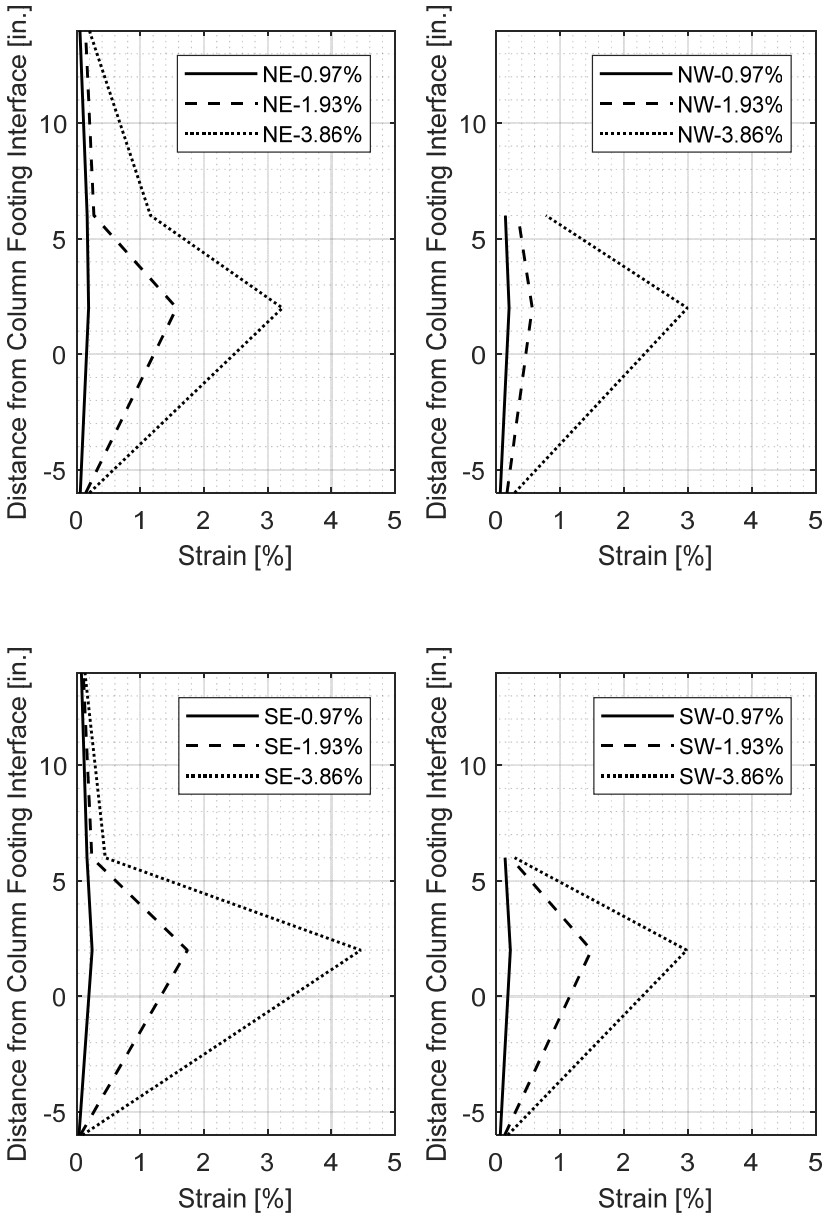


Figure 5-19 Distribution of the longitudinal rebars strains within plastic hinge region for UHPC specimen S1.

### *5.2.3. Moment-Curvature Behavior*

The moment curvature hysteretic curve relationship is obtained and shown in Figure 5-23. The maximum moment capacities in the push and pull loading sides are 933 kip-in and 1,276 kip-in, respectively. The moment curvature backbone curves and the idealized elasto-plastic curves are shown in Figure 5-24. The curvature ductility is determined to be equal to 15.4, which is comparable to typical ductile NSC columns.

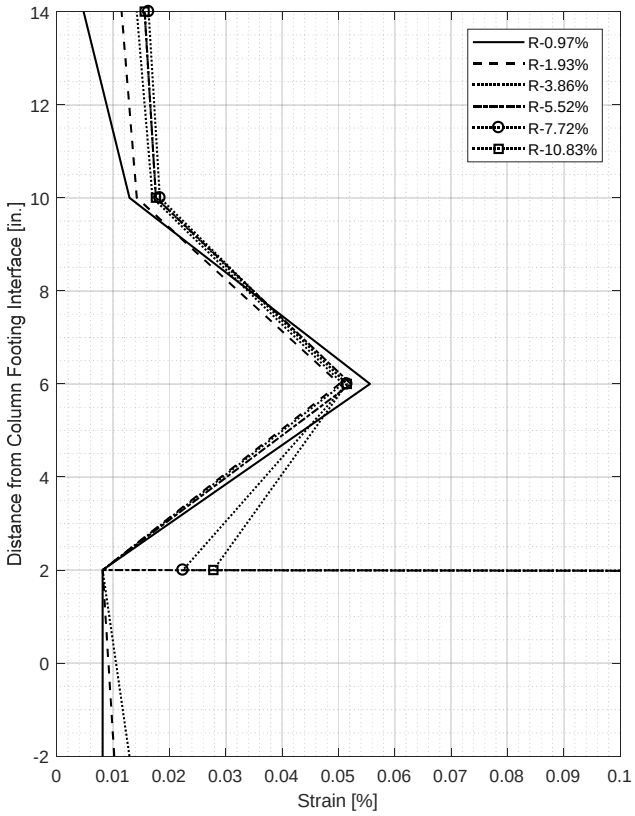


Figure 5-20 Distribution of the transverse rebars strains within plastic hinge region for S1.

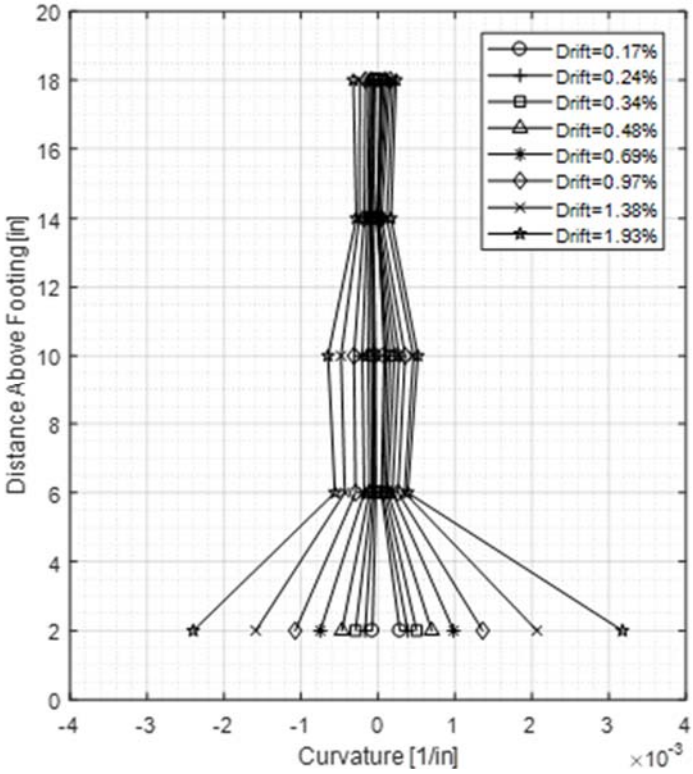


Figure 5-21 Plastic hinge curvatures for lower drift levels from S1 tests.

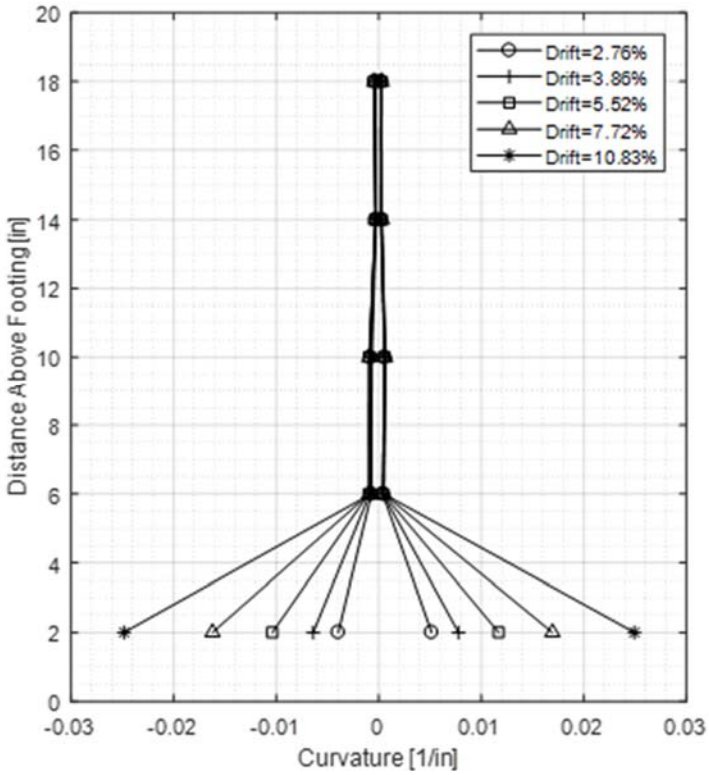


Figure 5-22 Plastic hinge curvatures for higher drift levels from S1 tests.

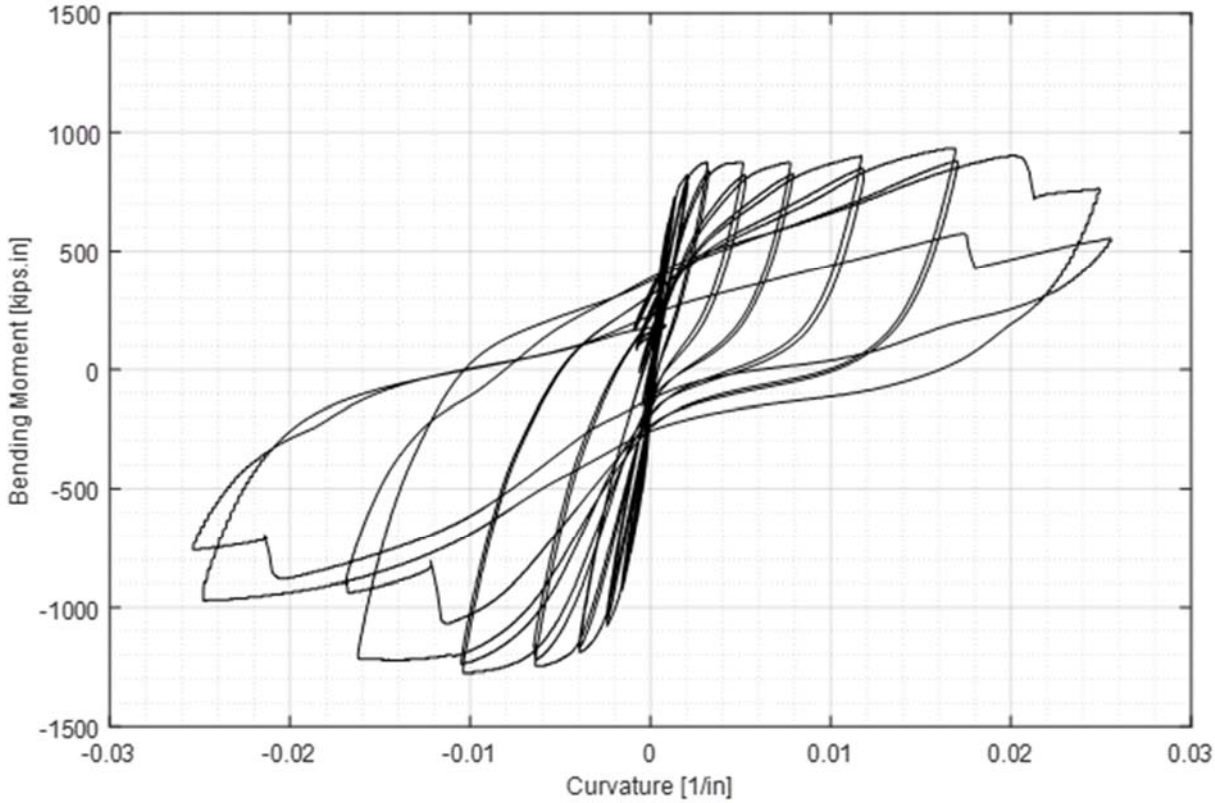


Figure 5-23 Moment-curvature relationship as obtained from test data for UHPC specimen S1.

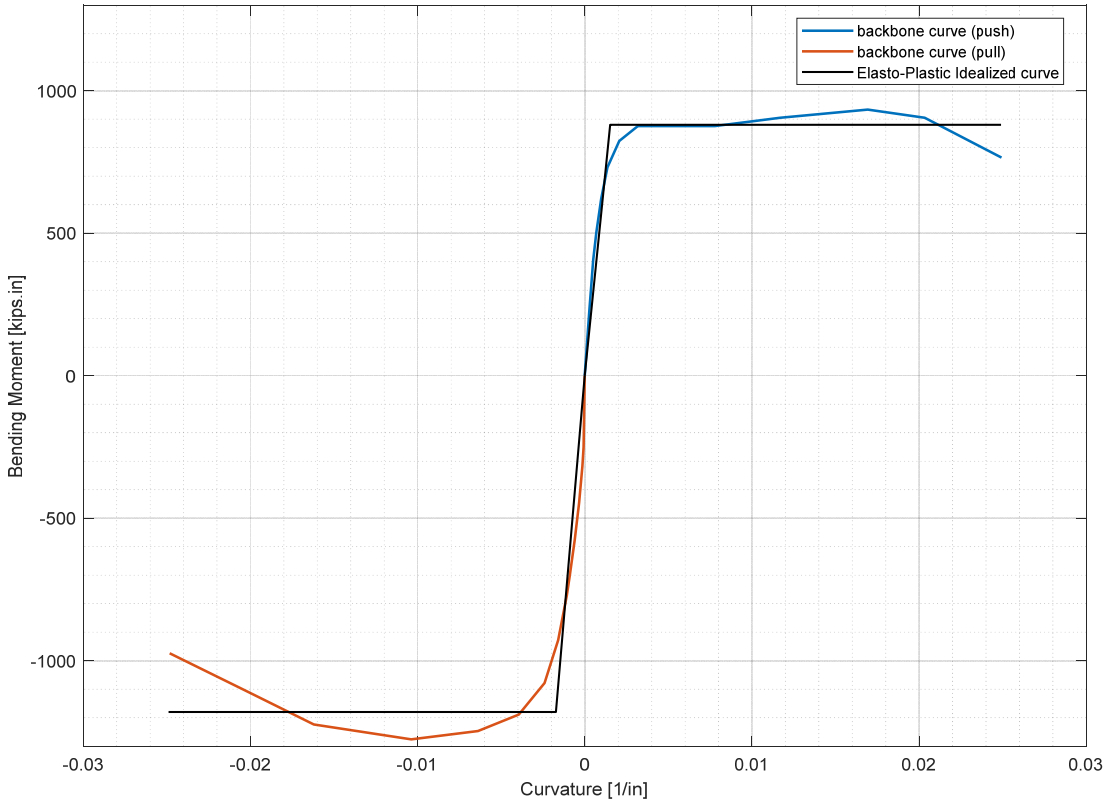


Figure 5-24 idealized elasto-plastic moment-curvature relationship for UHPC specimen S1.

## 5.3. Comparison between NSC and UHPC Columns (S0 versus S1)

Analytical methods were used to establish a comparison with a hypothetical NSC column of 5 ksi concrete compressive strength and with the same dimensions, longitudinal and transverse reinforcement ratios as the UHPC specimen S1. For this purpose, the finite element platform OpenSEES (Mckenna et al. 2000) was used to conduct pushover and nonlinear analysis under the same cyclic loads as the UHPC column. A three-dimensional two-node fiber-section model was developed for S0 specimen. A nonlinear force-based element, *forceBeamColumn*, with *linear* geometric stiffness matrix was used for the column element. Six integration points were used and distributed along the element length. Gauss-Lobatto integration rule with the same sections at each integration point was used. It is noted that the first and the last integration points were located at the column element ends.

The column cross-section was defined using a fiber section that was divided into two parts, the core part material modeled using confined concrete while the cover part modeled using unconfined concrete. The confined concrete properties were calculated using Mander's model (Mander et al. 1998). Both concrete parts were modeled using the *Concrete01* material model while the reinforcement was modeled using *Steel02* material model. The core section was meshed into 30 radial divisions and 10 theta divisions while the cover section was meshed into 10 radial divisions and 10 theta divisions. For better comparison, the longitudinal rebars locations inside the section were adopted to match the as-built distorted rebar locations of specimen S1. The comparison between specimens S0 and S1 was made with respect to the global and the local column behaviors as discussed next.

### *5.3.1. Global Behavior*

The envelops of the force-drift relationship for S0 (obtained from OpenSEES) and S1 (obtained from experimental test) are shown in Figure 5-25. By comparing the global response of S0 and S1, it is shown that using UHPC of almost 6 times the strength of NSC has led to a significant increase in the lateral load capacity of the column with an increase of 69% in the push direction and 94% in the pull direction. The OpenSEES model was not intended to capture rebar rupture or low-cycle fatigue effects and in turn, there was not a terminating criterion for the nonlinear analysis. Thus, for the sake of pushover analysis, the column was pushed up to about 11.5% drift and the maximum or peak displacement capacity of So was interpreted at a value that corresponded to the longitudinal rebars reach an ultimate strain of about 19%. Thus, a maximum drift ratio of 9.62% can be reported for S0 which is about 11% less than the value found from the test for S1. This comparison shows that not only the strength of the column increases but also the displacement capacity of UHPC columns can be slightly higher than NSC columns.

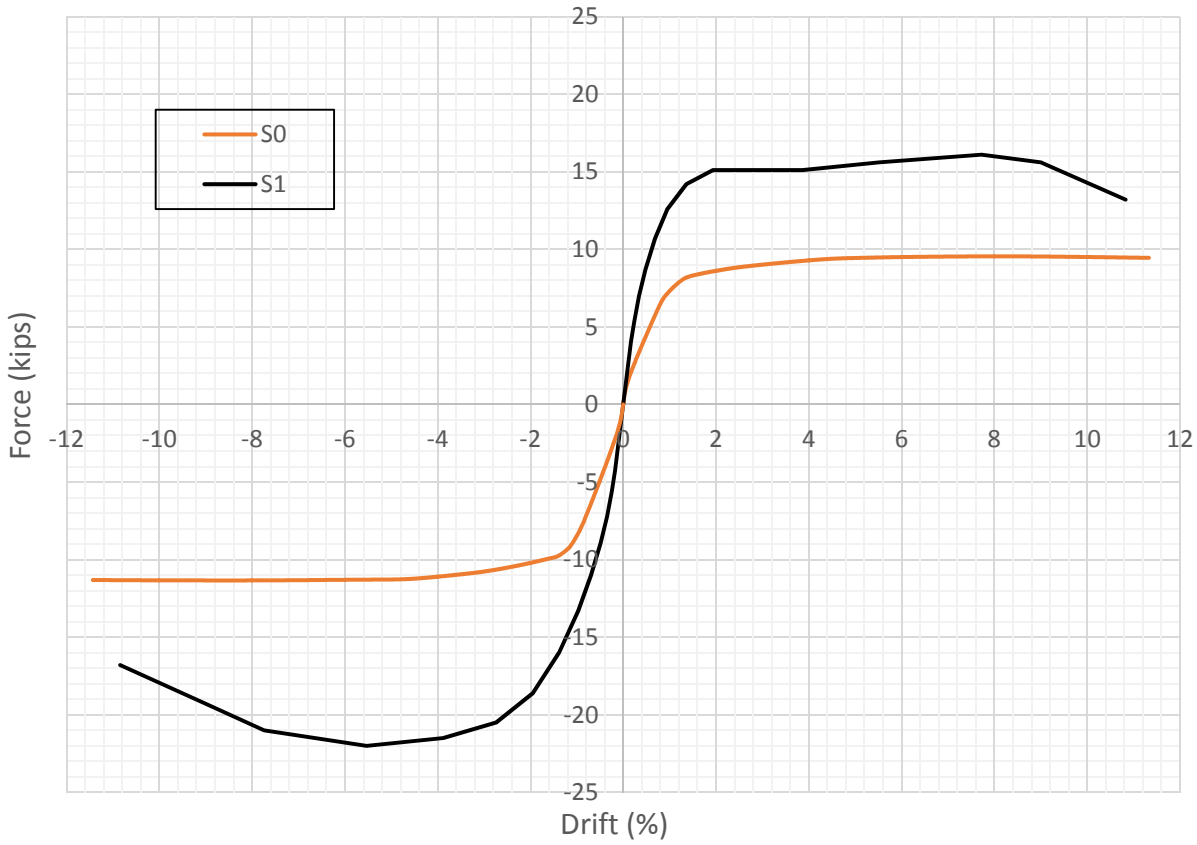


Figure 5-25 Comparison of Force-Drift Curve for S0 and S1.

### *5.3.2. Local Behavior*

Comparing specimen S0 to S1 with respect to their local behavior is represented by the moment-curvature relationships shown in Figure 5-26. The figure can shows that using UHPC has led to a significant increase in the moment capacity of the column with an increase of 36% in the push direction and 61% in the pull direction. The OpenSEES model shows that the maximum reached curvature of the NSC column was 0.016 1/in. which is less than that of S1 by 36%. This also confirms that the UHPC column has a comparable curvature ductility as NSC seismic columns.

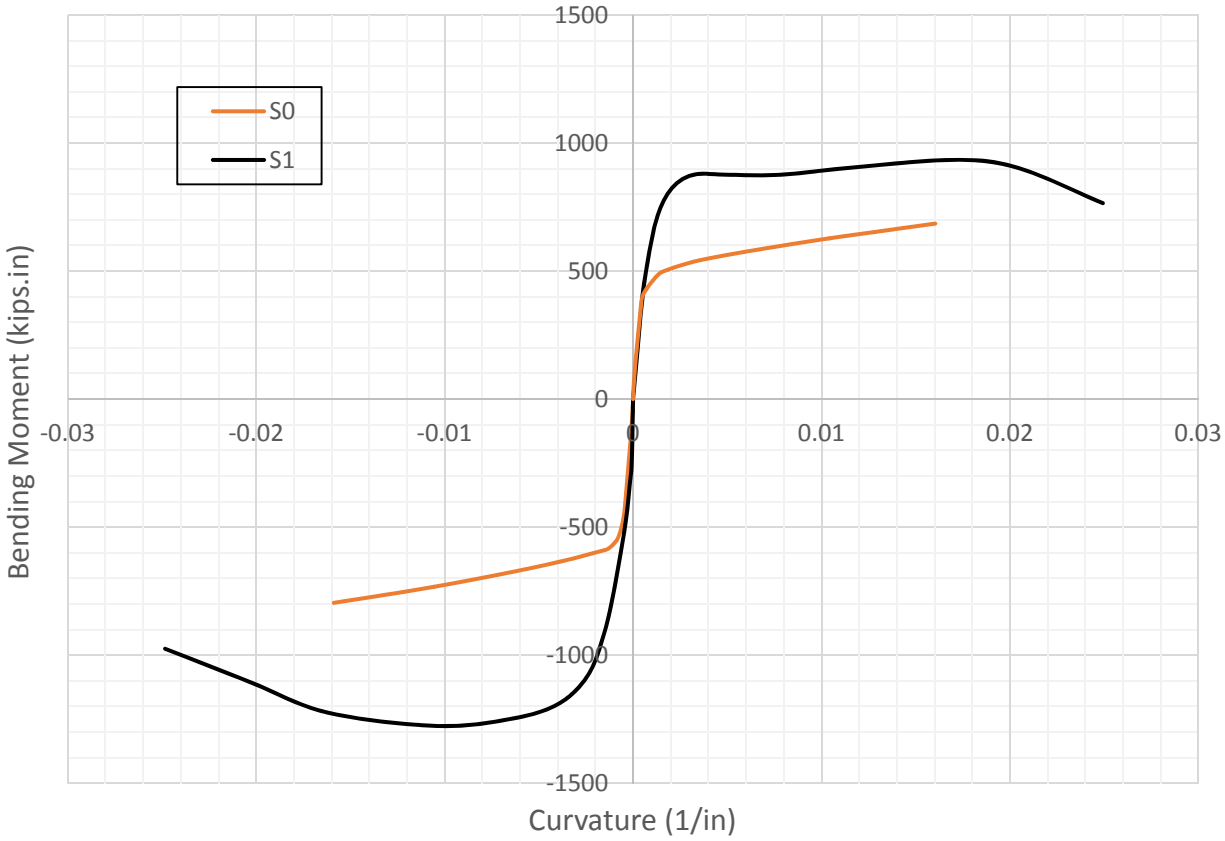


Figure 5-26 Comparison of Bending Moment-Curvature Curve for S0 and S1.

# Chapter 6. TEST RESULTS AND DISCUSSION OF GROUP II SPECIMENS

This chapter presents the experimental test results of the UHPC specimens S2, S3 and S4 of Group II with respect to the global and the local behavior. A comprehensive comparison between the two groups of UHPC columns that varied in steel grade is also provided in this chapter. The comparisons show the effect of using HSS rebars instead of Gr 60 rebars and the effect of changing the transverse or longitudinal reinforcement ratios on the behavior of UHPC columns. The reader is reminded that all three specimens used HSS for longitudinal rebars where S2 used same longitudinal and transverse reinforcement ratio as S1 before while S3 and S4 used lower values for the transverse and longitudinal reinforcement, respectively.

## 6.1. Columns Global Behavior

### *6.1.1. Plastic Hinge Damage and Mode of Failure*

The observed mode of failure for all of the UHPC columns of Group II was the fracture of reinforcing bars. The test was stopped after the rupture of the four outer-most rebars in the north and south directions of the column and before the rupture of the two middle rebars for test setup stability purposes. The observed sequence and progression of damage of the three specimens is discussed in order in the next three paragraphs.

For specimen S2, i.e. 2.37% HSS longitudinal reinforcement and 1.1% transverse reinforcement, no cracks were observed until reaching 0.97% drift ratio. The crushing of UHPC in compression was observed to happen after the column reached 7.72% drift ratio and the first significant crack started to appear at the column-footing interface after reaching 4% drift ratio with 0.03 in crack width. A wide crack appeared at the column-footing interface at drift ratio 8% with almost 0.1 in crack width. The first bar ruptured at the second cycle of almost 8% drift ratio in the south side while the other three bars ruptured at the first cycle of the 10.83% drift ratio run. There was no evidence of rebar buckling. Furthermore, no concrete spalling or reinforcement exposure was observed until the end of the test. Figures 6-1 through 6-9 show the progression of damage at the plastic hinge region of the column at selected different drift ratios for specimen S2.

For specimen S3, i.e. 2.37% HSS longitudinal reinforcement and 0.55% transverse reinforcement, no cracks were observed until reaching 0.97% drift ratio. The crushing of UHPC in compression was discovered to happen after the column reached 7.72% drift ratio and the first significant crack started to appear at the column-footing interface after reaching 4% drift ratio with 0.03 in crack width. A wide crack appeared at the column-footing interface at drift ratio 8% with almost 0.1 in crack width. The first bar ruptured at the first cycle of almost 8% drift ratio in the south side while the other three bars ruptured at the second cycle of the same drift ratio in the south side then the north side. There was no evidence of rebar buckling. Furthermore, no concrete spalling or reinforcement exposure was observed until the end of the test. Figures 6-10 through 6-16 show the progression of damage at the plastic hinge region at selected different drift ratios for specimen S3.

For specimen S4, i.e. 1.48% HSS longitudinal reinforcement and 1.1% transverse reinforcement, no cracks were observed until reaching 1.38% drift ratio. The crushing of UHPC in compression was discovered to happen after the column reached 2.76% drift ratio and the first

significant crack started to appear at the column-footing interface after reaching 4% drift ratio with 0.03 in crack width. A wide crack appeared at the column-footing interface at drift ratio 8% with almost 0.2 in crack width. The first two bars ruptured at the first cycle of almost 8% drift ratio in the north side while the other two bars ruptured at the second cycle of the same drift ratio in the south side. There was no evidence of rebar buckling. Furthermore, no concrete spalling or reinforcement exposure was observed until the end of the test. Figures 6-17 through 6-24 show the progression of damage at the plastic hinge region at selected different drift ratios for specimen S4.

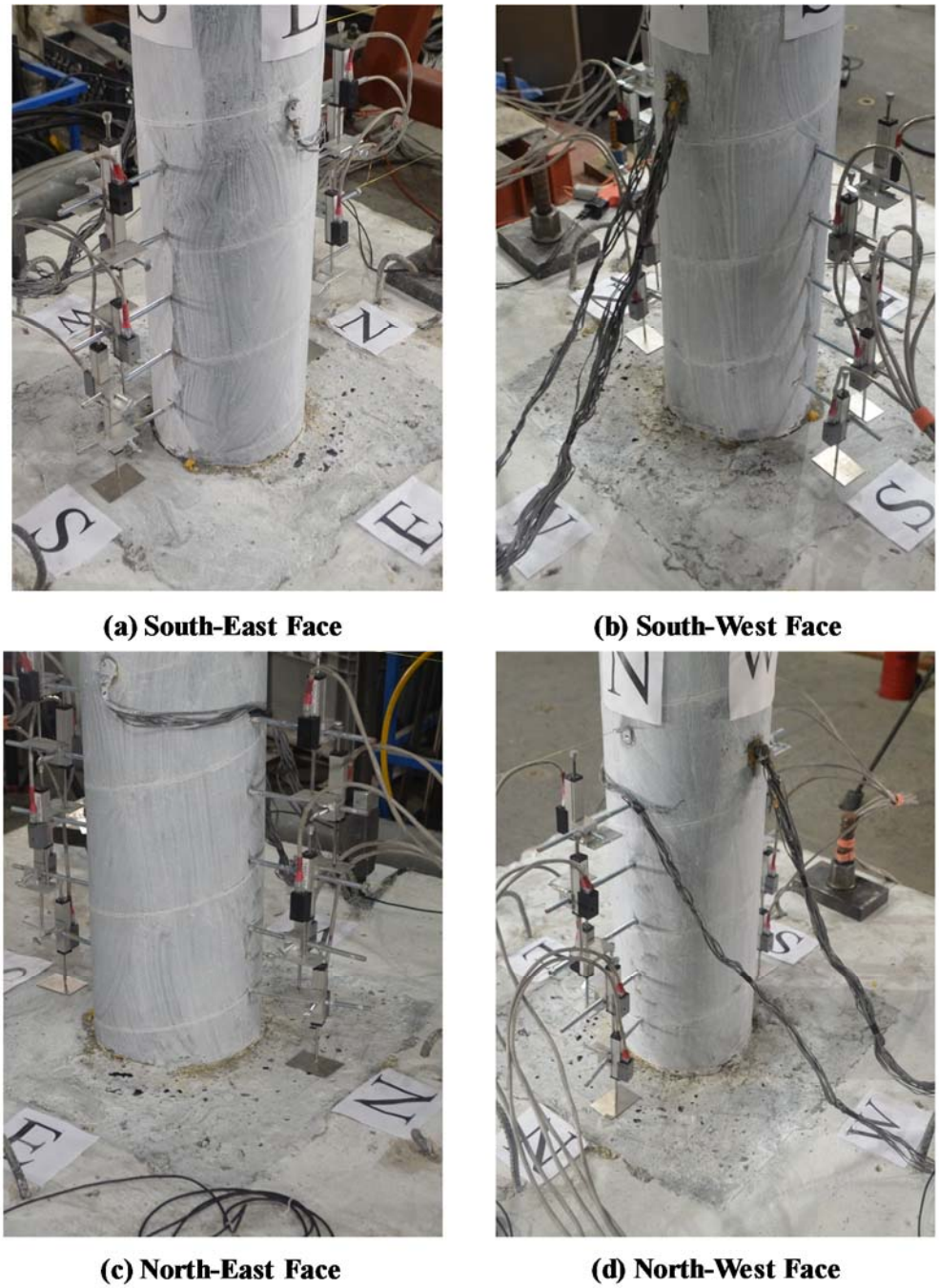


Figure 6-1 Damage observed at second cycle of 0.69% drift for specimen S2.

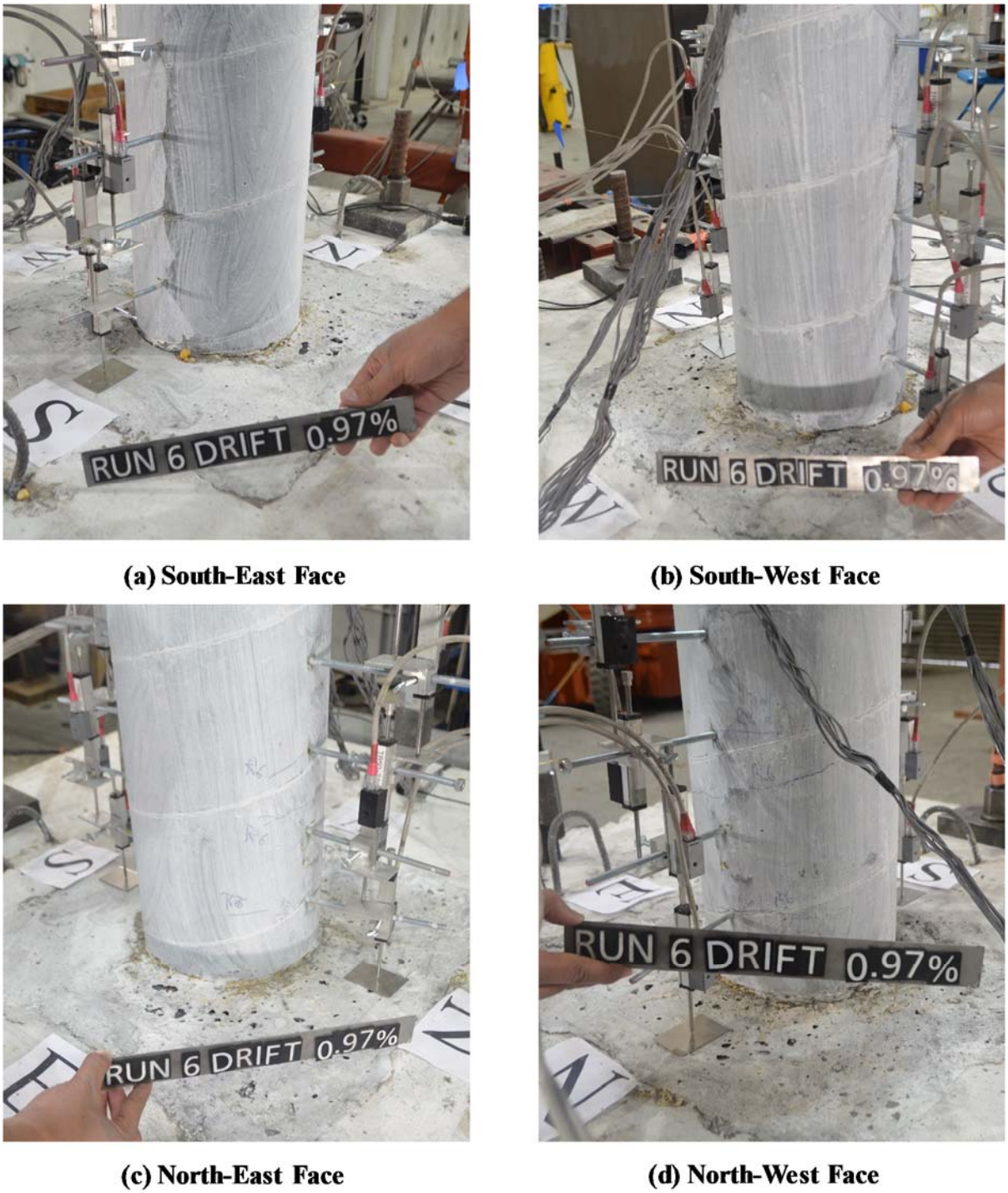


**(a) South-East Face** **(b) South-West Face**

**(c) North-East Face** **(d) North-West Face**

Figure 6-2 Damage observed at second cycle of 0.97% drift for specimen S2.

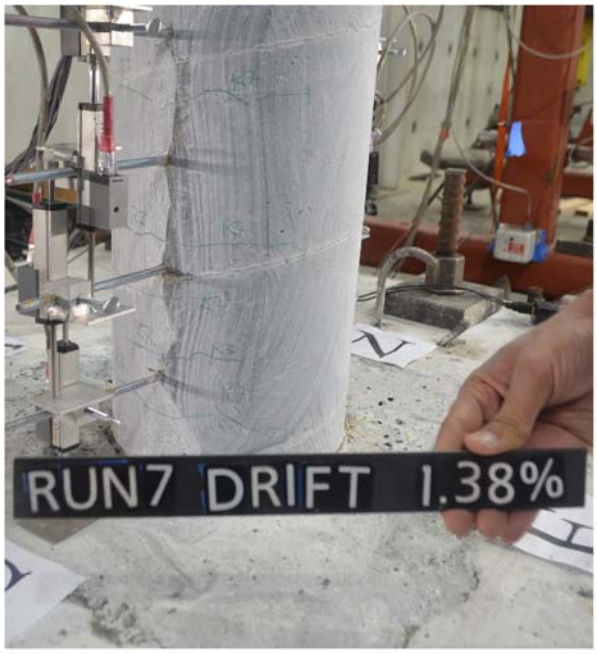


(a) South-East Face

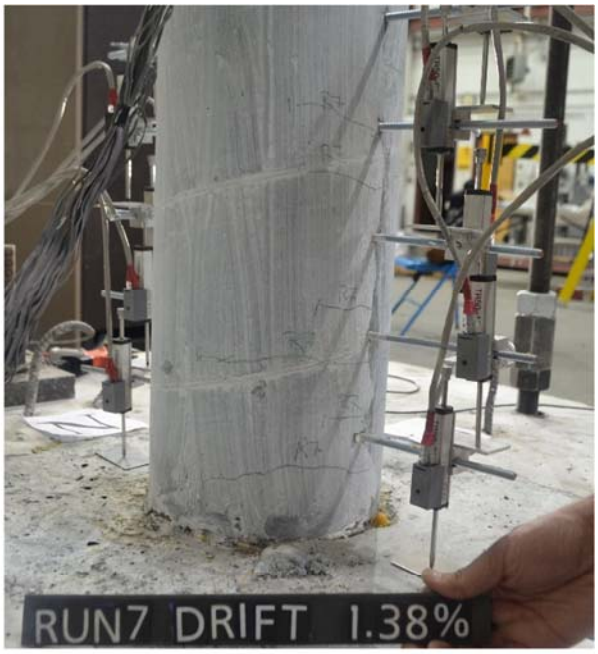


(b) South-West Face


(c) North-East Face


(d) North-West Face

Figure 6-3 Damage observed at second cycle of 1.38% drift for specimen S2.

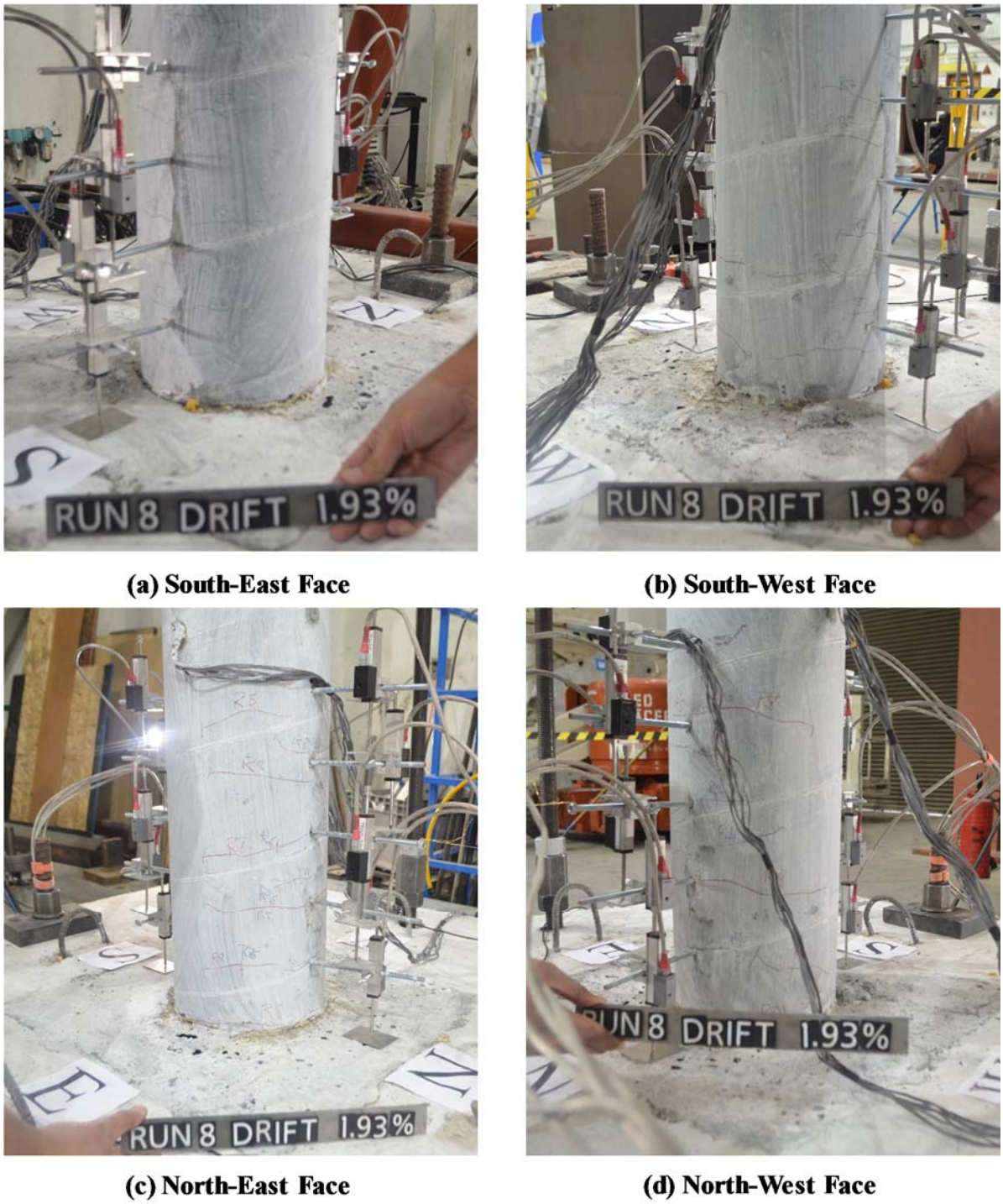


(a) South-East Face

(b) South-West Face

(c) North-East Face

(d) North-West Face

Figure 6-4 Damage observed at second cycle of 1.93% drift for specimen S2.

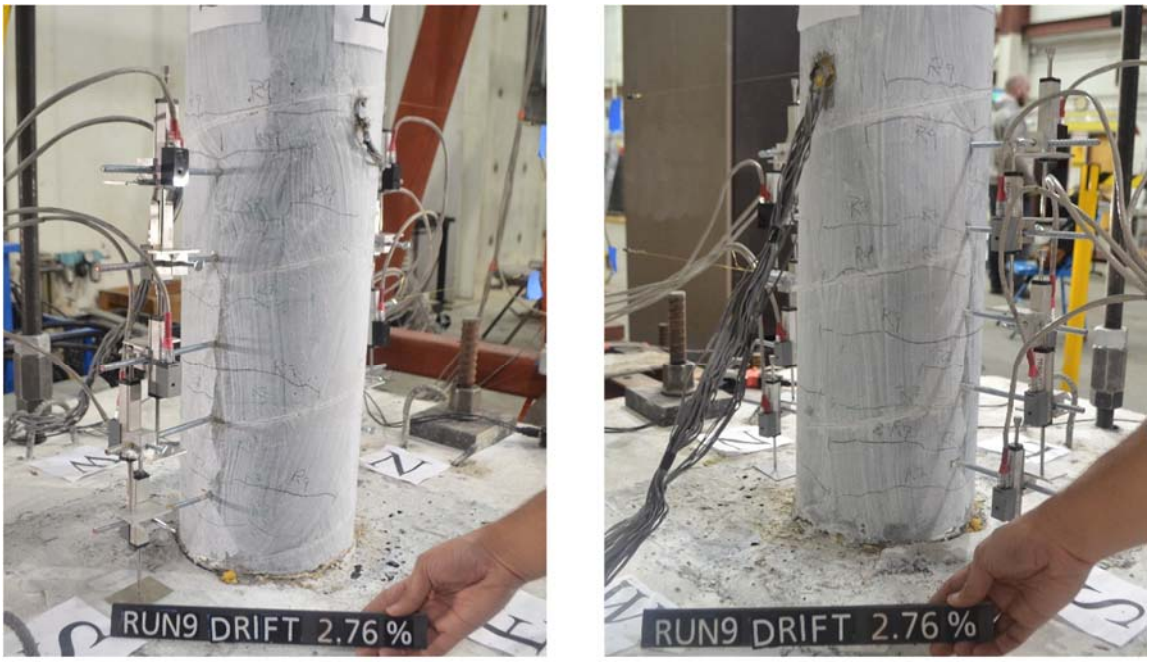


(a) South-East Face (b) South-West Face

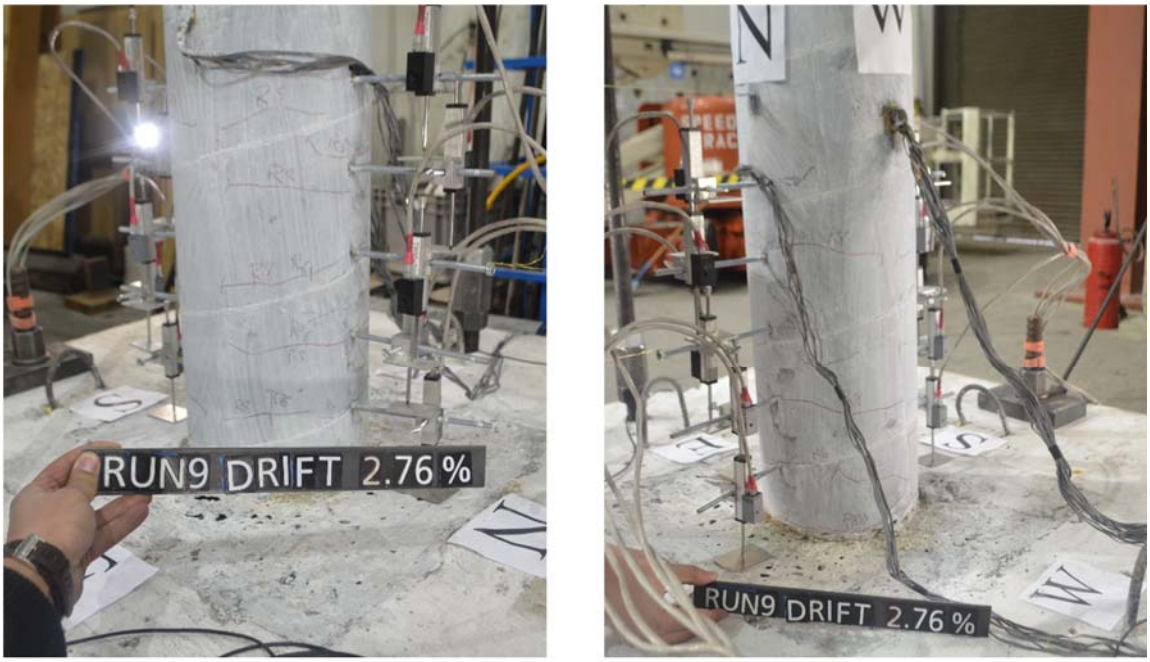


(c) North-East Face (d) North-West Face

Figure 6-5 Damage observed at second cycle of 2.76% drift for specimen S2.

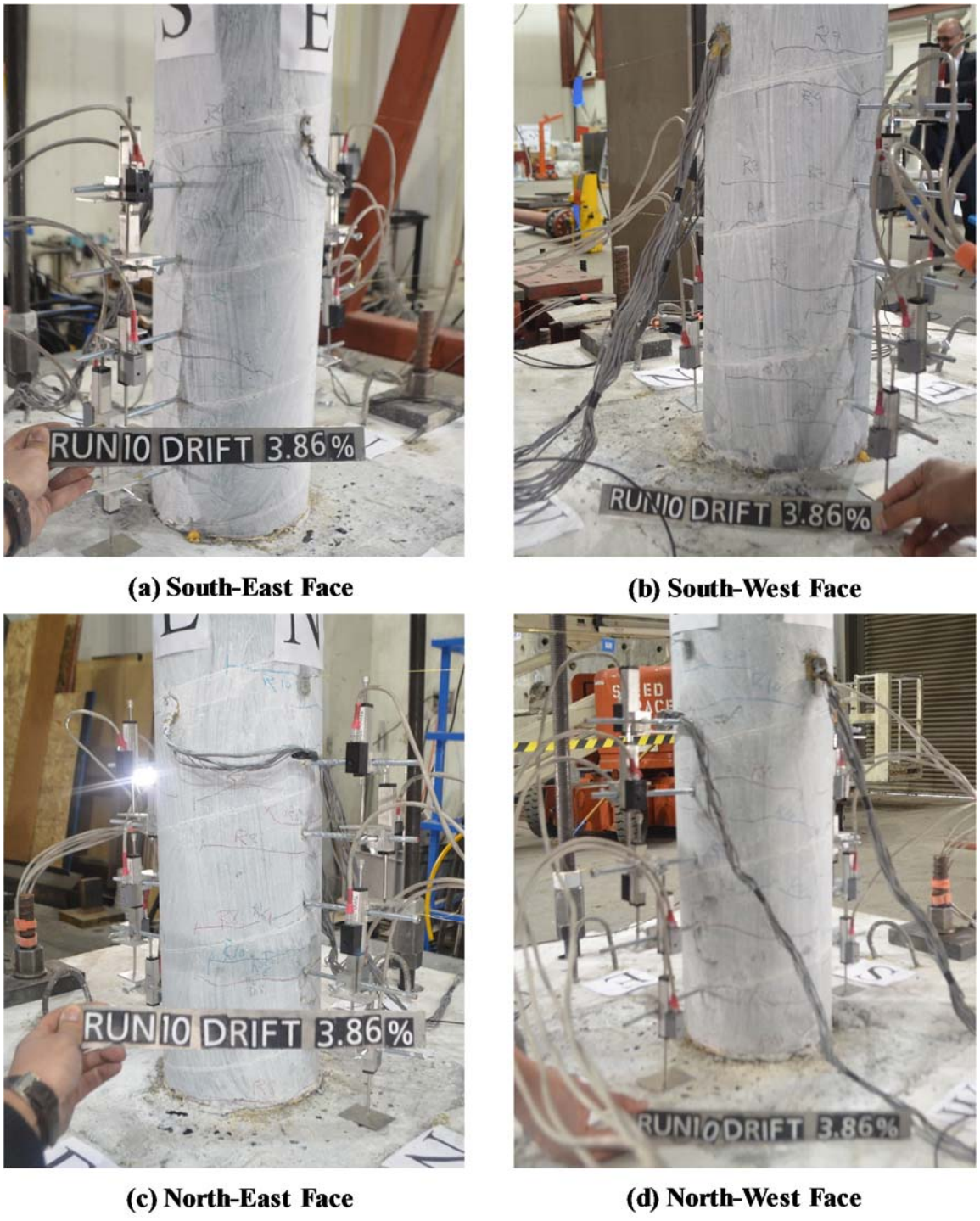


**(a) South-East Face** **(b) South-West Face**

**(c) North-East Face** **(d) North-West Face**

Figure 6-6 Damage observed at second cycle of 3.86% drift for specimen S2.

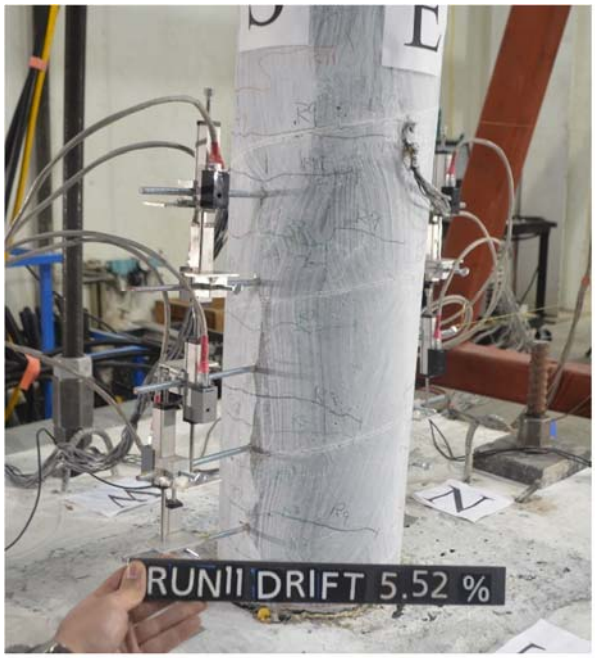


(a) South-East Face

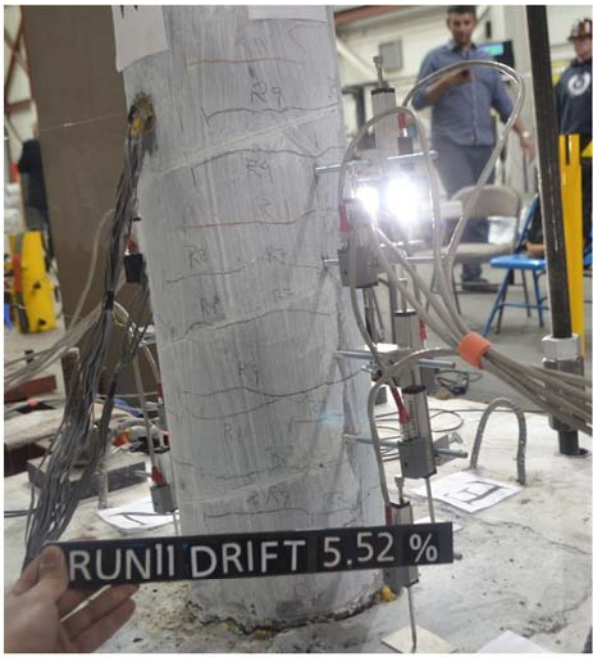


(b) South-West Face

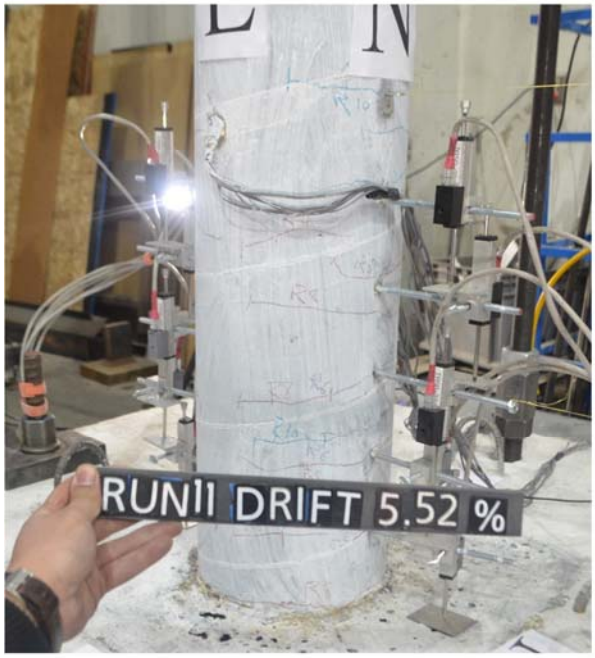


(c) North-East Face


(d) North-West Face

Figure 6-7 Damage observed at second cycle of 5.52% drift for specimen S2.

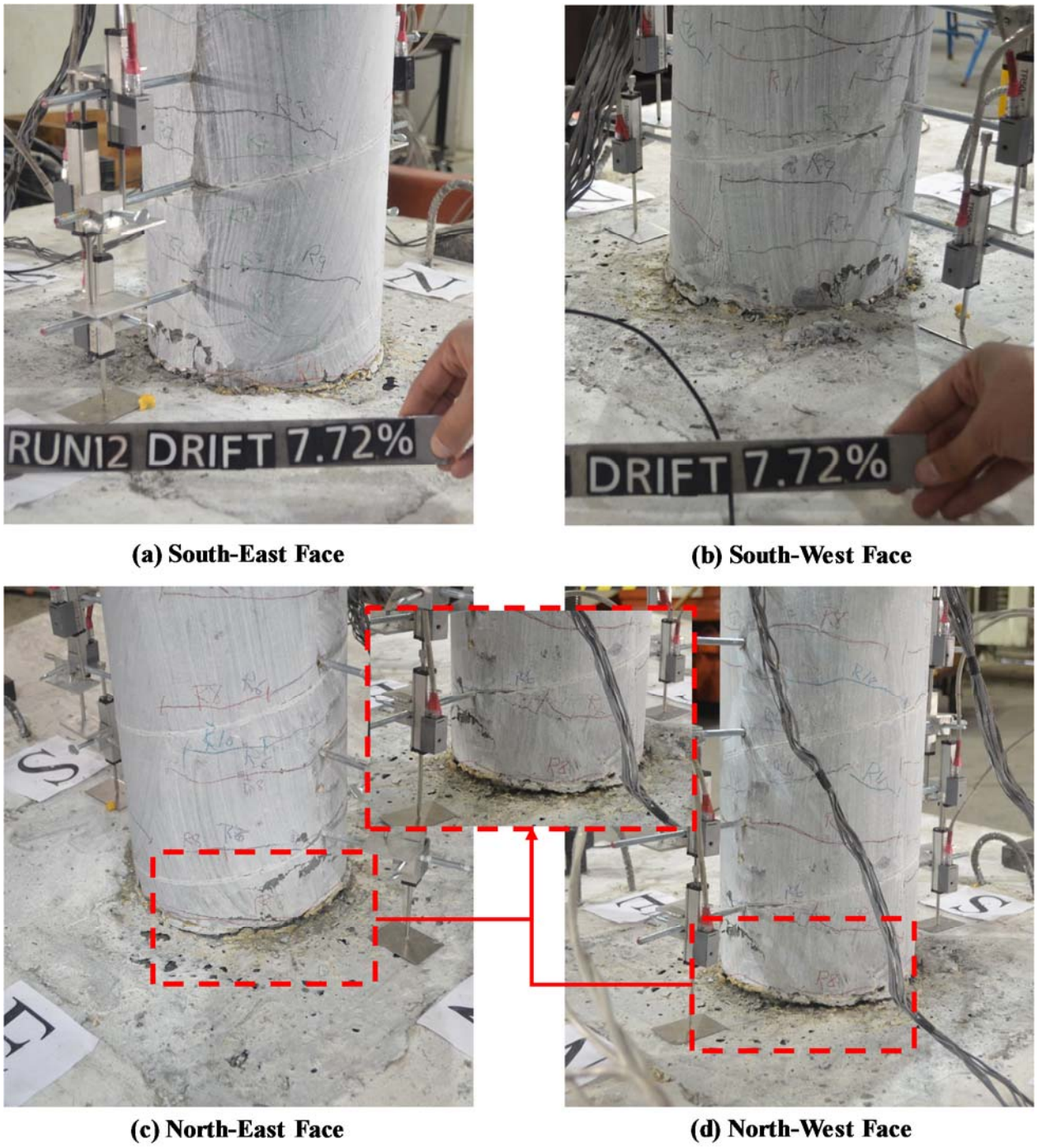


Figure 6-8 Damage observed at second cycle of 7.72% drift for specimen S2.


(a) South-East Face

(b) South-West Face


(c) North-East Face

(d) North-West Face

Figure 6-9 Damage observed at second cycle of 10.83% drift for specimen S2.


**(a) South-East Face** **(b) South-West Face**

**(c) North-East Face** **(d) North-West Face**

Figure 6-10 Damage observed at second cycle of 0.97% drift for specimen S3.

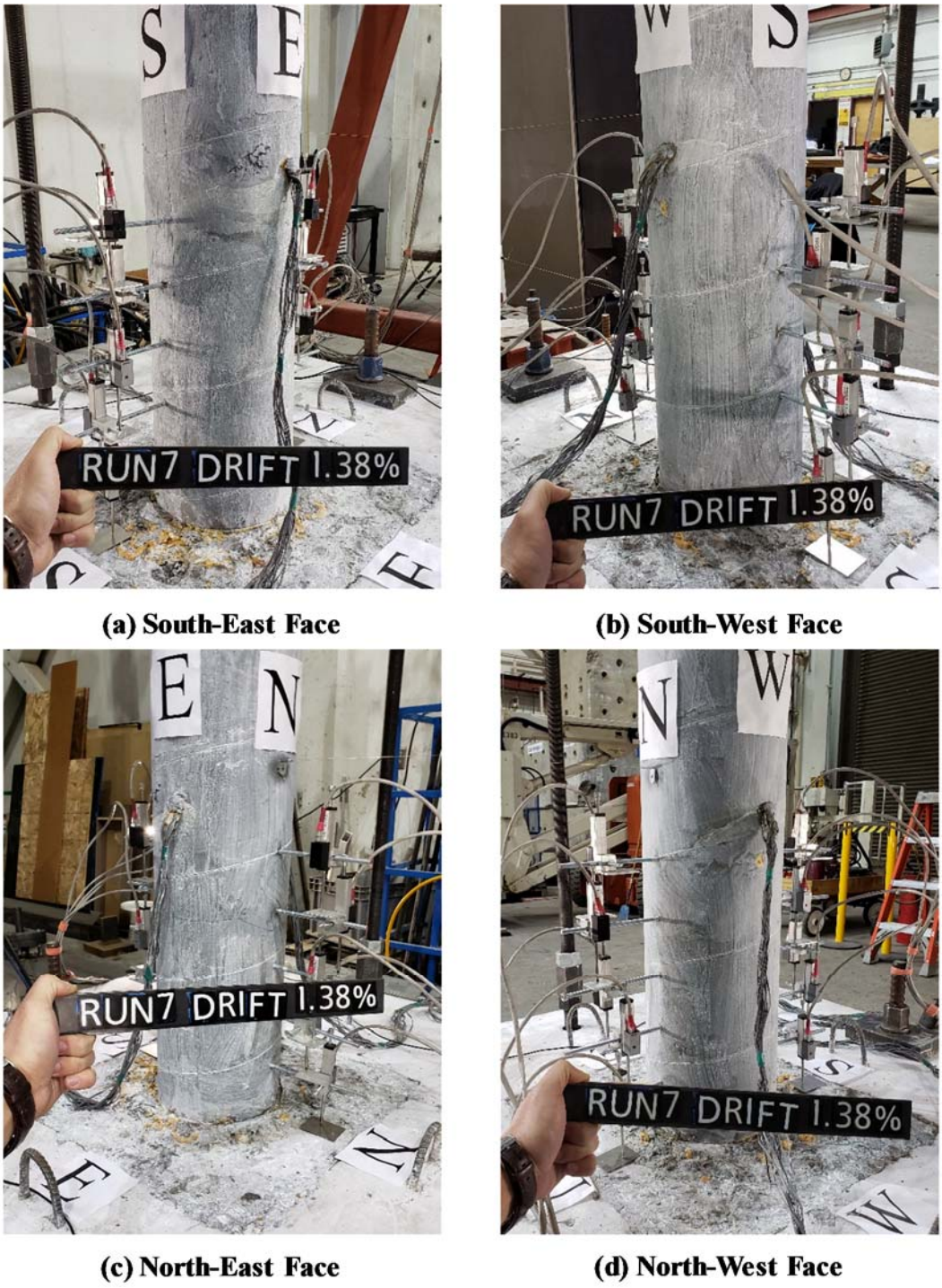


(a) South-East Face (b) South-West Face

(c) North-East Face (d) North-West Face

Figure 6-11 Damage observed at second cycle of 1.38% drift for specimen S3.

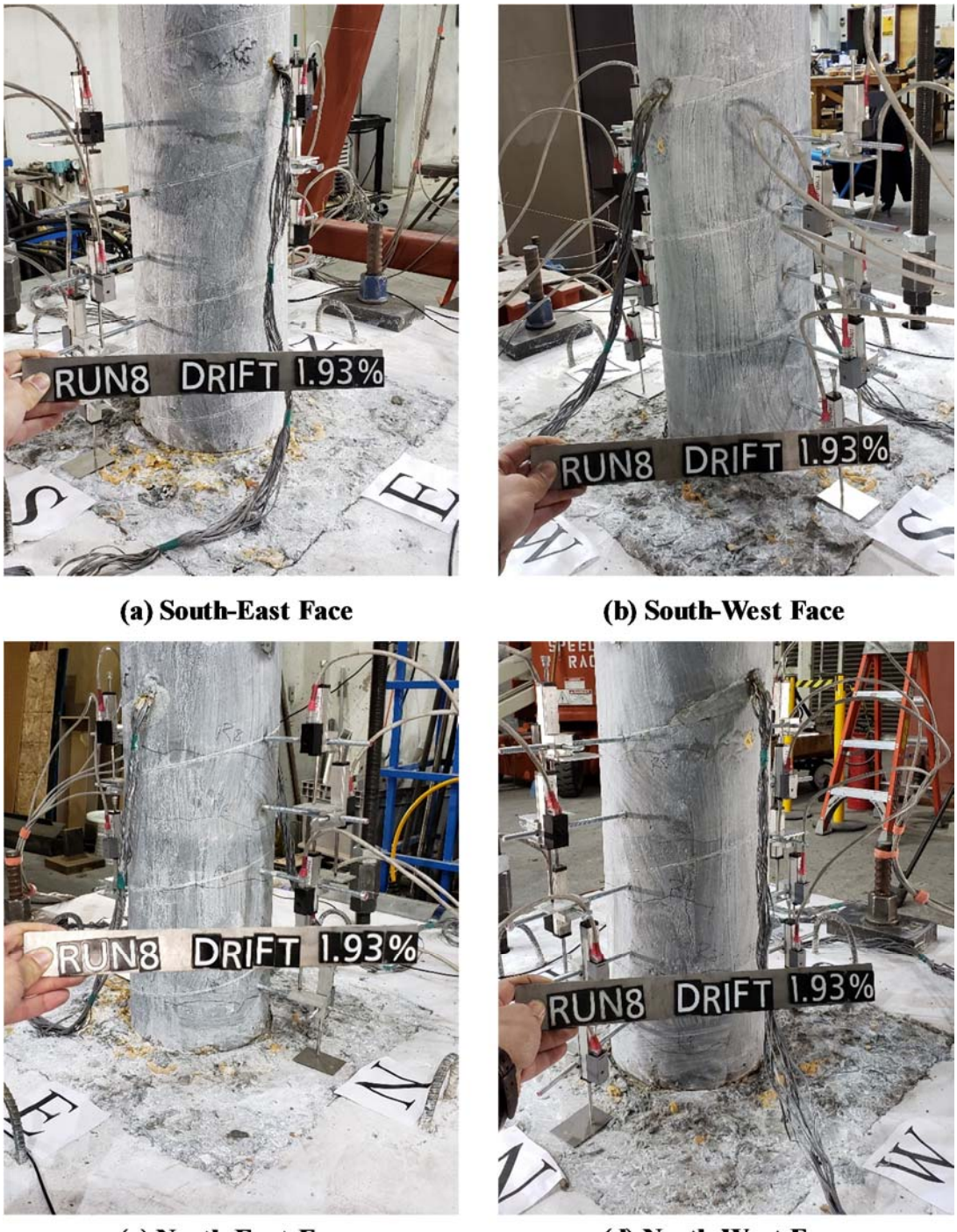


(a) South-East Face (b) South-West Face

(c) North-East Face (d) North-West Face

Figure 6-12 Damage observed at second cycle of 1.93% drift for specimen S3.


(a) South-East Face (b) South-West Face

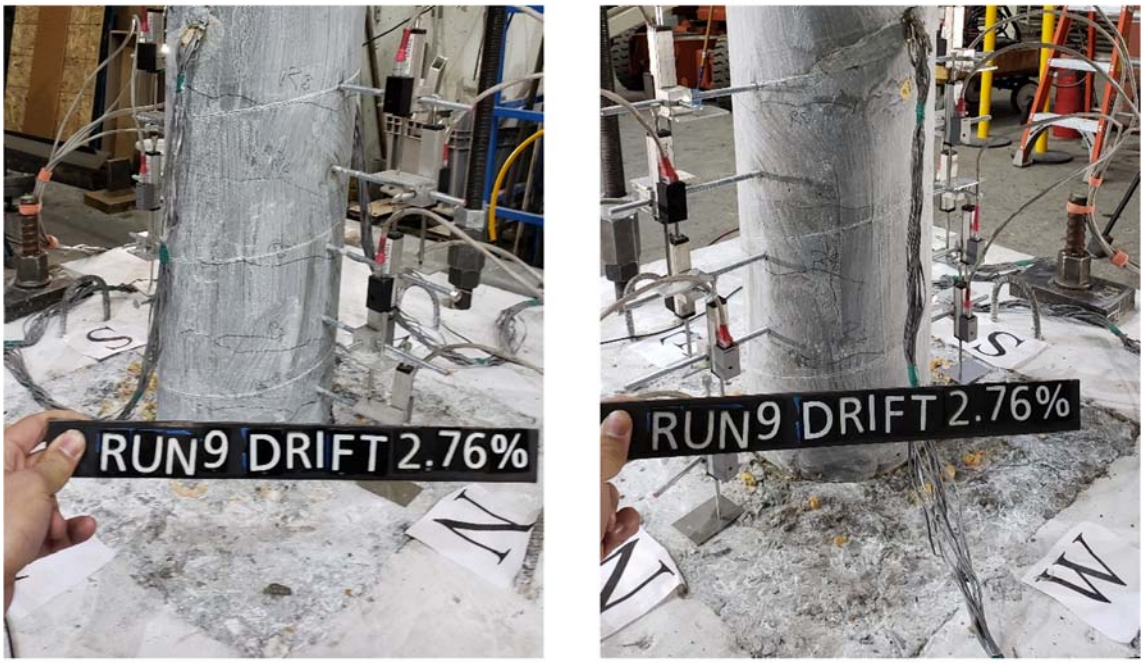


(c) North-East Face (d) North-West Face

Figure 6-13 Damage observed at second cycle of 2.76% drift for specimen S3.

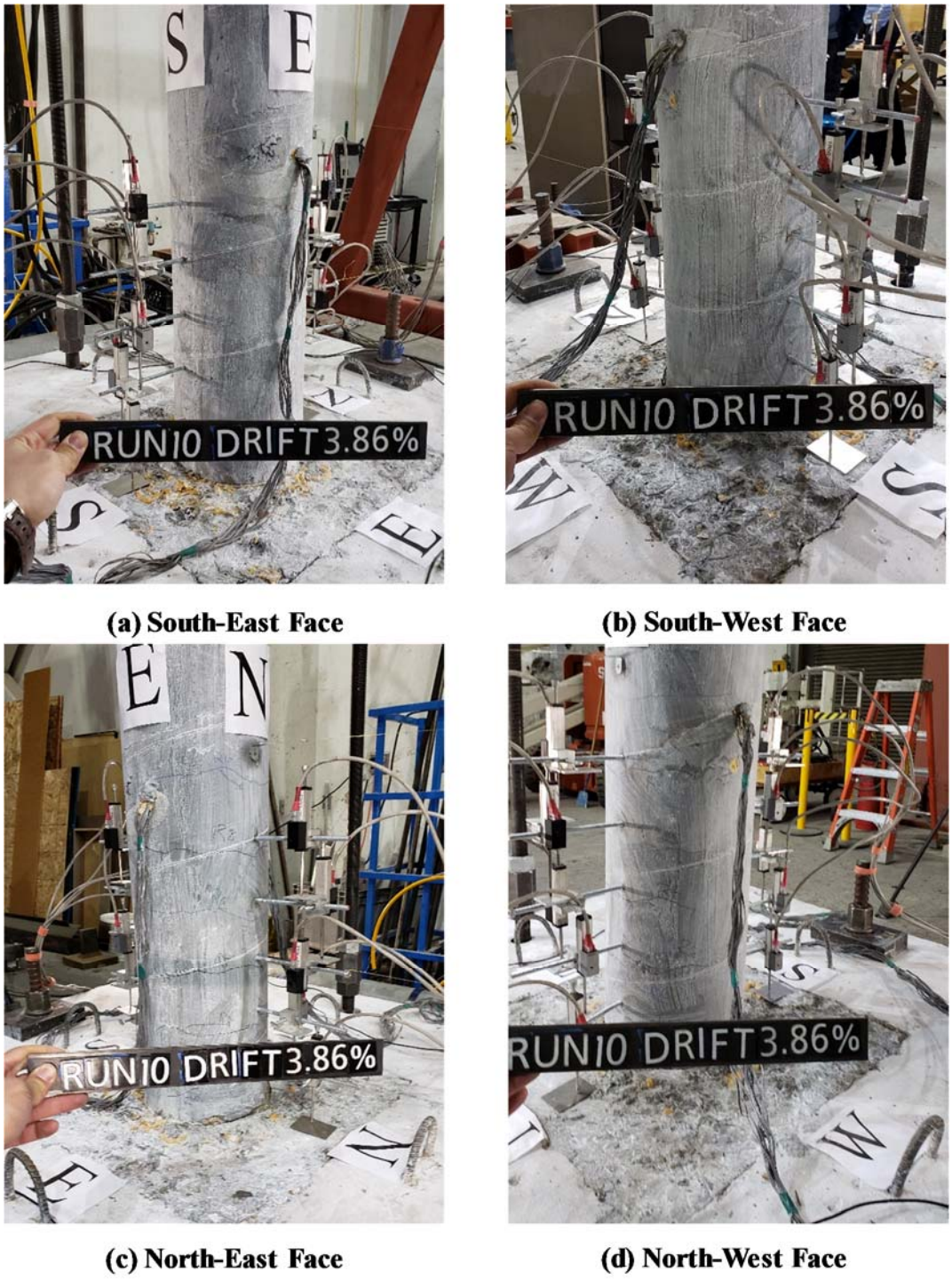


(a) South-East Face (b) South-West Face

(c) North-East Face (d) North-West Face

Figure 6-14 Damage observed at second cycle of 3.86% drift for specimen S3..

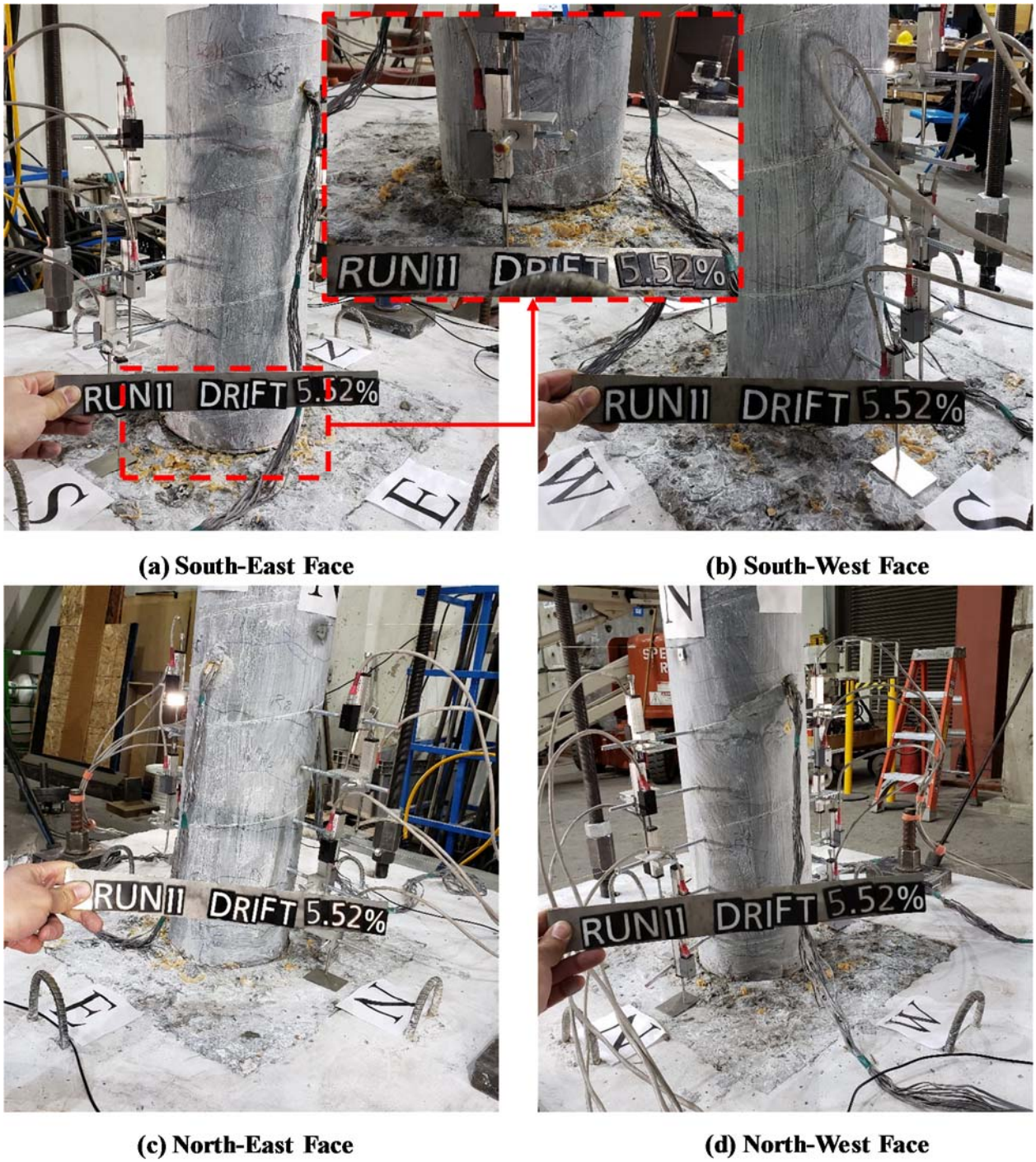


(a) South-East Face

(b) South-West Face

(c) North-East Face

(d) North-West Face

Figure 6-15 Damage observed at second cycle of 5.52% drift for specimen S3..

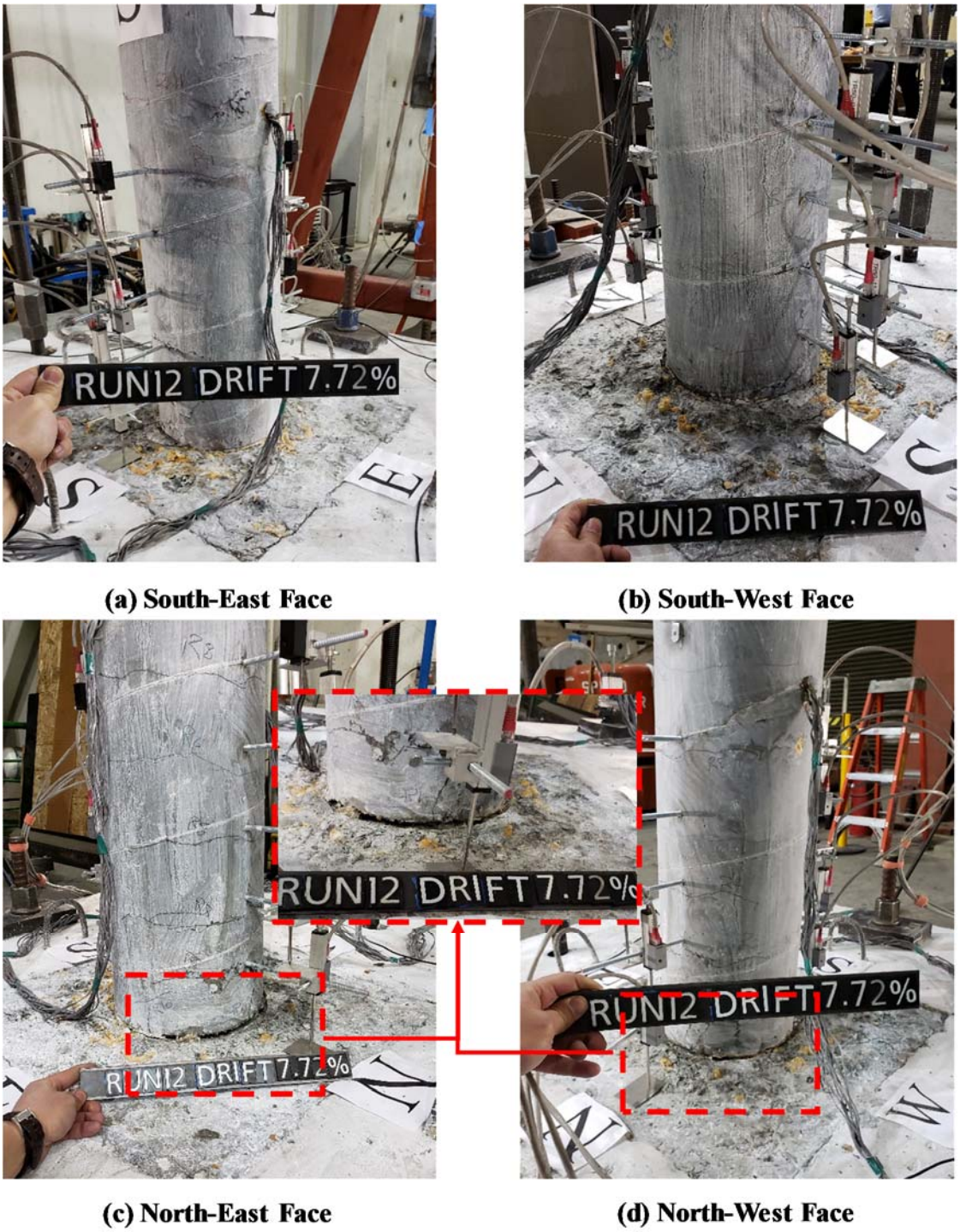


Figure 6-16 Damage observed at second cycle of 7.72% drift for specimen S3.

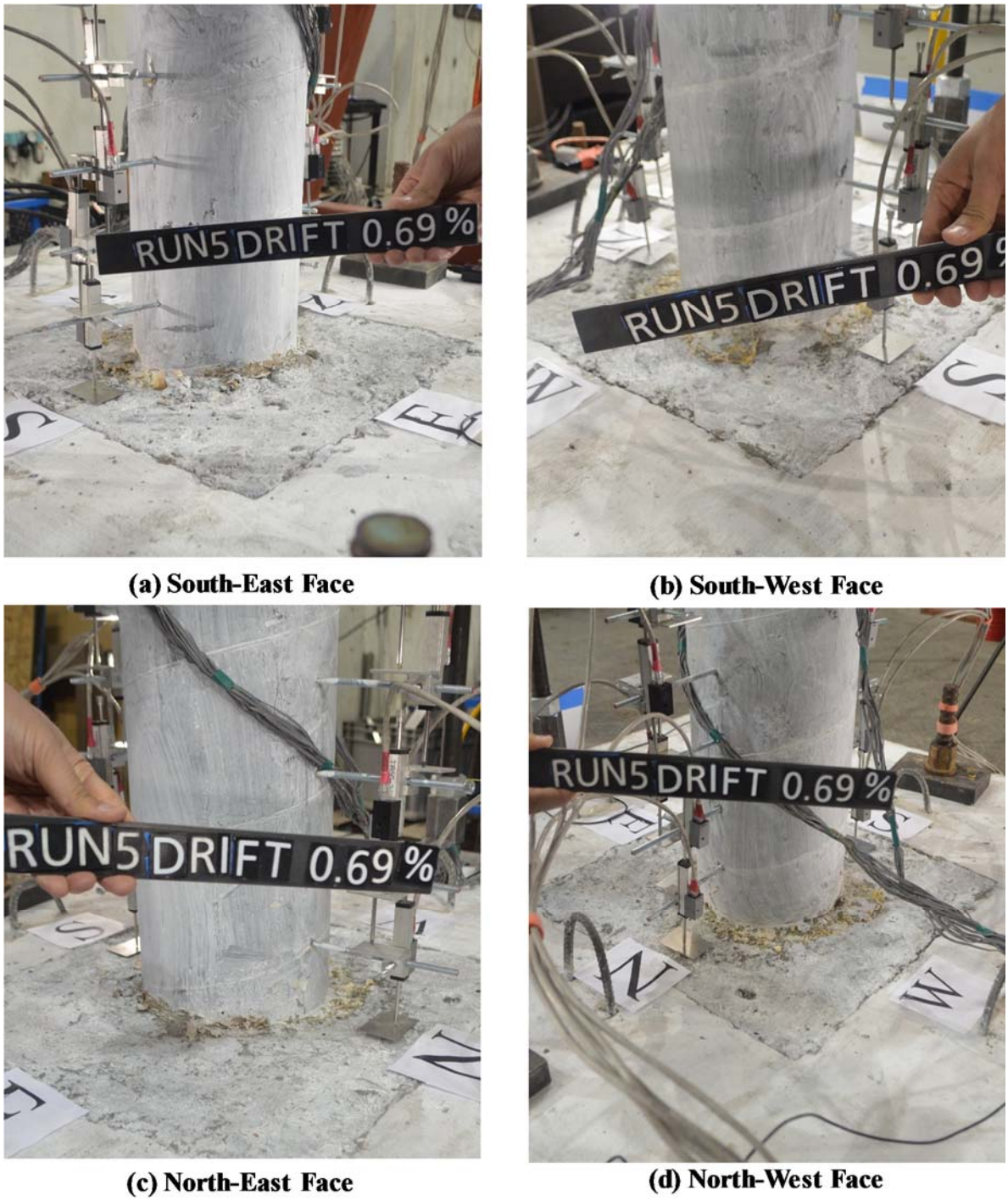


(a) South-East Face

(b) South-West Face

(c) North-East Face

(d) North-West Face

Figure 6-17 Damage observed at second cycle of 0.69% drift for specimen S4.

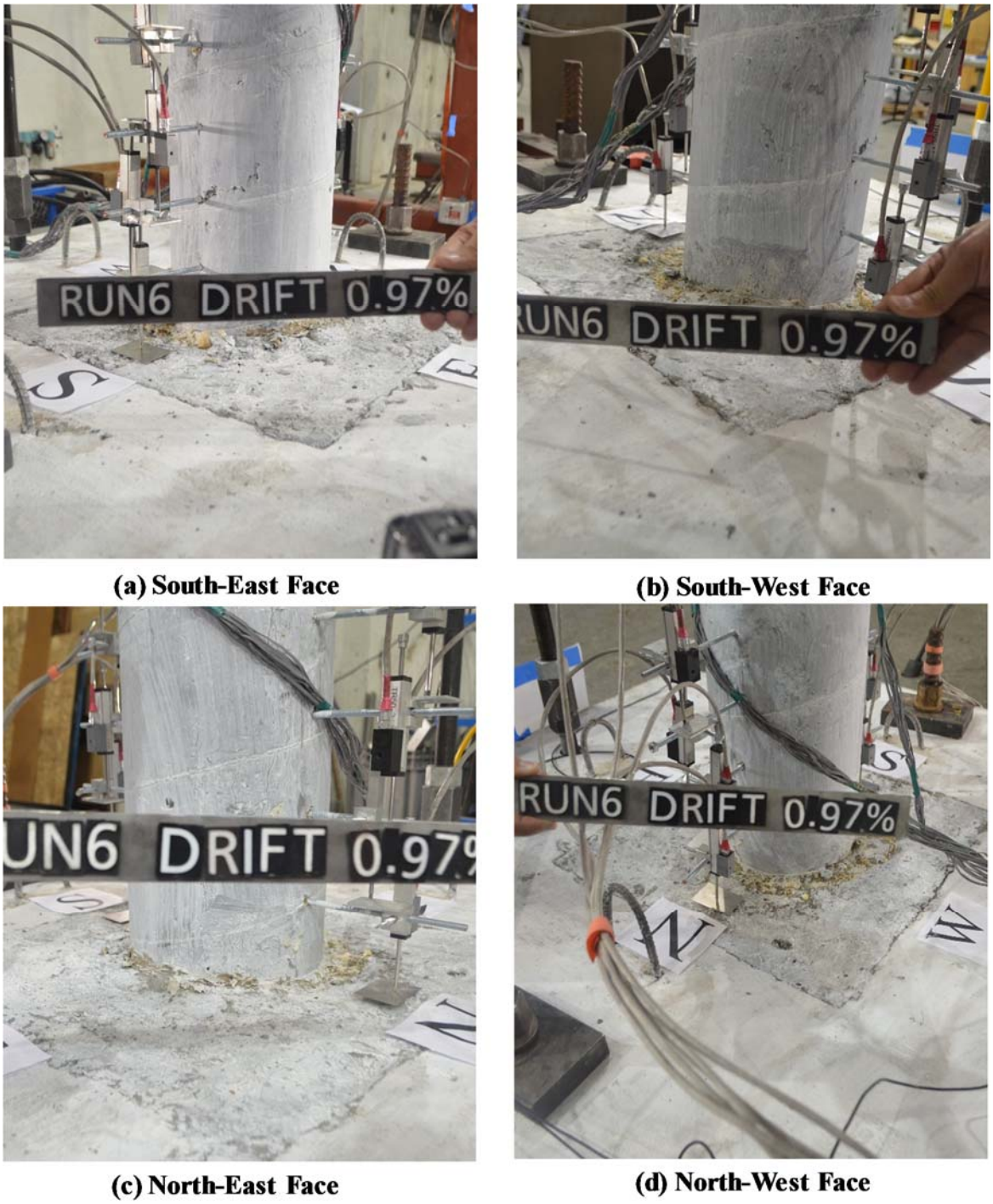


Figure 6-18 Damage observed at second cycle of 0.97% drift for specimen S4.

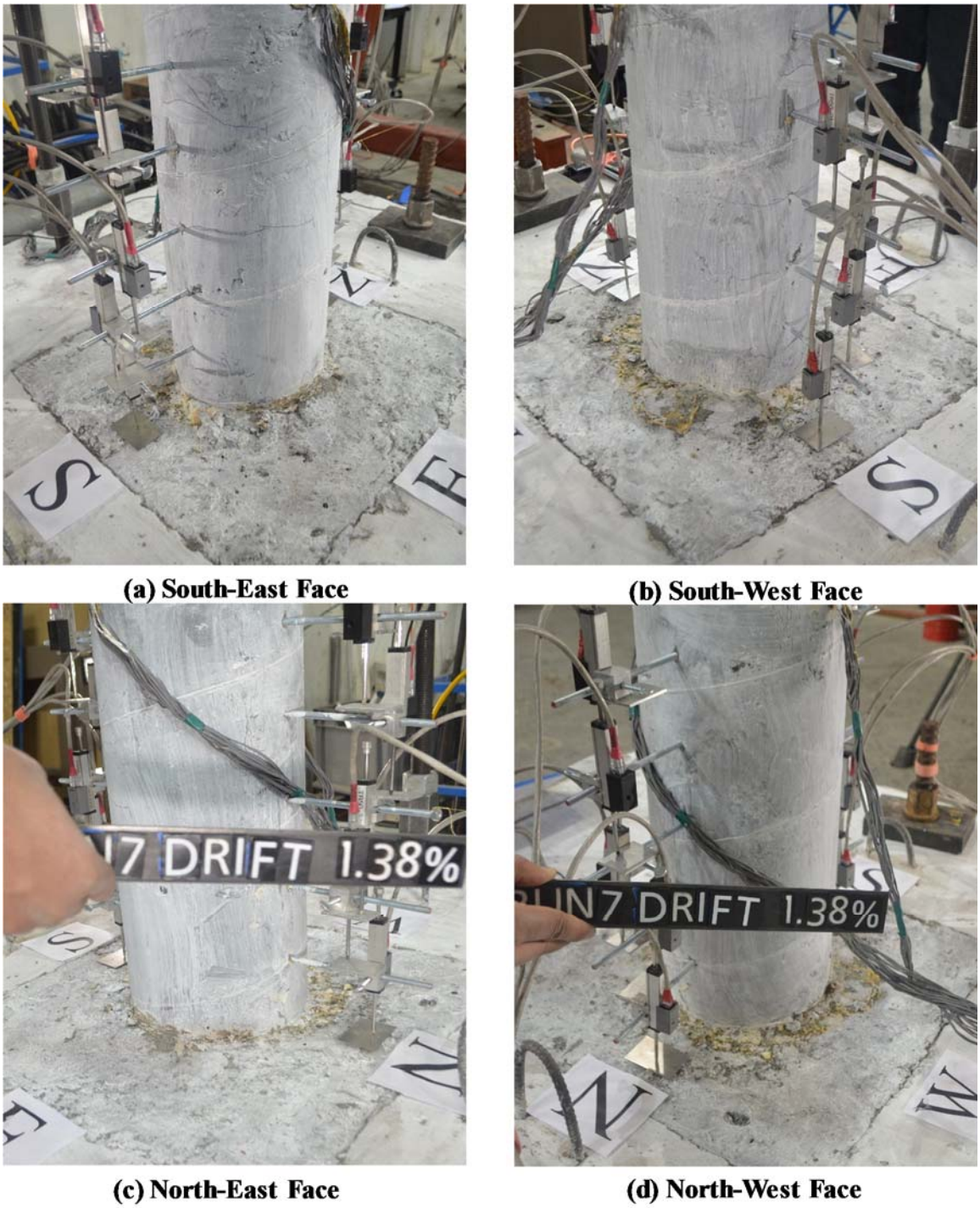


Figure 6-19 Damage observed at second cycle of 1.38% drift for specimen S4.

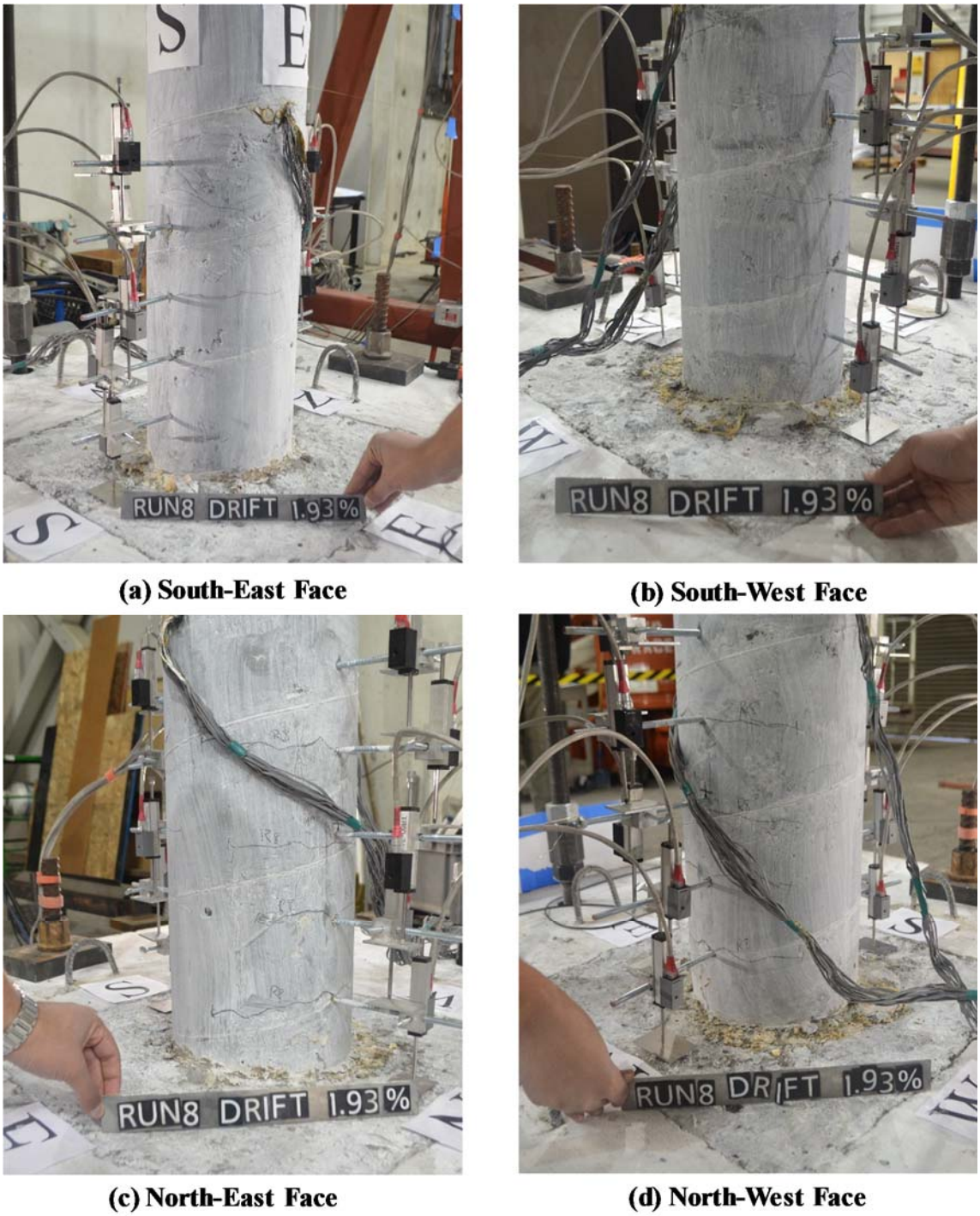


(a) South-East Face (b) South-West Face

(c) North-East Face (d) North-West Face

Figure 6-20 Damage observed at second cycle of 1.93% drift for specimen S4.

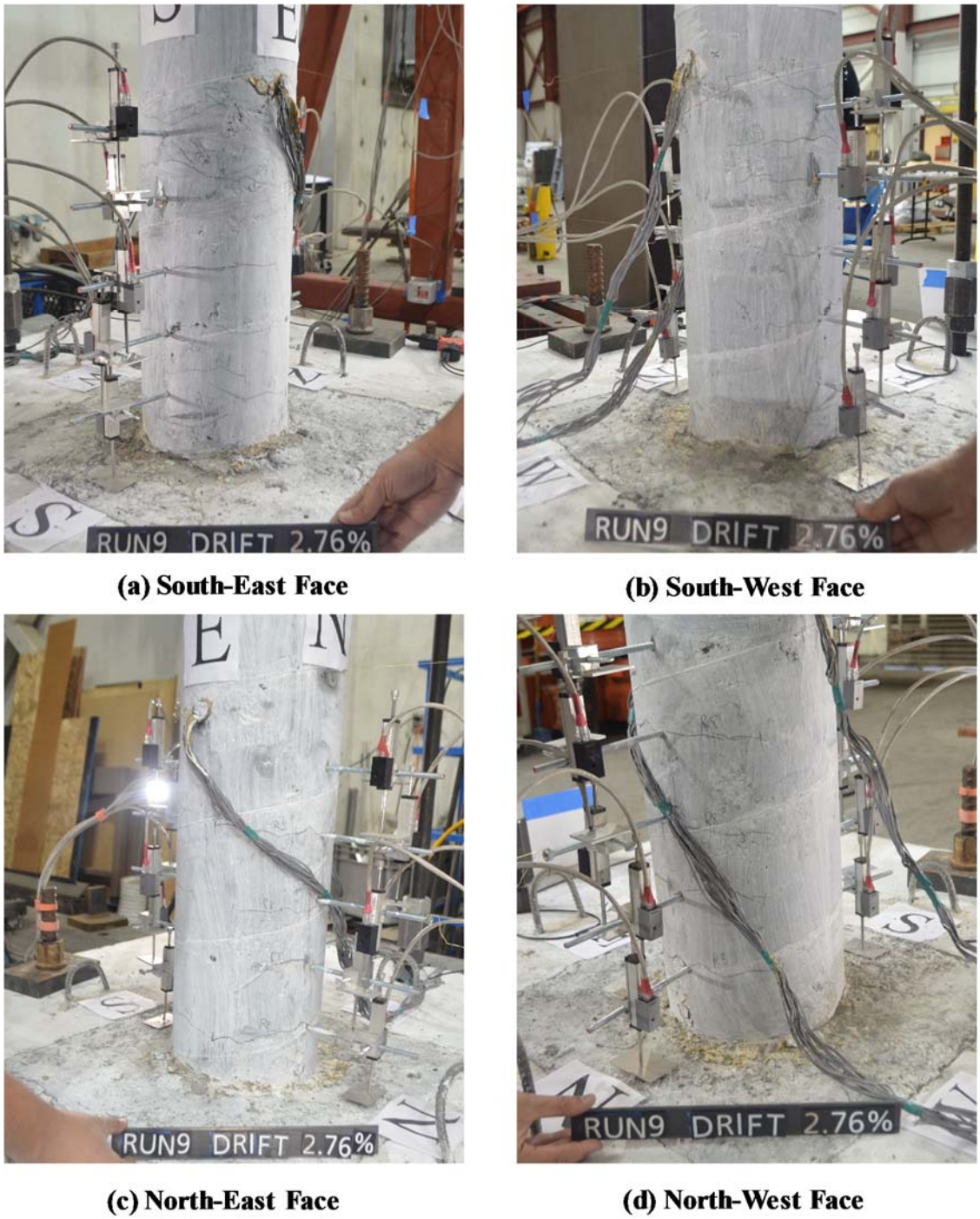


**(a) South-East Face** **(b) South-West Face**

**(c) North-East Face** **(d) North-West Face**

Figure 6-21 Damage observed at second cycle of 2.76% drift for specimen S4.


(a) South-East Face

(b) South-West Face

(c) North-East Face

(d) North-West Face

Figure 6-22 Damage observed at second cycle of 3.86% drift for specimen S4.

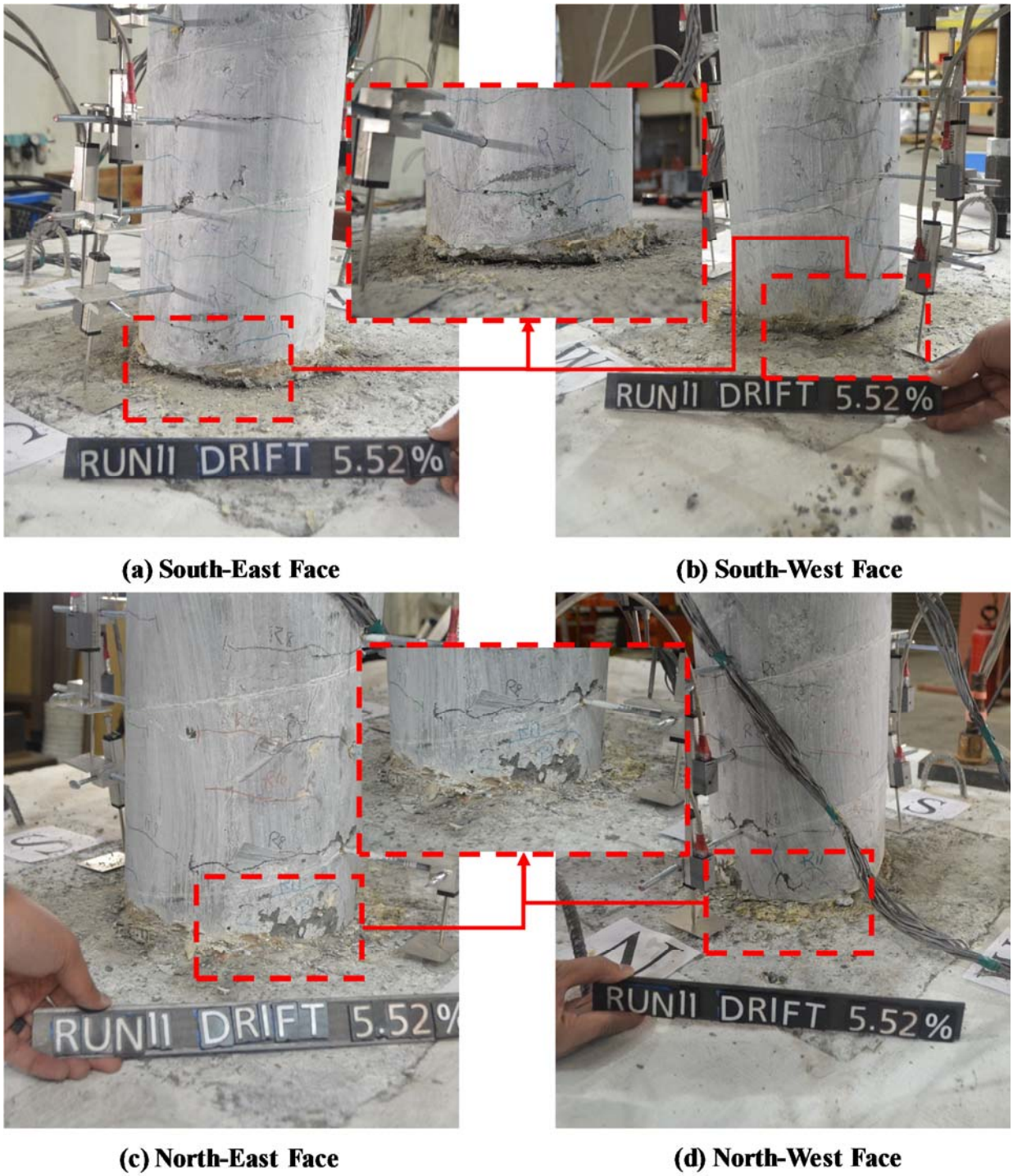


(a) South-East Face (b) South-West Face

(c) North-East Face (d) North-West Face

Figure 6-23 Damage observed at second cycle of 5.52% drift for specimen S4.

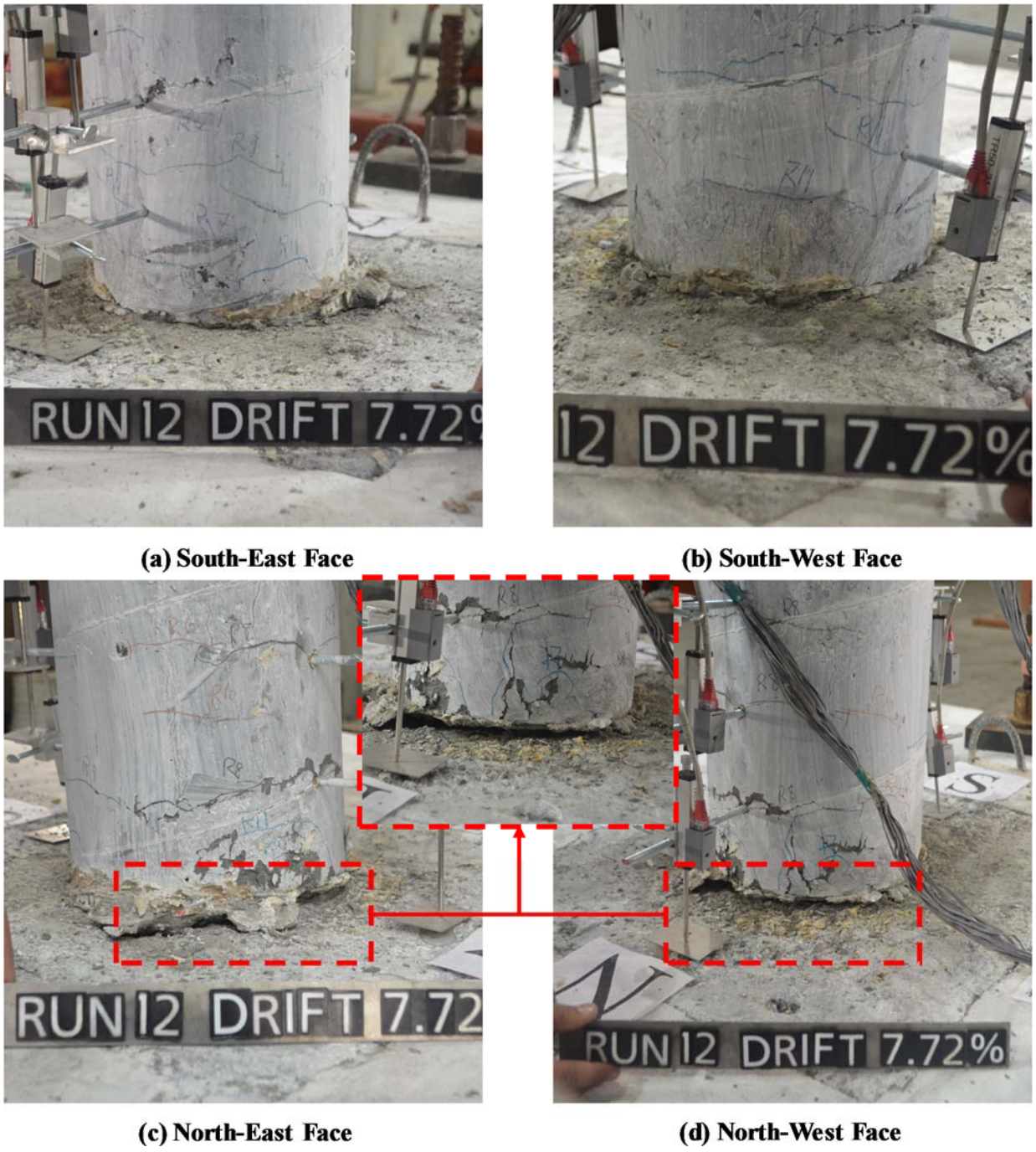


**(a) South-East Face** **(b) South-West Face**

**(c) North-East Face** **(d) North-West Face**

Figure 6-24 Damage observed at second cycle of 7. 27% drift for specimen S4.

### *6.1.2. Force-Drift Relationship*

Similar to S1 before, Figures 6-25 through 6-27 show the hysteretic behavior of the UHPC columns S2, S3 and S4, respectively. The positive values on the plot indicate pushing the column to the north direction. The force shown in this plot was recorded directly from the load cell while the column displacement was measured using several string potentiometers attached to the column head.

For specimen S2, the peak strength was reached and maintained at drift ratio of 5.52% for the push and pull directions, where the maximum reported lateral loads were 22.9 kips and 23.9 kips for the push and pull directions, respectively. For specimen S3, the peak strength was reached and maintained at drift ratio of 5.52% for the push and pull directions, where the maximum reported lateral loads were 20.2 kips and 24.7 kips for the push and pull directions, respectively. The asymmetric response in specimen S3 can be attributed to rebars misalignment during construction as previously observed in S1 and shown in Figure 6-28 for S3. For specimen S4, the peak strength was reached and maintained at drift ratios 5 % and 5.53% for the push and pull directions, respectively, where the maximum reported lateral loads were 19.6 kips and 20 kips for the push and pull directions, respectively.

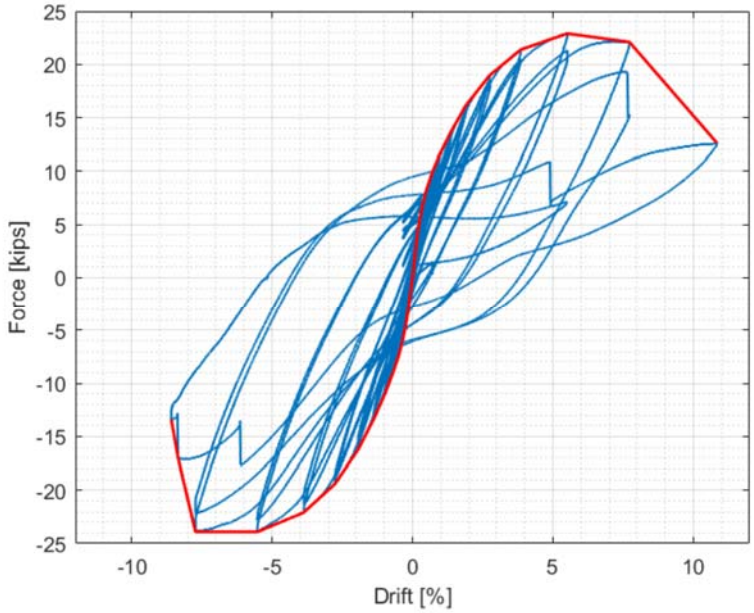


Figure 6-25 Global force-drift relationship for specimen S2.

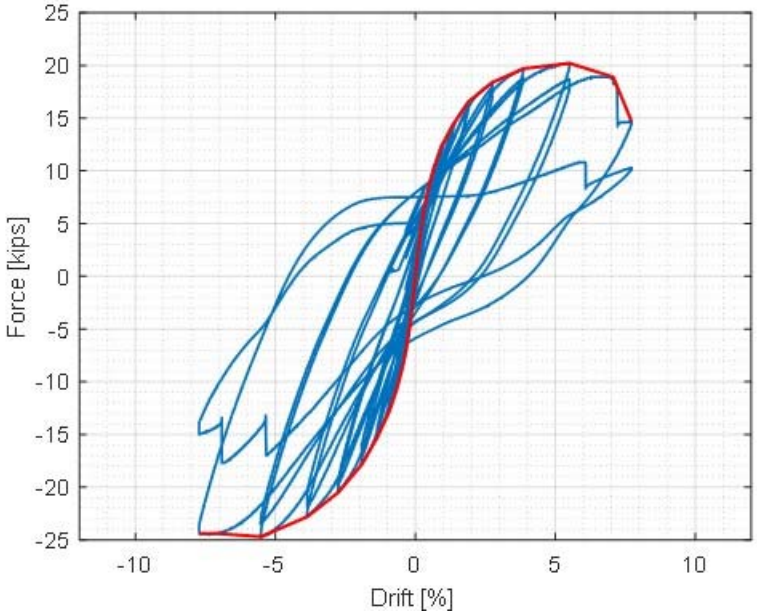


Figure 6-26 Global force-drift relationship for specimen S3.

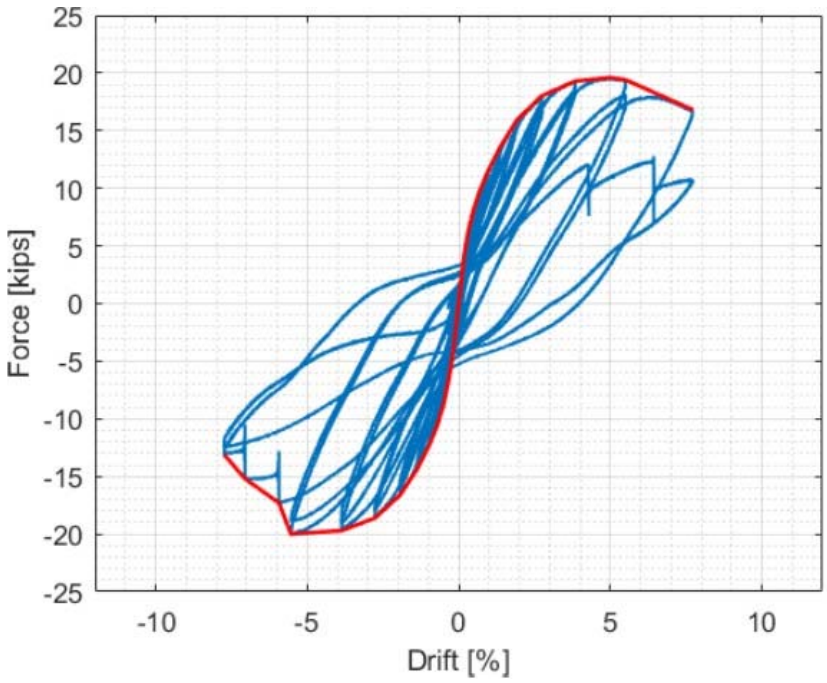


Figure 6-27 Global force-drift relationship for specimen S4.

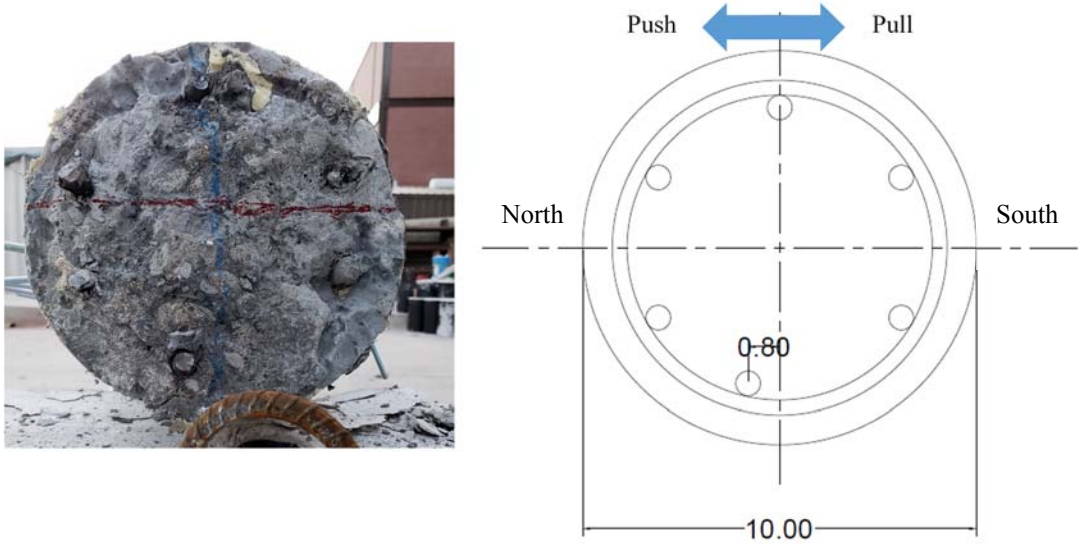


Figure 6-28 As-built S3 column cross-section observed after column separation from footing.

For Specimen S2, the first rebar to reach the proof strain was observed to be the south-west rebar at drift ratio of 2.21% at the first cycle of the 2.76% drift ratio run which can be observed from the strain history of the rebars at level 2 ( at 2 in above the footing level) shown in Figure 6-29. For Specimen S3, the first rebar to reach the proof strain was the south-east rebar at drift ratio of 1.39% at the first cycle of the 1.93% drift ratio run which can be observed from the strain history of the rebars also at level 2 shown in Figure 6-30. For Specimen S4, the first rebar to reach the proof strain was the south-west rebar at drift ratio of 2.1% at the first cycle of the 2.76% drift ratio run which can be observed from the strain history of the rebars at level 2 shown in Figure 6-31.

The first bar to rupture in specimen S2 was observed on the south-west rebar at drift ratio of 7.7% at the second cycle of the 7.72% drift ratio run which can be implied from the sudden drop of the strain at level 3 (at 6 in above the footing level) shown in Figure 6-32 and the sudden drop of the measured force in the force history relation showed in Figure 6-33. The first bar to rupture in specimen S3 was observed on the south-west rebar at drift ratio of 7.2% at the first cycle of the 7.72% drift ratio run which can be implied from the sudden drop of the strain at level 3 shown in Figure 6-34 and force drop illustrated in Figure 6-35. The first bar to rupture in specimen S4 was observed on the north-east rebar at drift ratio of 5.86% at the first cycle of the 7.72% drift ratio run which can be implied from the sudden drop of the strain and force as shown in Figures 6-36 and 6-37, respectively.

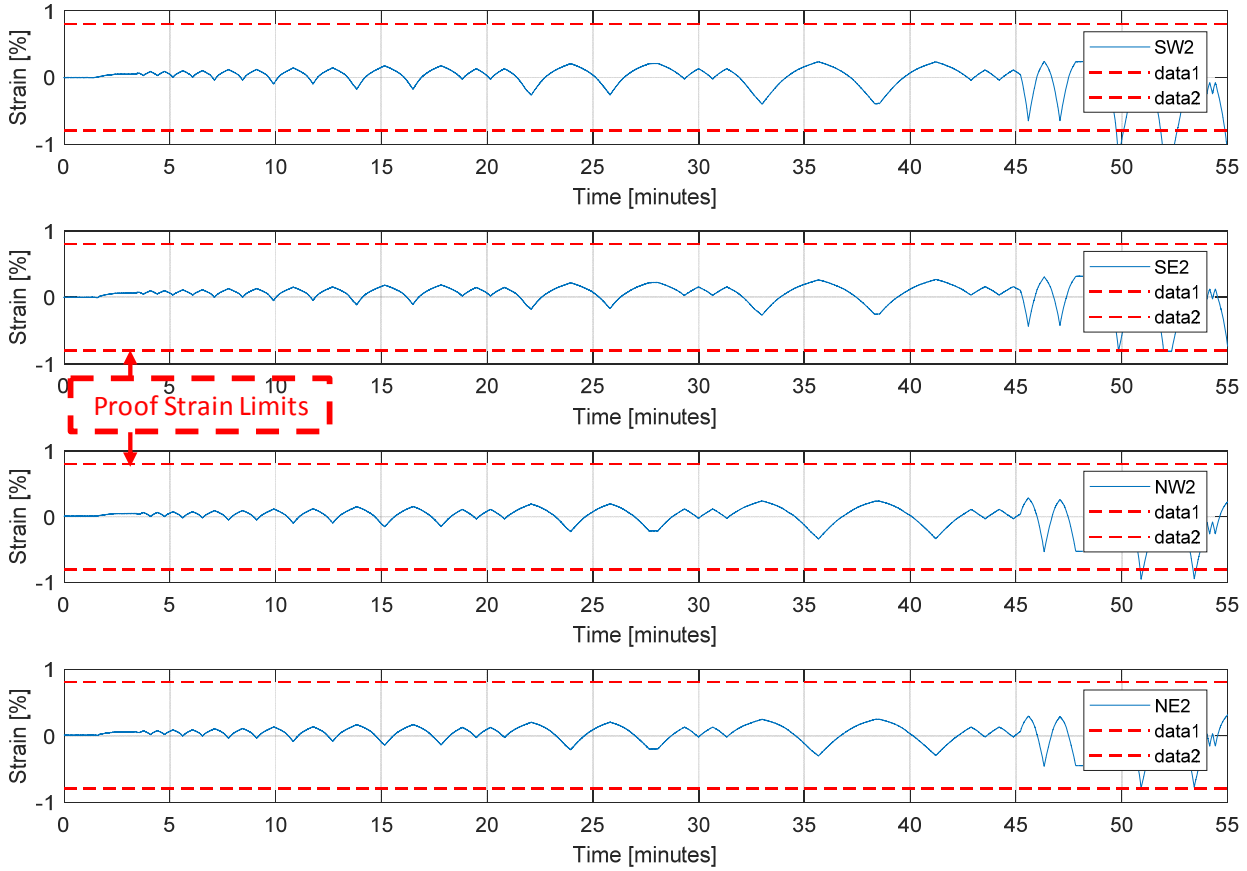


Figure 6-29 Rebars strain history at level 2 at 2 in above footing for specimen S2.

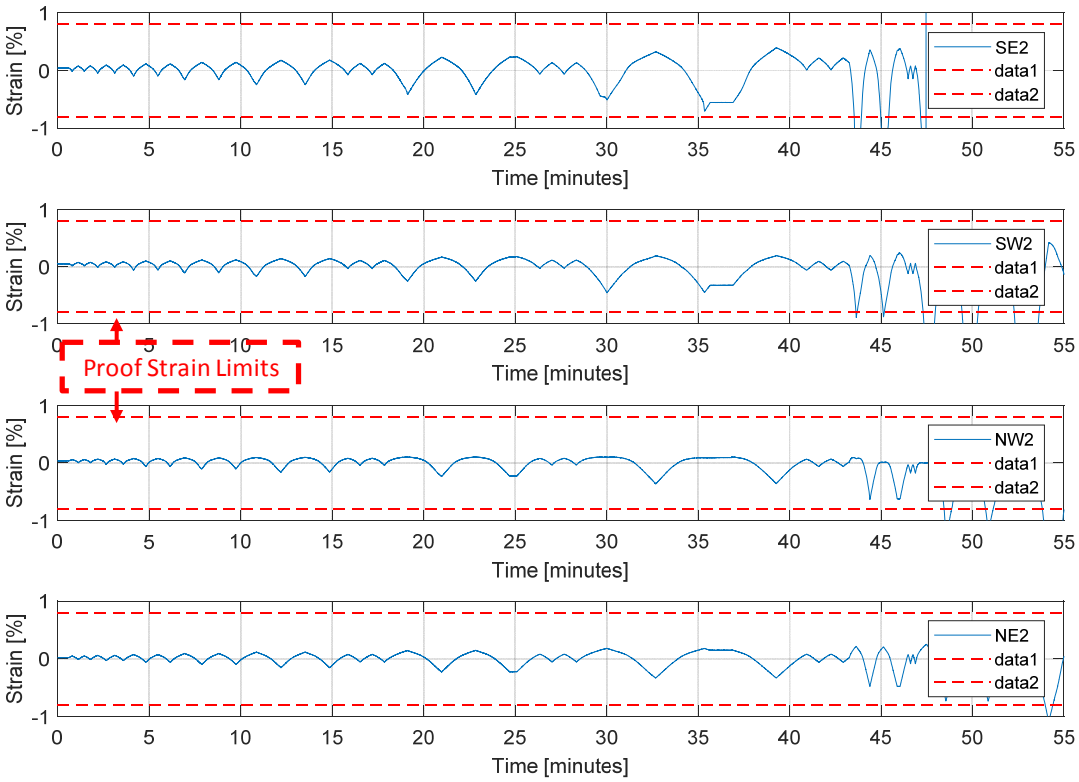


Figure 6-30 Rebars strain history at level 2 at 2 in above footing for specimen S3.

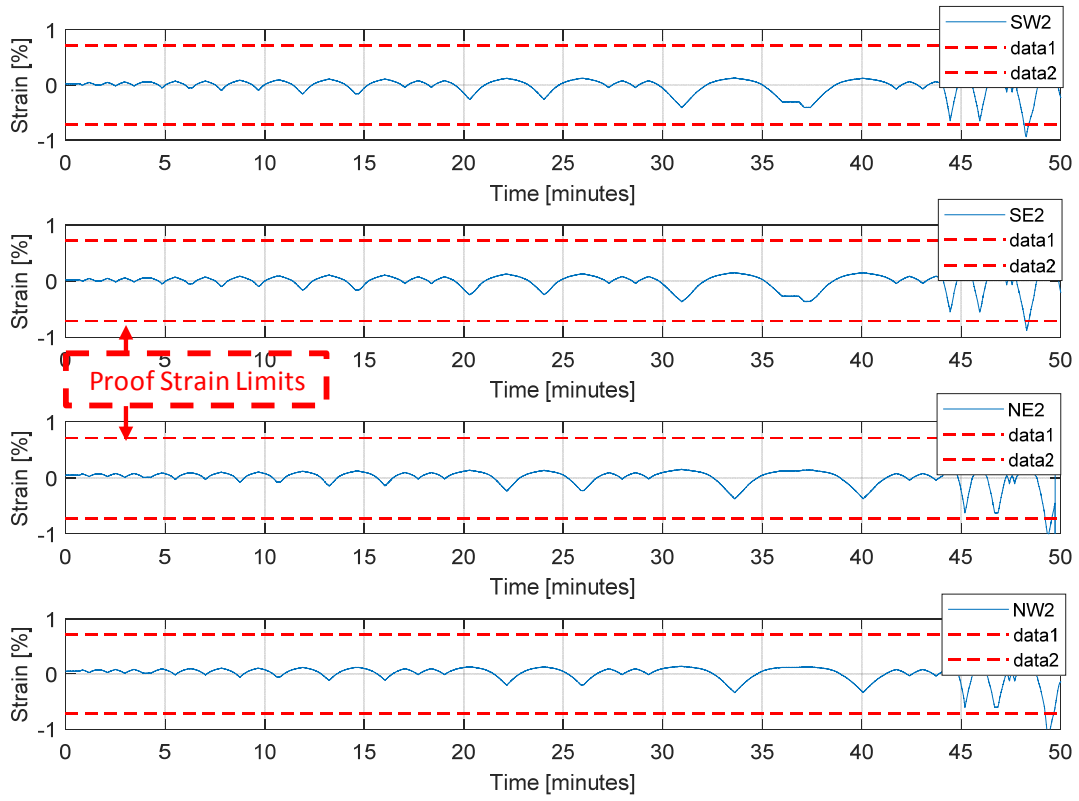


Figure 6-31 Rebars strain history at level 2 at 2 in above footing for specimen S4.

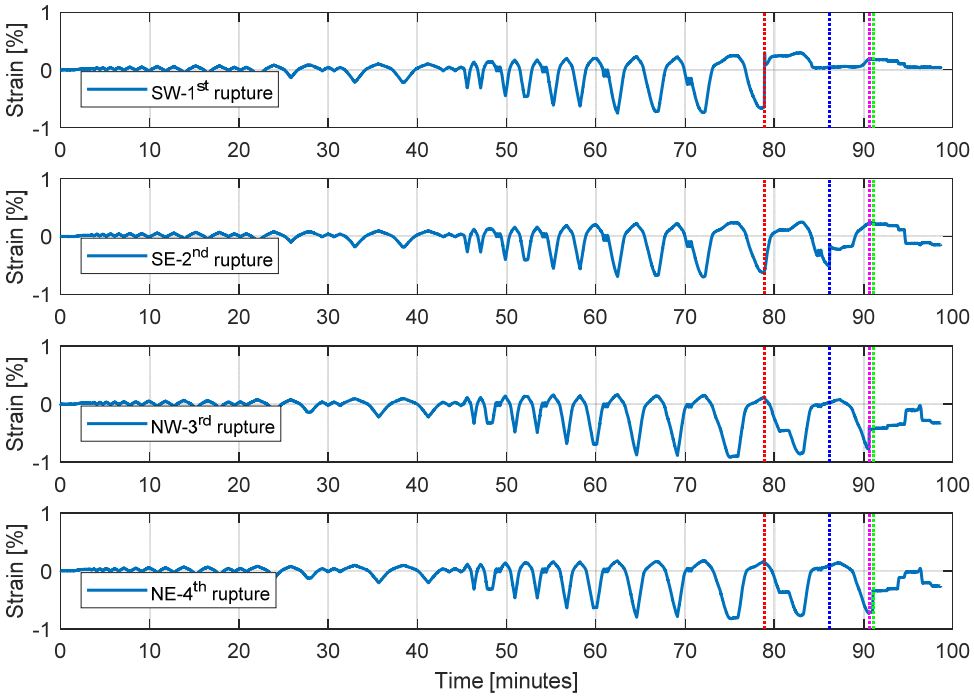


Figure 6-32 Rebars strain history at level 3 at 6 in above footing for specimen S2 where sequence of rebars rupture can be implied.

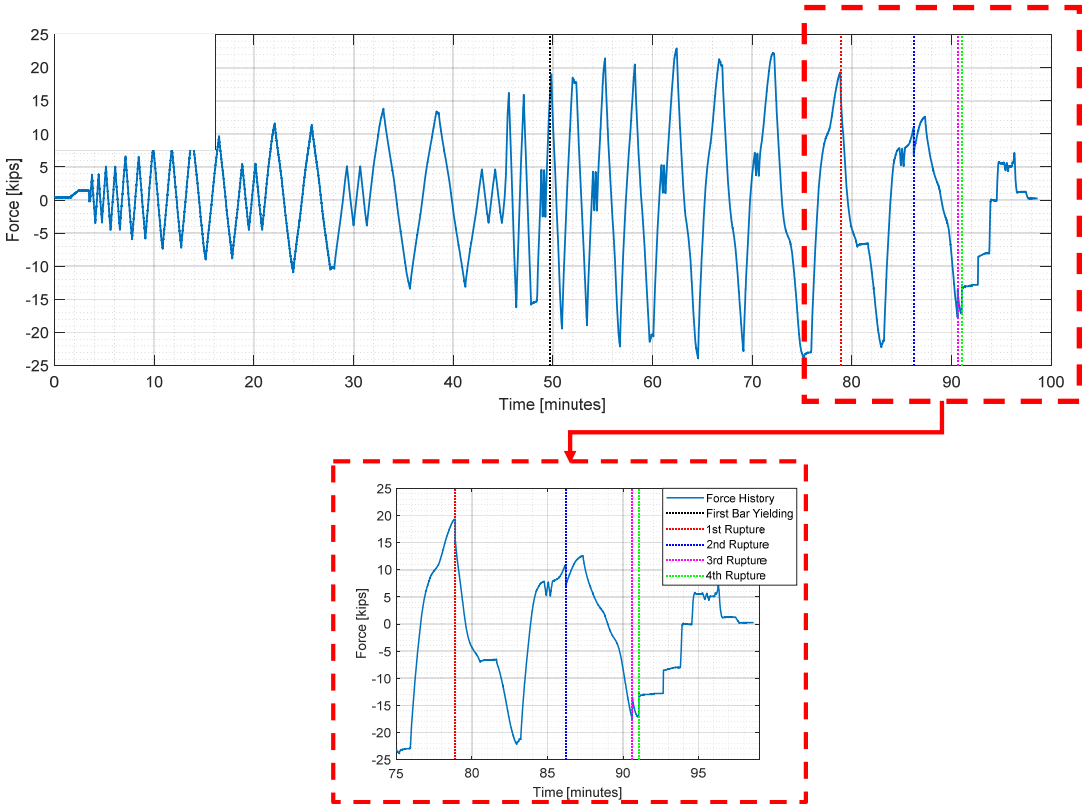


Figure 6-33 Lateral force history for S2 test and sequence of rebar rupture identified.

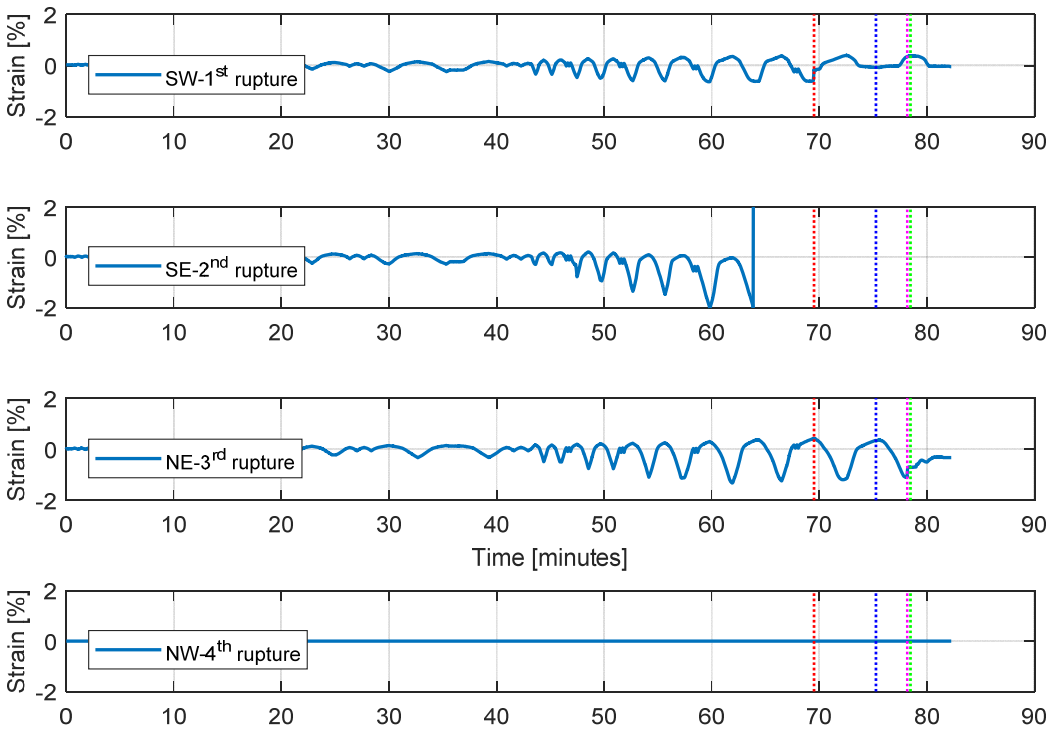


Figure 6-34 Rebars strain history at level 3 at 6 in above footing for specimen S3 where sequence of rebars rupture can be implied.

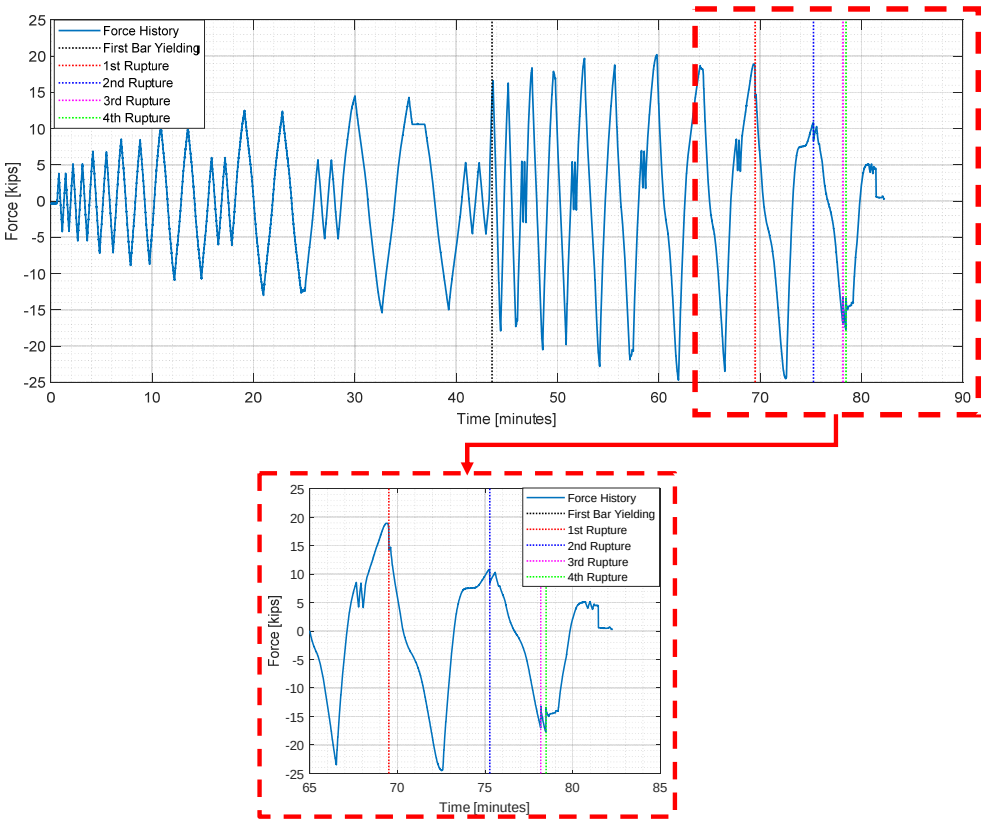


Figure 6-35 Lateral force history for S3 test and sequence of rebar rupture identified.

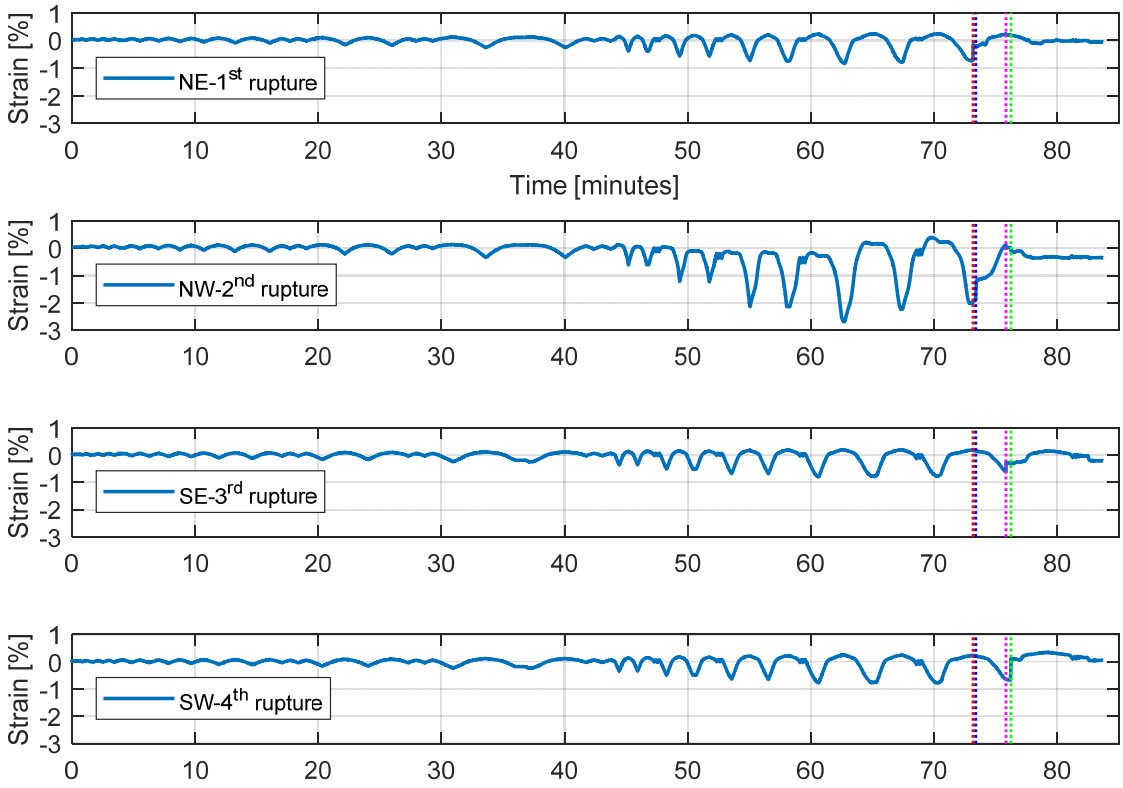


Figure 6-36 Rebars strain history at level 3 at 6 in above footing for specimen S4 where sequence of rebars rupture can be implied.

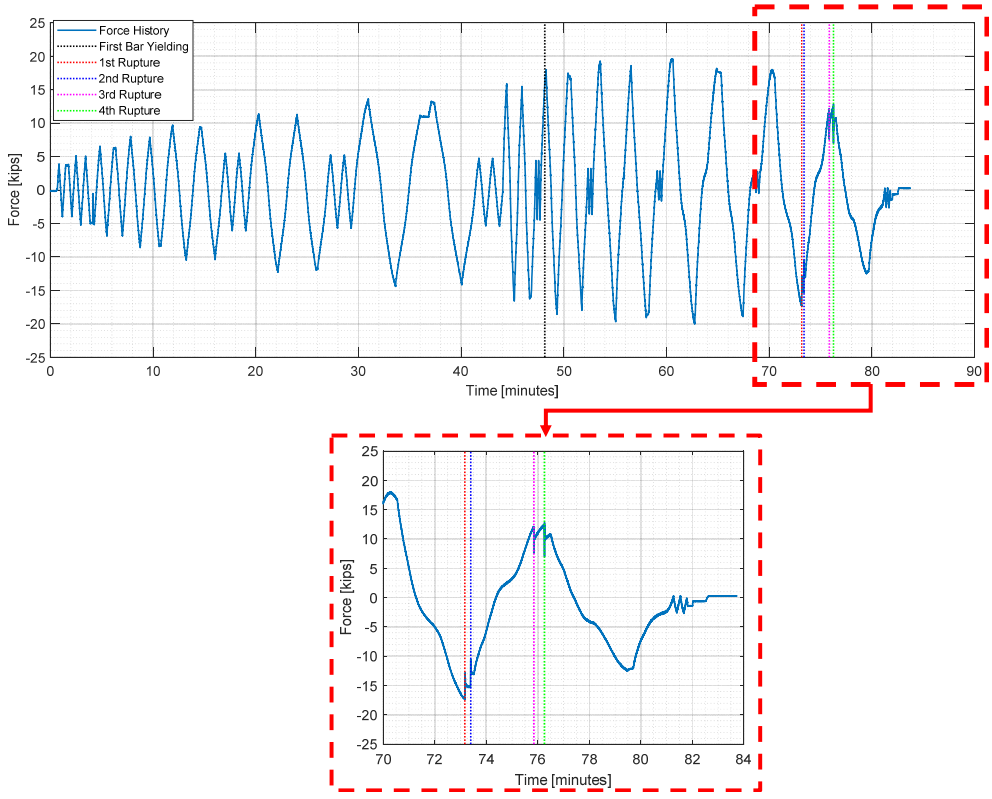


Figure 6-37 Lateral force history for S4 test and sequence of rebar rupture identified.

The backbone of the hysteresis curves in the positive and negative displacement regions and their idealized elasto-plastic idealization are shown in Figures 6-38 through 6-40 for specimens S2, S3 and S4, respectively. The recorded drift histories with the projected first bar yielding and the rebar rupture sequence are shown in Figures 6-41 through 6-43 for S2, S3 and S4, respectively.

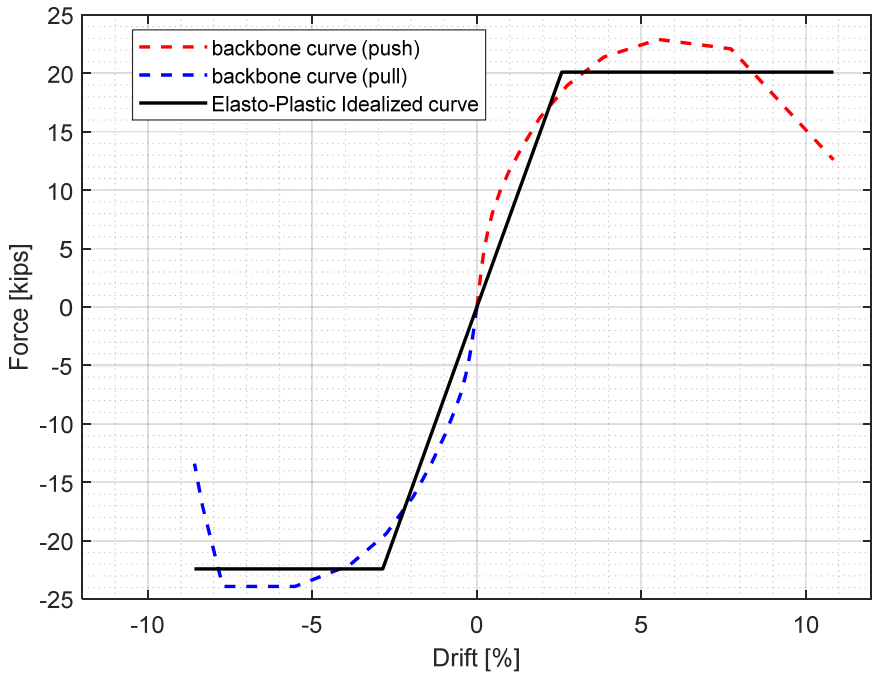


Figure 6-38 Backbone for force-drift relationship and elasto-plastic idealization for S2.

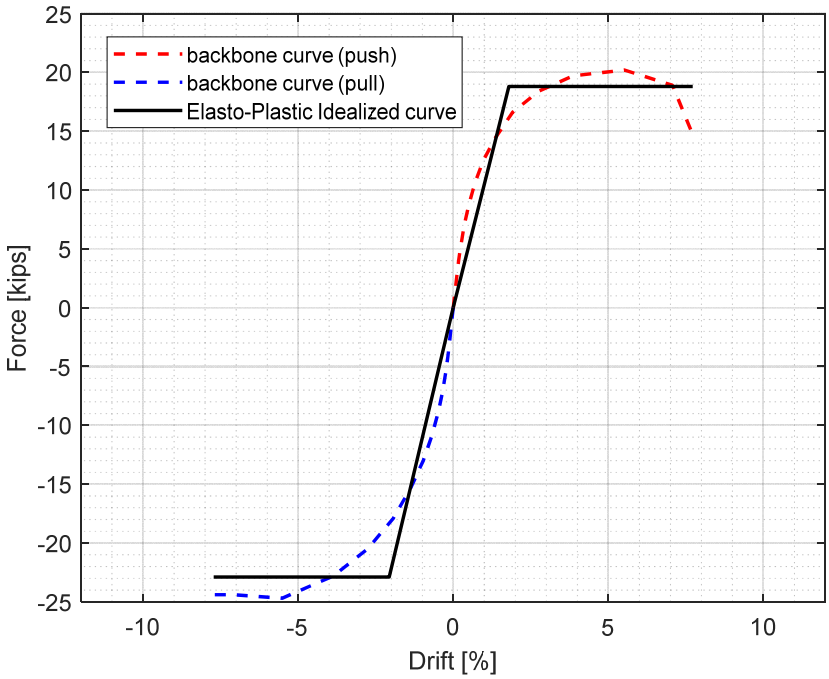


Figure 6-39 Backbone for force-drift relationship and elasto-plastic idealization for S3.

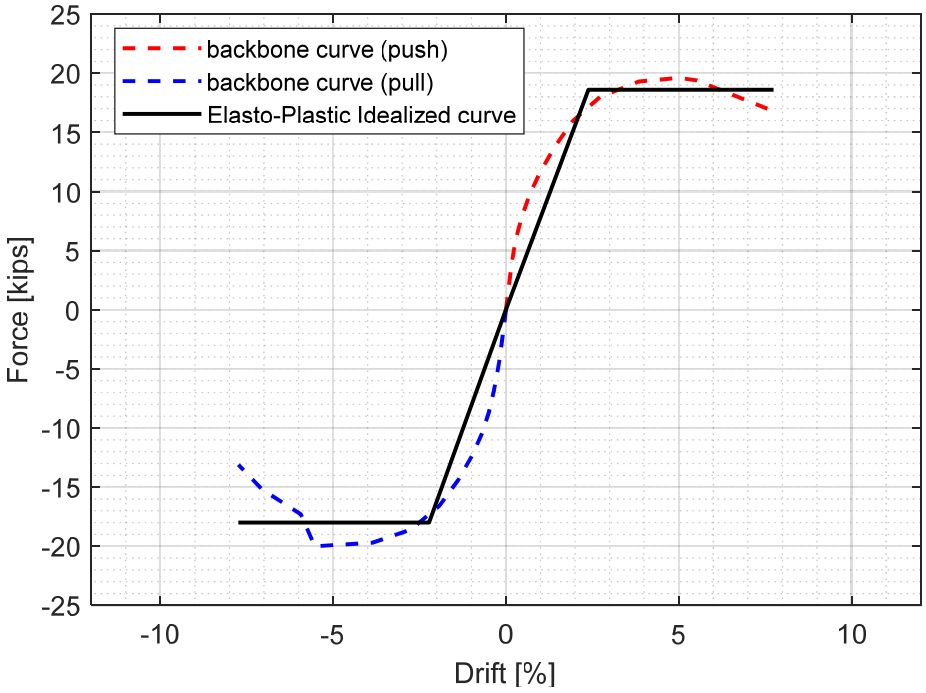


Figure 6-40 Backbone for force-drift relationship and elasto-plastic idealization for S4.

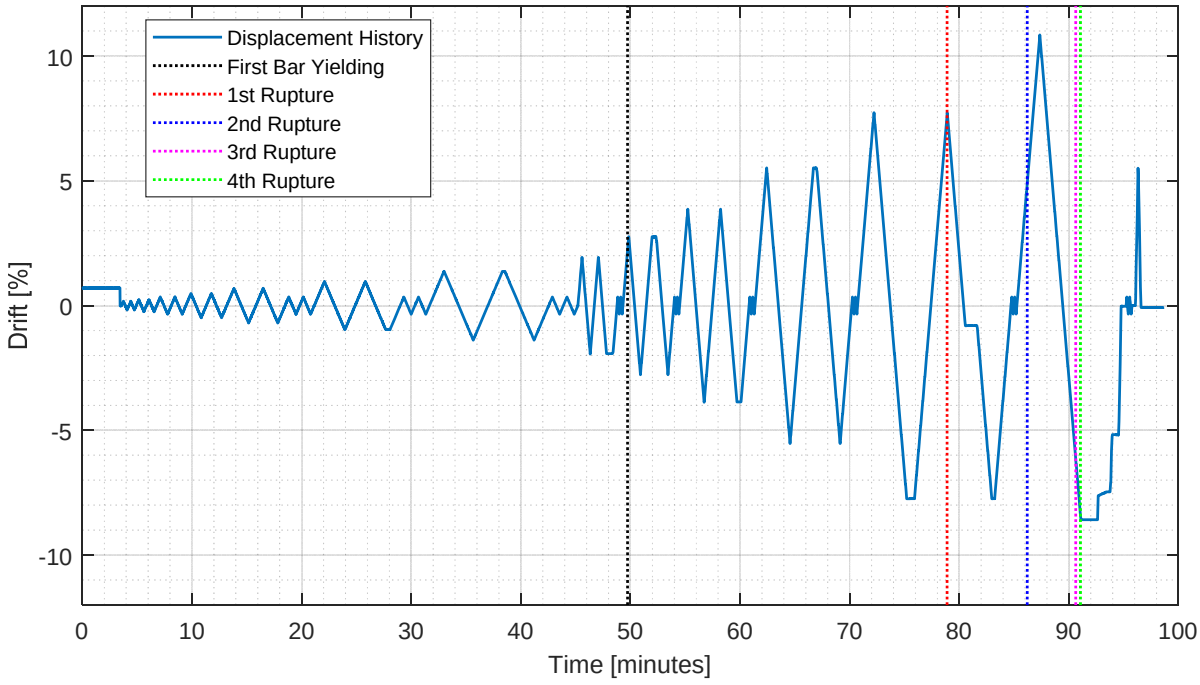


Figure 6-41 Recorded drift history and rebar rupture sequence for specimen S2.

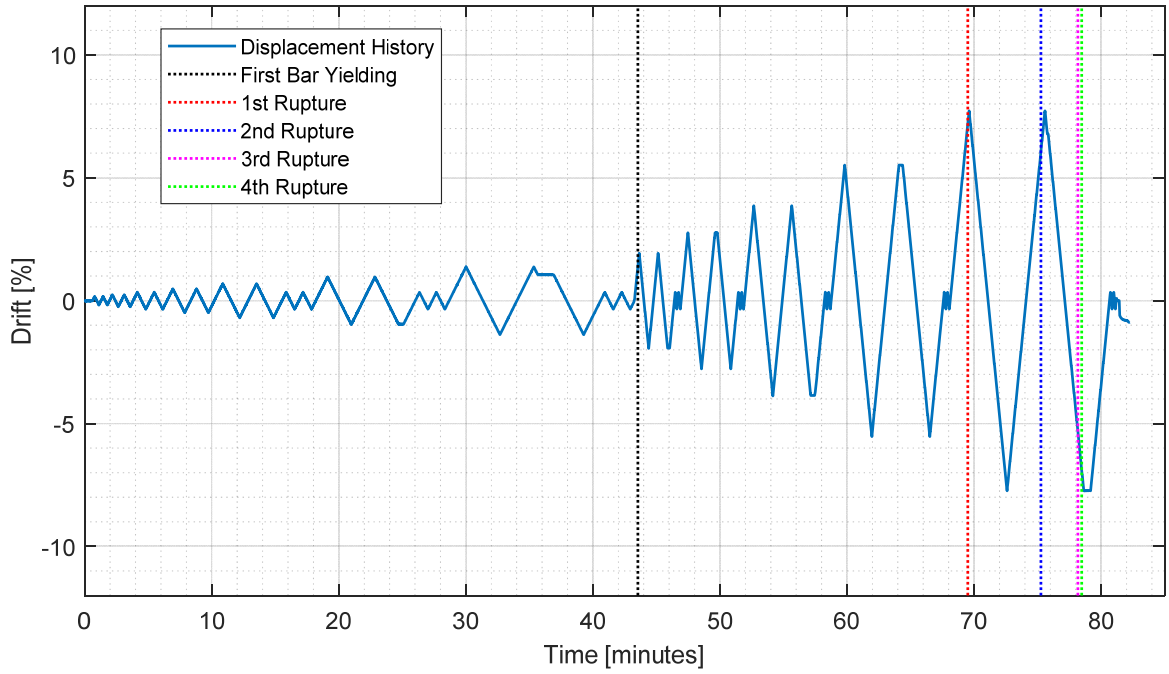


Figure 6-42 Recorded drift history and rebar rupture sequence for specimen S3.

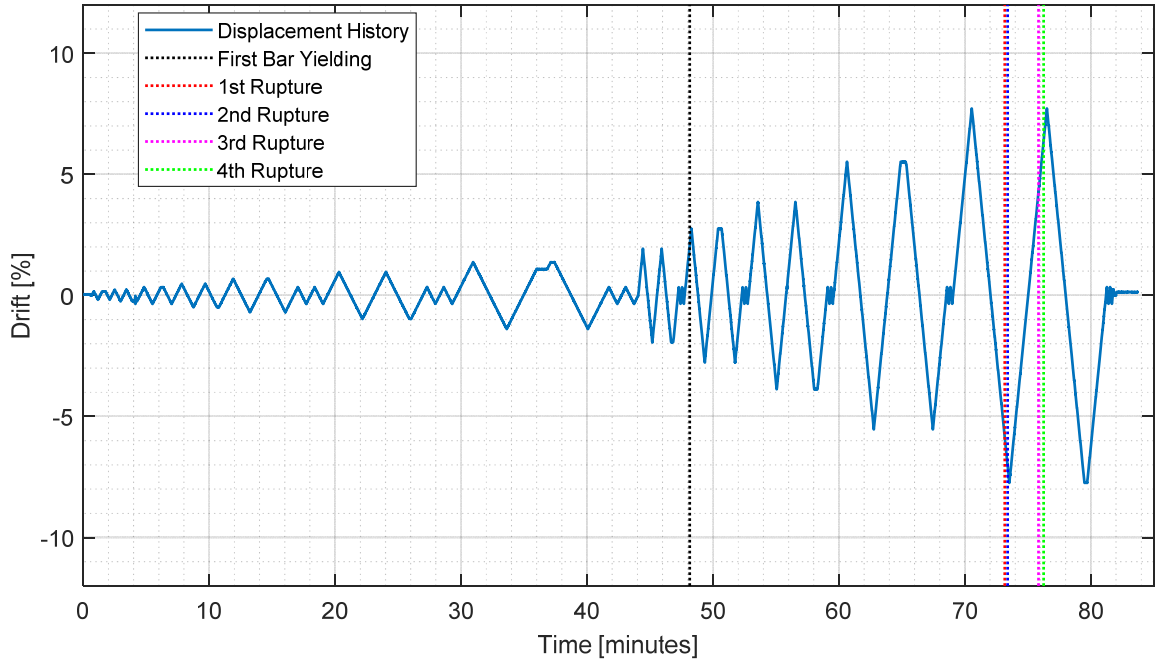


Figure 6-43 Recorded drift history and rebar rupture sequence for specimen S4.

### *6.1.3. Stiffness Degradation*

The stiffness degradation of Group II UHPC columns was investigated at different drift ratios. As shown in Figure 6-44, all three columns lost about 50% of the initial stiffness at about 2% drift ratio. The initial stiffness determined form the tests were 37.1, 40.7 and 40.1 kips/in for specimens S2, S3 and S4, respectively. Those values were found to be corresponding to an initial stiffness of about 0.60, 0.64 and 0.65 $E_cI_g$ for specimens S2, S3 and S4, respectively.

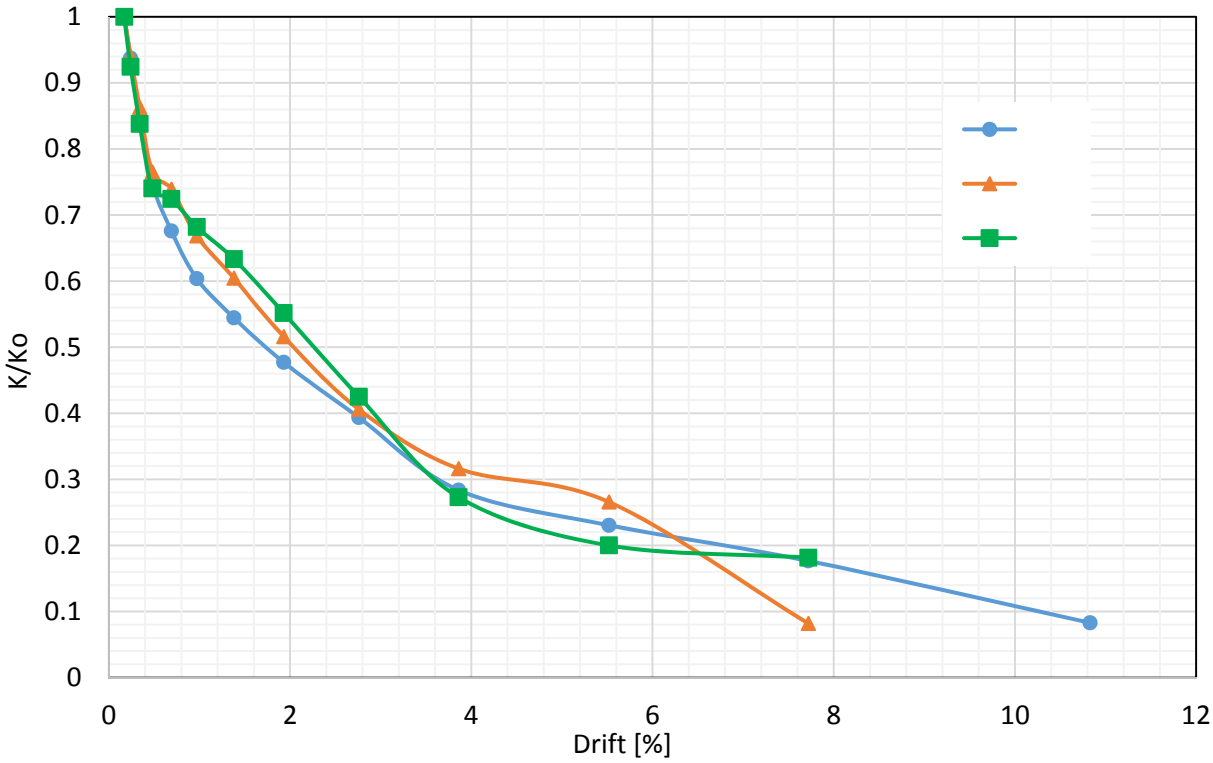


Figure 6-44 Stiffness degradation of S2, S3, and S4 as relates to drift ratio.

## 6.2. Column Local Behavior

### *6.2.1. Strains*

The longitudinal reinforcement strain profiles at the plastic hinge region are shown in Figures 6-45 through 6-47 for specimens S2, S3 and S4, respectively. The strains values reported in the figures are the maximum absolute strains of the two complete cycles at each drift ratio. A sample of the strain gage profiles is reported and shown at 0.97, 1.93 and 3.86% drift ratios. It can be seen that the reinforcing bar strains were well distributed in the plastic hinge region of the column-footing interface as they had the maximum strains near the column-footing interface and small strains away from it. The transverse reinforcement strain profiles at the plastic hinge region are shown in Figures 6-48 for all three specimens S2, S3 and S4. A sample of the strain gage profiles is reported and shown at 0.97, 1.93, 3.86, 5.52, 7.72 and 10.83% drift ratios. For specimen S3, it is noted that the strain gauge at level 1 (2 in below footing level) have stopped working after the 3.86% drift run, while for specimen S4, the same strain gauge has stopped working after the 5.52% drift run. It is observed that none of the hoops yielded and the recorded strains were very small which did not exceed 0.1% strain. The low values of hoops strains indicates that confinement is not activated especially that no cover spalling happened in the plastic hinge region or rebars were exposed or buckled. Moreover, the UHPC itself provides a good confinement due to the steel fibers without engaging the transverse reinforcement.

### *6.2.2. Curvature Profiles*

The curvature profiles at the plastic hinge region reported at different drift levels are shown in Figures 6-49 through 6-51 for specimens S2, S3 and S4, respectively. Curvatures were measured

indirectly by using displacement transducers mounted on both loading sides of the columns as illustrated before in Figure 4-20. Curvatures at each level were computed as the ratio of the section rotations of that level to the vertical distance of the transducers, where in turn, the rotations were the ratio of the summation of the relative displacements to the horizontal distance between the transducers in the same level. The curvature was measured at five levels. The curvature of the columns at the base was the highest mainly because of yield penetration at the column-footing interface.

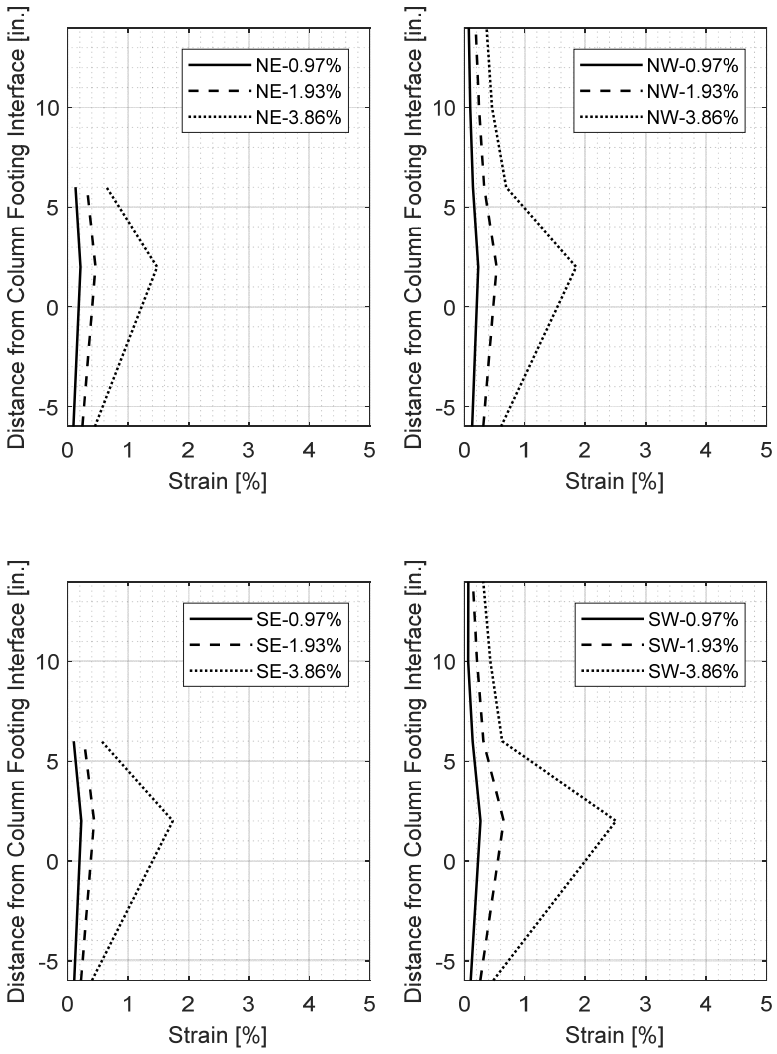


Figure 6-45 Distribution of the longitudinal rebars strains within the plastic hinge region for specimen S2.

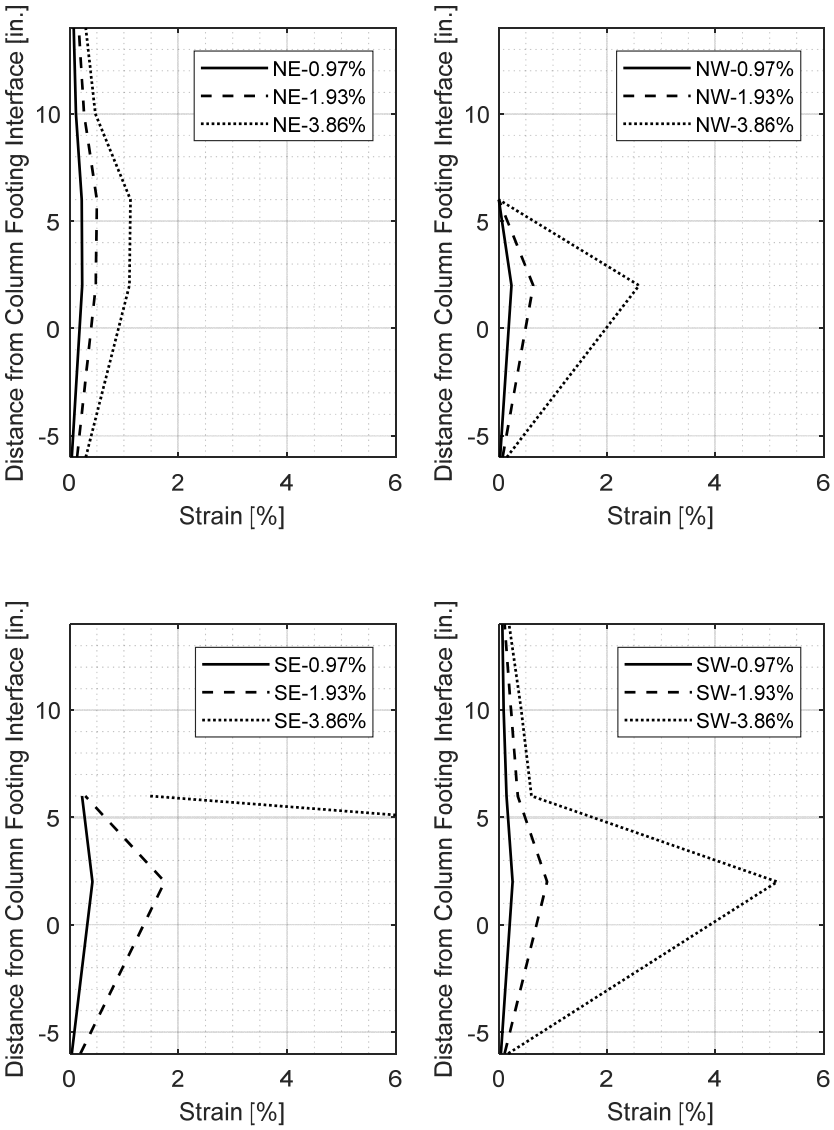


Figure 6-46 Distribution of the longitudinal rebars strains within the plastic hinge region for specimen S3.

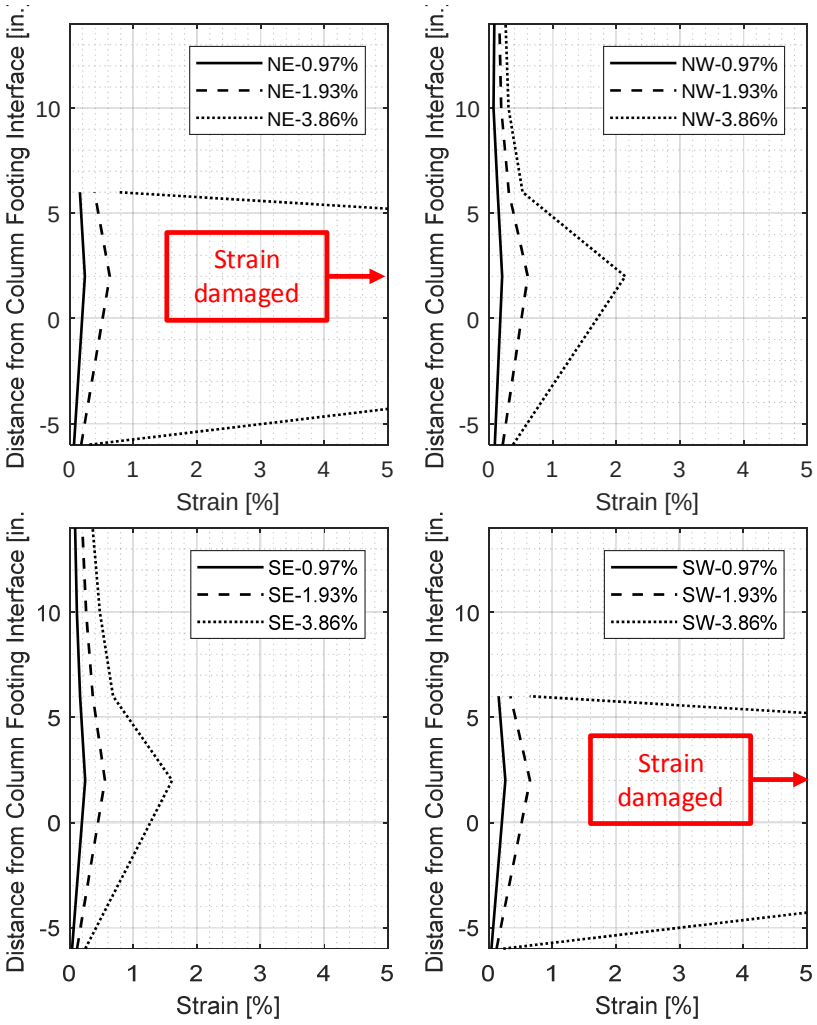


Figure 6-47 Distribution of the longitudinal rebars strains within the plastic hinge region for specimen S4.

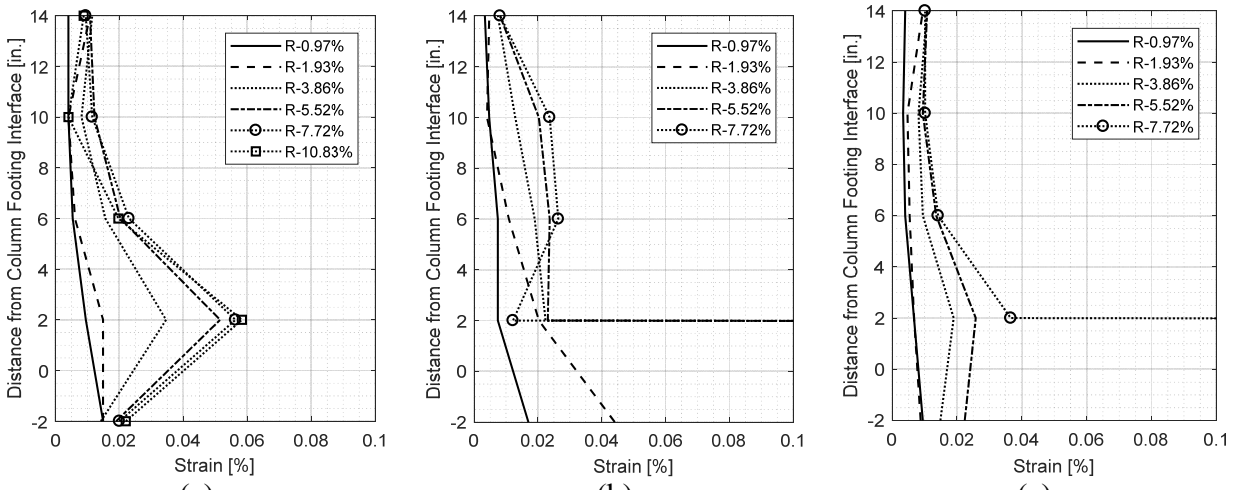


(a) (b) (c)

Figure 6-48 Distribution of the transverse reinforcement (hoops) strains within the plastic hinge region for specimens: (a) S2, (b) S3, and (c) S4.

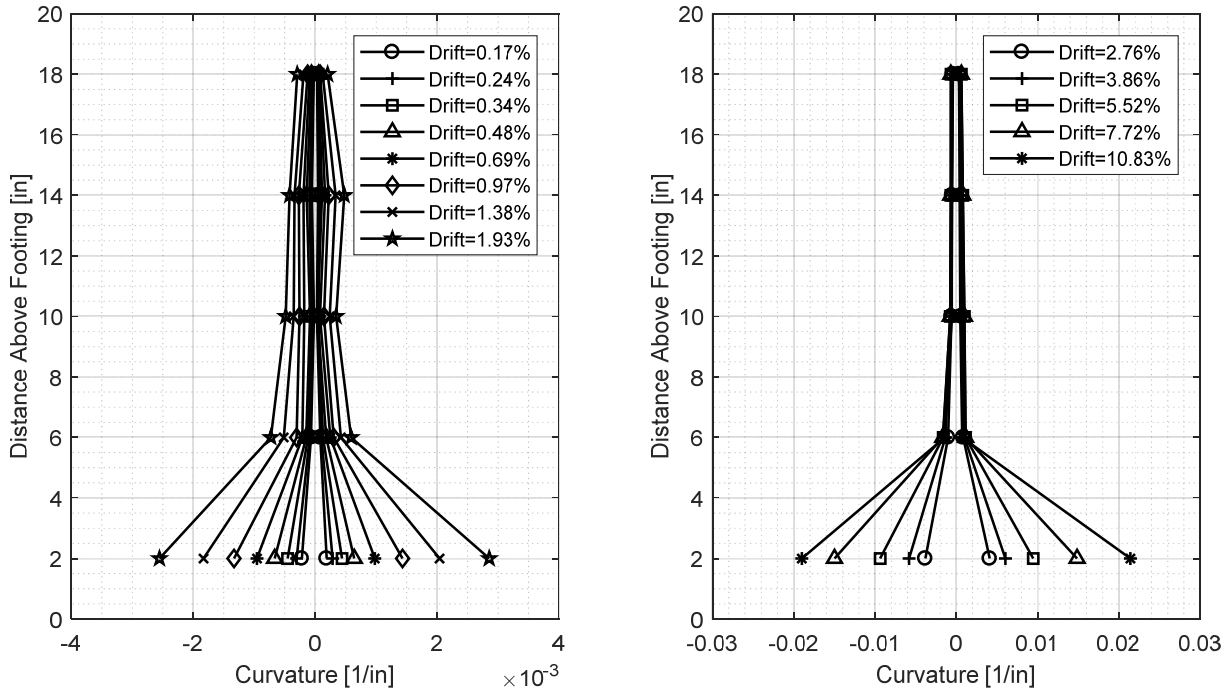


Figure 6-49 Curvature profile along the plastic hinge zone for specimen S2.

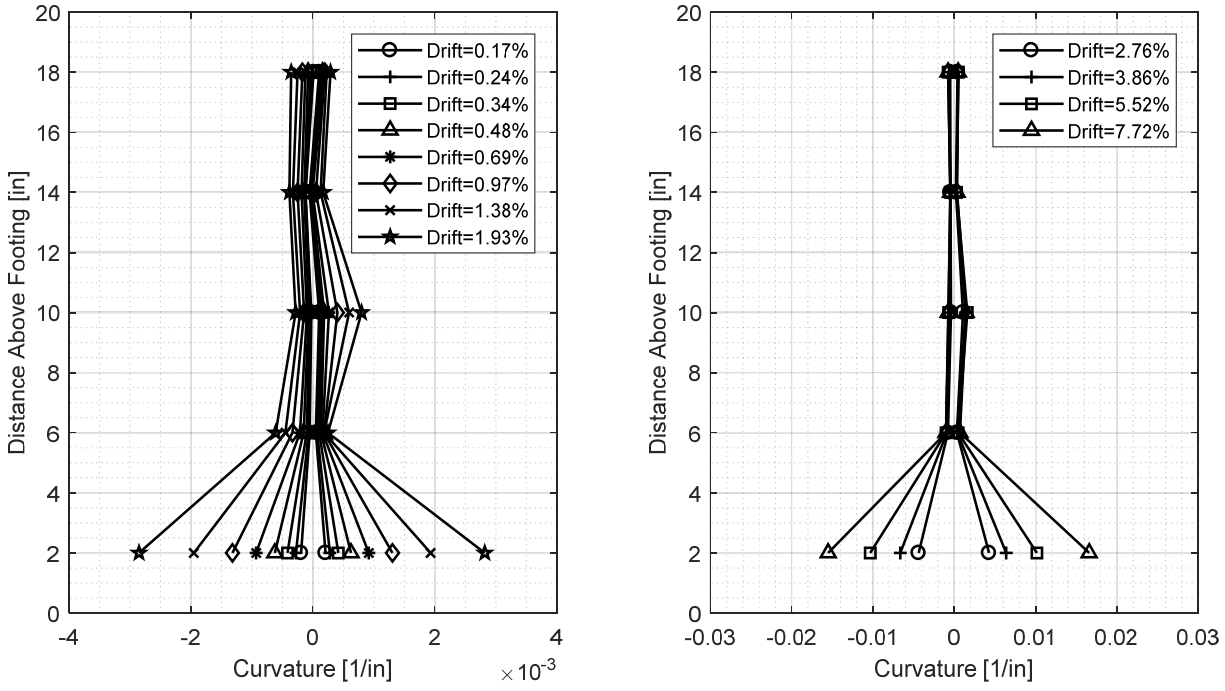


Figure 6-50 Curvature profile along the plastic hinge zone for specimen S3.

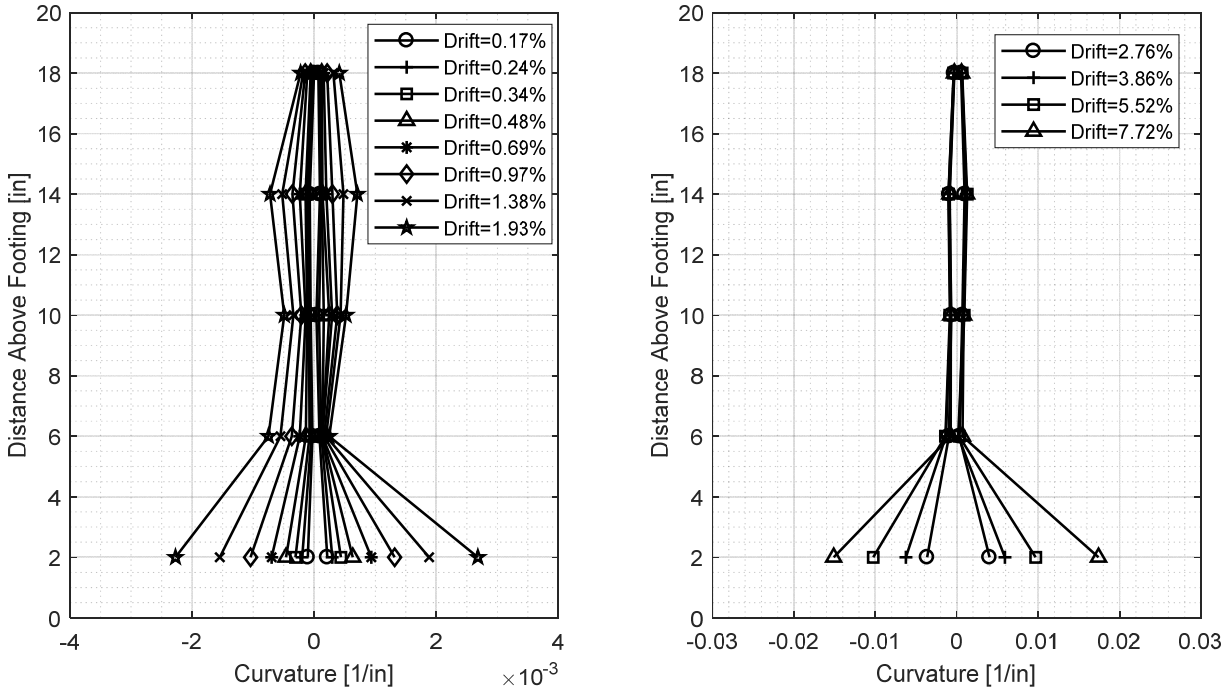


Figure 6-51 Curvature profile along the plastic hinge zone for specimen S4.

### *6.2.3. Moment-Curvature Behavior*

The moment curvature hysteretic curves of specimens S2, S3 and S4 were obtained and shown in Figures 6-52 through 6-54, respectively. The moment curvature backbone curves and the idealized elasto-plastic curves were also obtained and shown in Figures 6-55 through 6-57 for specimens S2, S3 and S4, respectively. For specimen S2, the maximum moment capacity in the push and pull loading sides is 1,328 kip-in and 1,386 kip-in, respectively. Using the idealized elasto-plastic curves, the curvature ductility is determined to be equal to 5.25. For specimen S3, the maximum moment capacity in the push and pull loading sides is 1,172 kip-in and 1,433 kip-in, respectively, while the curvature ductility is determined to be equal to 6.15. For specimen S4, the maximum moment capacity in the push and pull loading sides are 1,137 kip-in and 1,160 kip-in, respectively, while the curvature ductility is determined to be equal to 5.65.

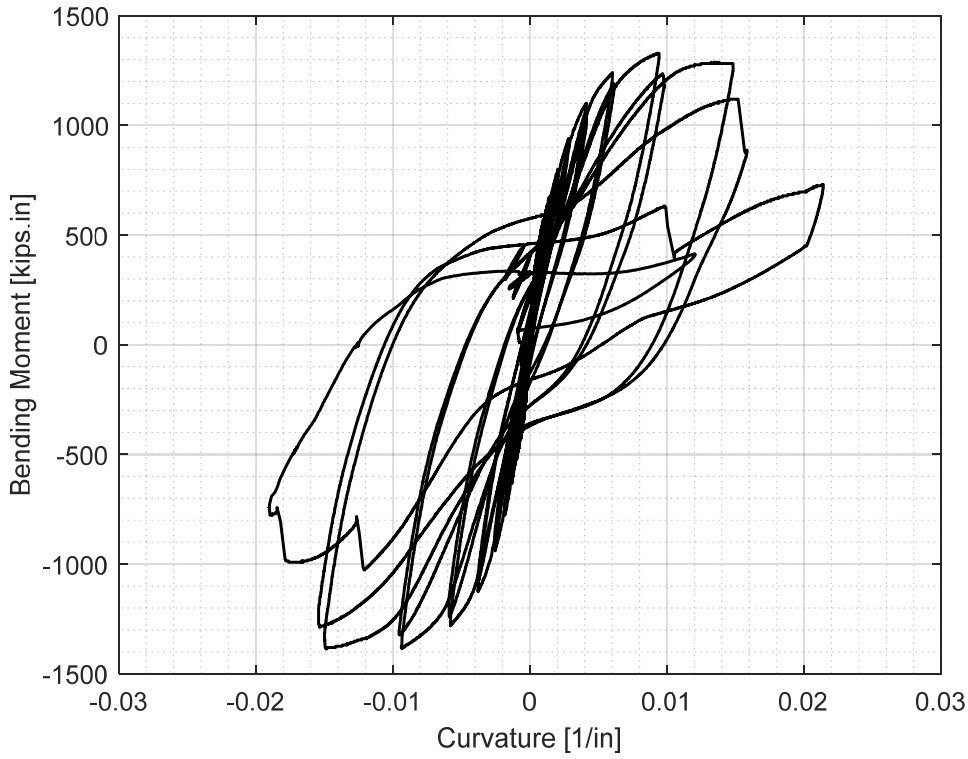


Figure 6-52 Moment-curvature relationship as obtained from S2 test.

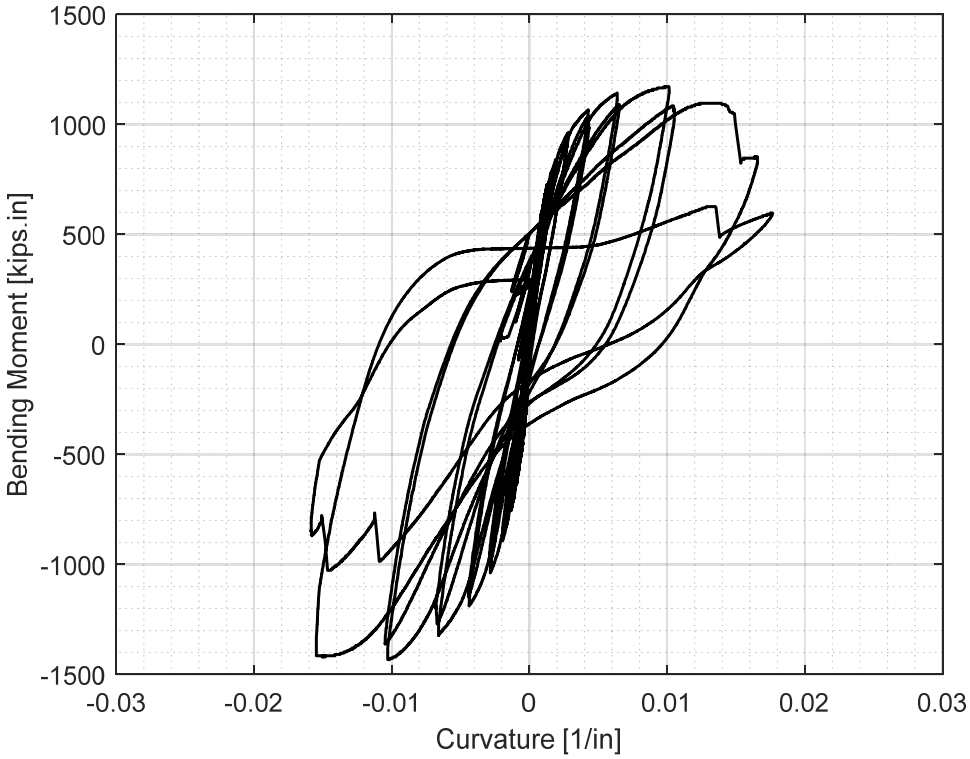


Figure 6-53 Moment-curvature relationship as obtained from S3 test.

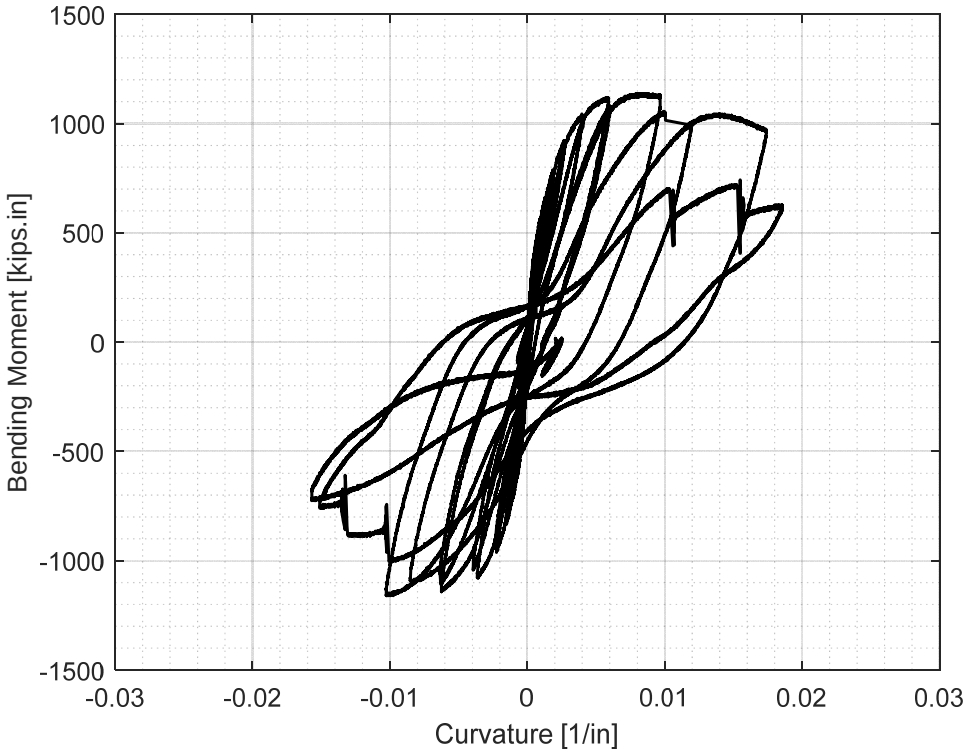


Figure 6-54 Moment-curvature relationship as obtained from S4 test.

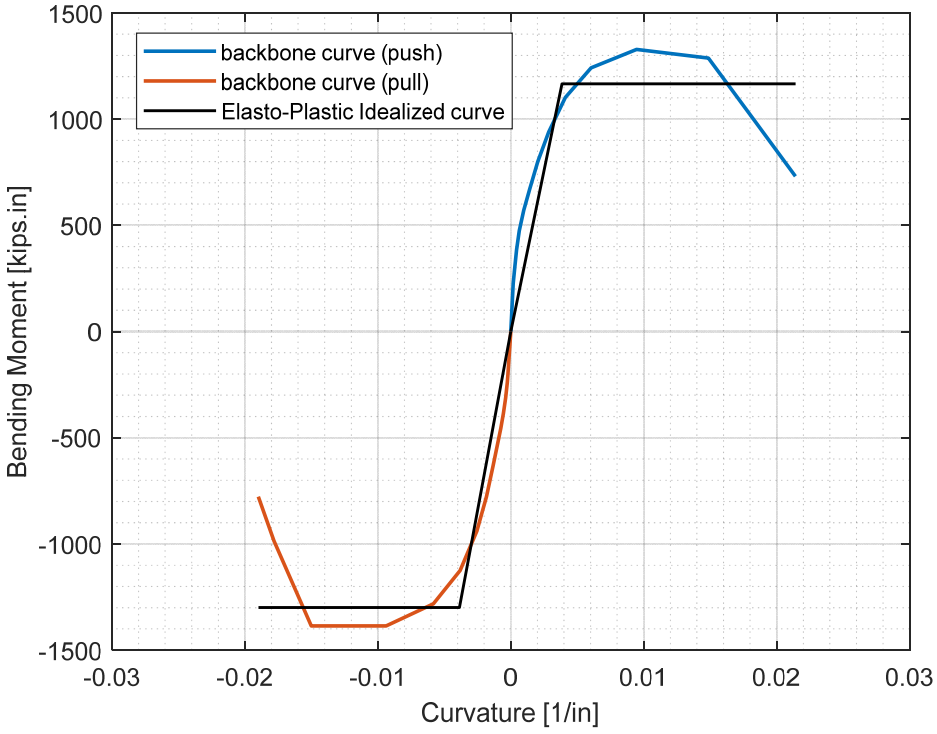


Figure 6-55 Moment-curvature backbone curves with elasto-plastic idealization for S2.

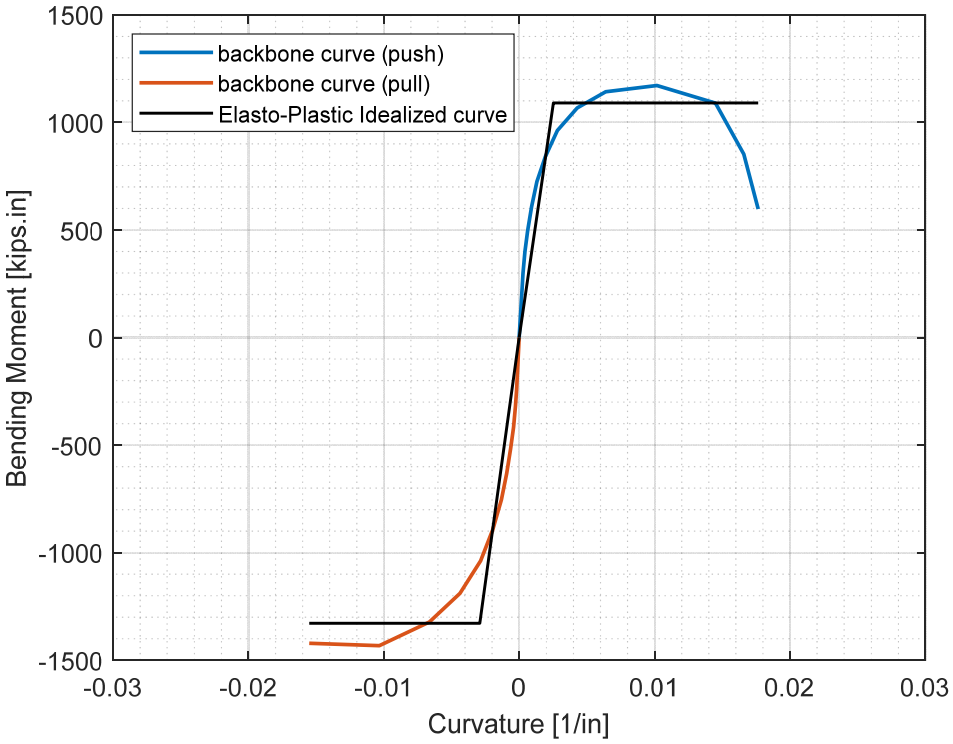


Figure 6-56 Moment-curvature backbone curves with elasto-plastic idealization for S3.

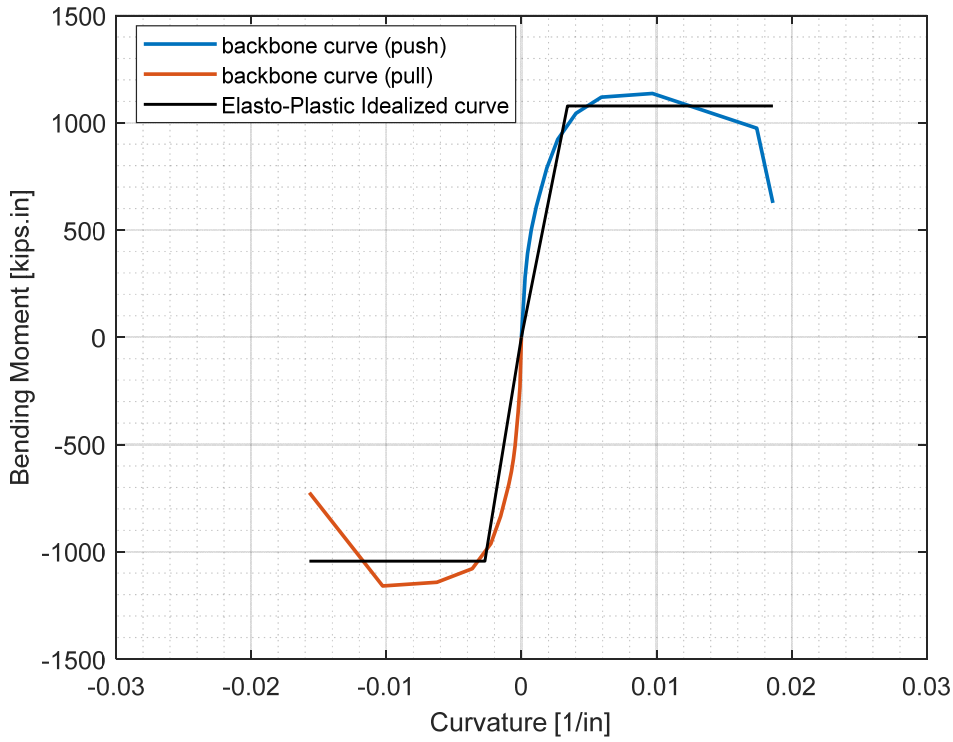


Figure 6-57 Moment-curvature backbone curves with elasto-plastic idealization for S4.

## 6.3. Comparison between Group I and Group II Specimens

### *6.3.1. Global Behavior*

For the sake of the comparison between the Group I and Group II specimens, an average backbone curve for the force-drift curves of the push and pull directions was obtained for every specimen. The average backbone curves for specimens S0 through S4 are plotted together for convenience as shown in Figure 6-58. A comparison between the two groups with respect to the maximum lateral force capacity and the corresponding drift ratio besides the ultimate drift ratio and their corresponding lateral force is given in Table 6-1. Another comparison is made between the two groups of specimens to show the maximum lateral load and the maximum drift ratio reached before the first bar yielded and before the first bar ruptured as shown in Table 6-2.

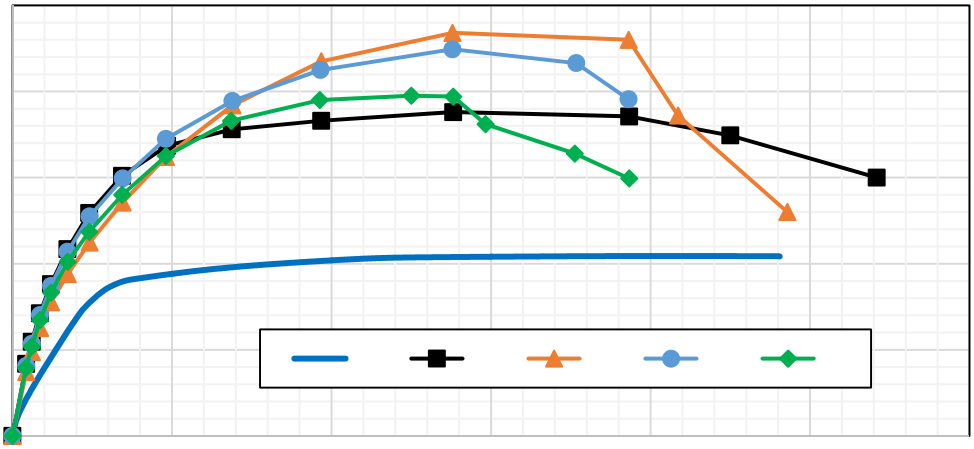

Figure 6-58 Comparison of force-drift backbone curves for all specimens from Groups I and II.

Table 6-1 Summary of the measured maximum lateral force and drift %.

| Specimen | Maximum lateral force (kips) | Maximum drift ratio (%) | Lateral force at ultimate drift (kips) | Ultimate drift ratio (%) |
|---|---|---|---|---|
| S0 | 10.44 | 6.1 | 10.43 | 9.62 |
| S1 | 18.80 | 5.53 | 15.00 | 10.84 |
| S2 | 23.40 | 5.52 | 13.00 | 9.72 |
| S3 | 22.45 | 5.52 | 19.55 | 7.72 |
| S4 | 19.75 | 5.00 | 14.95 | 7.73 |

Table 6-2 Summary of maximum measured force and drift before first rebar yield and rupture.

| Specimen | Maximum load reached before first yield (kips) | Maximum drift reached before first yield (%) | Maximum load before first rupture (kips) | Maximum drift reached before first rupture (%) |
|---|---|---|---|---|
| S0 | 6.90 | 0.82 | 10.43 | Not available |
| S1 | 12.40 | 0.92 | 18.80 | 7.73 |
| S2 | 17.10 | 2.21 | 23.40 | 7.73 |
| S3 | 15.00 | 1.39 | 22.45 | 7.20 |
| S4 | 16.70 | 2.10 | 19.75 | 7.73 |

From Figure 6-58 and Tables 6-1 and 6-2 above, and based on the varied parameters between each of the specimens as listed before in Table 4-1, the following can be observed:

- Comparing S0 to S1, it can be observed that using UHPC instead of NSC has led to an increase of almost 80% in the lateral load capacity of the column while both columns almost reached the same ultimate drift ratio. It is observed that specimen S0 would experience a first rebar yield earlier than S1 with a difference in the recorded force at first yield of about 44%.
- Comparing S1 to S2, it can be observed that using Gr 100 longitudinal rebars instead of Gr 60 rebars with an increase of 60% of the rebar ultimate strength has led to an increase of almost 25% in the lateral load capacity of the column while both columns have almost reached the same ultimate drift ratio. It can also be observed that S1 would exhibit a first rebar yield earlier than S2 when yield is defined using the proof strain with a difference in the corresponding force at yield of 38%. Both columns reached their maximum lateral load capacity and a corresponding drift % of 7.73% before the first rebar rupture.
- Comparing S2 to S3, it can be observed that decreasing the column confinement by decreasing the transverse reinforcement ratio to 50% of its value in S2 has led to an insignificant decrease of only 4% in the lateral load capacity of the column. However, the lower confinement resulted in a significant decrease in the ultimate drift ratio by 20%. The S3 test results indicated that the first rebar proof strain was reached before it did for S2 with the difference in the recorded force at the proof strain was 14%. Again, both columns reached their maximum lateral load capacity before the first rebar rupture. Yet, specimen S3 experienced the first rebar rupture at about 7% lower drift ratio than S2.
- Comparing S2 to S4, it can be observed that decreasing the column longitudinal reinforcement ratio to 65% of its value in S2 has led to a decrease of 15.6% in the lateral load capacity of the column and it resulted in a significant decrease in the ultimate drift ratio by 20%. It can also be observed that both of them reached the first rebar proof strain at the same drift ratio, while the difference in the recorded force at the proof strain was only 2.4%. It is noted that both columns S2 and S4 reached their maximum lateral load capacity and a drift ratio of 7.73% before the first rebar rupture.
- Comparing S4 to S1, it can be observed that using a longitudinal reinforcement ratio of 1.53% of Gr 100 rebars will result in almost the same lateral load column capacity (only 5% difference was observed) of a UHPC column with 2.37% Gr 60 longitudinal reinforcement. However, it is noted that although both specimens had almost the same lateral load capacity, there was a significant difference in the ultimate drift ratio. Specimen S4 that used Gr 100 steel had a 31.5% less drift capacity as compared to specimen S1 with Gr 60 steel. This agrees with the fact that HSS is overall less ductile than Gr 60 steel.

For the sake of comparing the displacement ductility of the specimens, the bilinear elasto-plastic curve method was used as shown in Figure 6-59. However, conclusions based on this method might be misleading and is not considered a good representation of the ductility of the columns reinforced with Gr 100 rebars. This is because it is completely dependent on the yield strain of the reinforcement so when the proof strain of Gr 100 rebars is approximately 4 times the yield strain of Gr 60, the effective yield displacement will be much higher which leads to small unrepresentative ductility values. The low ductility values do not necessarily reflect a lower drift or displacement capacity. For this reason, Group II specimens are compared to Group I specimens with respect to their drift capacity, which is defined to be the lesser of the ultimate drift ratio and the measured drift ratio at 80% of the maximum lateral load capacity.

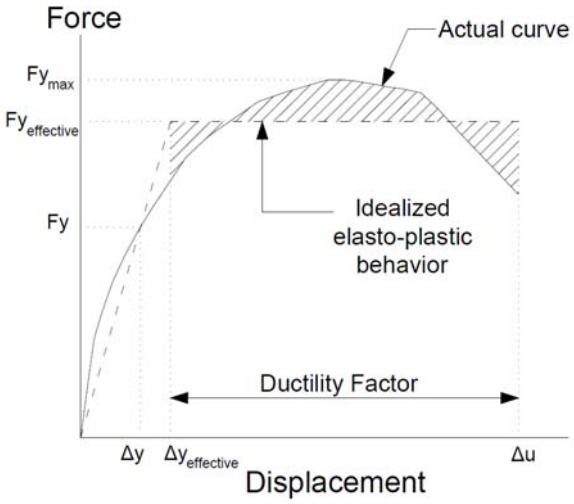


Figure 6-59 Bilinear Force-Displacement curve for Displacement Ductility Evaluation.

The bilinear elasto-plastic curve method defines the displacement ductility as the ratio of the ultimate displacement to the effective yield displacement, which can be calculated using a bilinear curve in which the area under the bilinear curve from the yield displacement to the ultimate displacement is equal to that of the actual column force displacement relationship from the yield to the ultimate point. The comparison between Group I with respect to the calculated ductility factor, and Group II with respect to the maximum drift ratio, is shown in Table 6-3. From the comparison showed in Tables 6-3, it can be observed that S0 and S1 have almost the same displacement ductility factors with an average value of 8.2 which is acceptable for bridge columns in high seismic zones. The UHPC column with 2.37% Gr 60 reinforcement was found to have the largest displacement/drift capacity which was higher than S0, S2, S3 and S4 by 11.25%, 23%, 28.8% and 31.5%, respectively. Moreover, comparing S2 to S3 to investigate the effect of using 50% of the column transverse reinforcement ratio shows that only 8% decrease was observed in the determined maximum drift ratio.

Table 6-3 Comparison of the estimated peak drift (%) capacity and displacement ductility factor.

| Specimen | Effective yield drift ratio (%) | Maximum drift ratio (%) | Displacement ductility factor | Drift capacity as related to S1 |
|---|---|---|---|---|
| S0 | 1.20 | 9.62 | 8.0 | 88.8% |
| S1 | 1.29 | 10.84 | 8.4 | 100% |
| S2 | -- | 8.34 | -- | 77.0% |
| S3 | -- | 7.72 | -- | 71.2% |
| S4 | -- | 7.43 | -- | 68.5% |

### *6.3.2. Local Behavior*

The average backbone curve for the moment-curvature curves of the push and pull directions of all Group I and Group II specimens was obtained and plotted as shown in Figure 6-60. A comparison between the two groups with respect to the maximum measured bending moment values and the measured ultimate curvatures was made and given in Table 6-4.

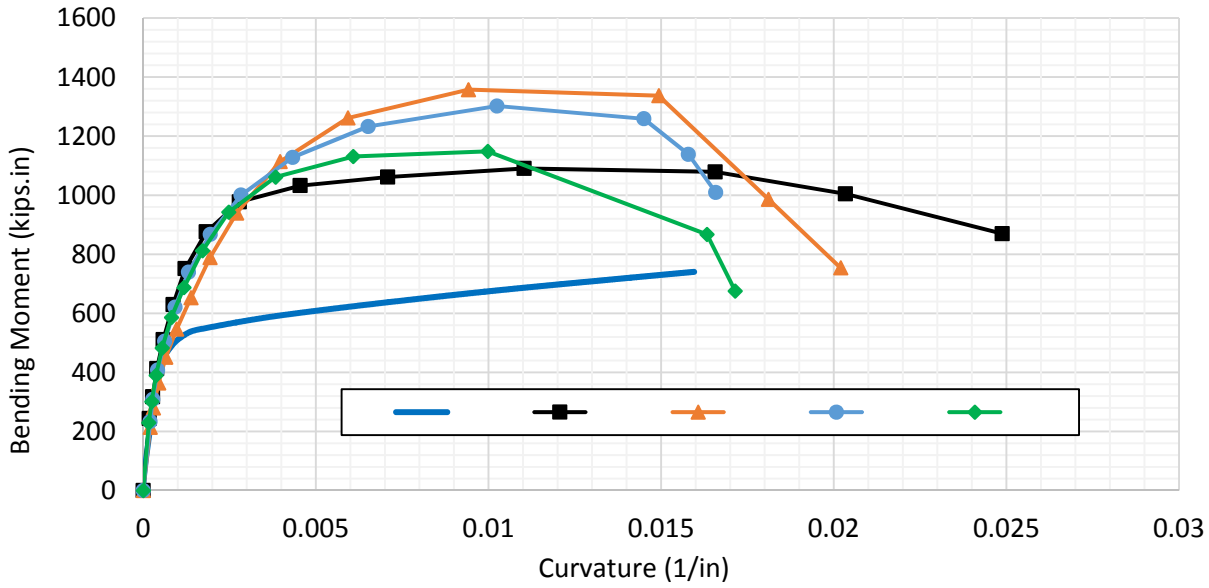


Figure 6-60 Comparison of moment-curvature curves for all specimens from Groups I and II.

Table 6-4 Maximum Measured Bending Moment and Drift Ratios.

| Specimen | Maximum Moment (kips.in) | Ultimate Curvature (1/in) |
|---|---|---|
| S0 | 740 | 0.016 |
| S1 | 1,090 | 0.025 |
| S2 | 1,357 | 0.020 |
| S3 | 1,302 | 0.017 |
| S4 | 1,148 | 0.017 |

From Figure 6-60 and Table 6-4, the following can be observed:

- Comparing S0 to S1, it can be observed that using UHPC instead of NSC has led to an increase of almost 47% in the bending moment capacity of the column and an increase of 56% in the ultimate curvature capacity.
- Comparing S1 to S2, it can be observed that using Gr 100 longitudinal rebars instead of Gr 60 rebars has led to an increase of almost 25% in the bending moment capacity but the measured ultimate curvature decreased by 20%.
- Comparing S2 to S3, it can be observed that decreasing the column confinement by decreasing the transverse reinforcement ratio to 50% of its value in S2 has led to an insignificant decrease of only 4% in the bending moment capacity of the column, although it resulted in a larger reduction in the ultimate curvature by 15%.
- Comparing S2 to S4, it can be observed that decreasing the column longitudinal reinforcement ratio to 65% of its value in S2 has led to a decrease of 15.4% in the moment capacity of the column and it resulted in a larger reduction in the ultimate curvature by 15%.
- Comparing S4 to S1, it can be observed that using a longitudinal reinforcement ratio of 1.53% of Gr 100 rebars will result in almost the same bending moment capacity of a column with 2.37% Gr 60 longitudinal reinforcement. The difference in the bending moment capacity was only 5% but a larger reduction of about 32% decrease was observed in the ultimate curvature.

# Chapter 7. SUMMARY, CONCLUSIONS, AND FUTURE WORK

## 7.1. Summary and Conclusions

This report presented results from extensive experimental testing that aimed at providing a better understanding of the fundamental behavior of UHPC columns. The experimental testing comprised two independent studies. The first study focused on uniaxial compression behavior of unconfined UHPC and UHPC cylinders confined by steel spirals. The obtained results included the stress-strain curves, modulus of elasticity, peak strength, and ultimate strain of UHPC. The second study is the core of this project and focused on investigating the structural and seismic response of UHPC columns with conventional Grade 60 and Grade 100 HSS under combined axial and cyclic loading. Results of four experimentally tested UHPC columns and one analytically investigated NSC column were presented and discussed with respect to their global and local behaviors with emphasis on the maximum measured lateral loads, ultimate drift ratios, maximum bending moments, ultimate curvatures, displacement ductility, reinforcement strains and stiffness degradation. This study investigated the effect of four tested variables on the seismic response of columns that included: using Gr 100 rebars instead of Gr 60 rebars; using low confinement ratios, i.e. less transverse reinforcement, and using different longitudinal reinforcement ratios. Overall, the UHPC columns exhibited larger moment capacity when compared to a NSC column of same design while maintaining an adequate ductile behavior. Reuslts from the confinement study and large-scale columns tests have led to several observations and conclusions which can be briefly summarized as follows:

- Based on the confinement study, the use of steel spirals improved the overall behavior of UHPC cylinders in term of strength and ductility. However, the ductility enhancement was more significant.
- The obtained confined stress-strain curves for UHPC exhibited three phases for the behavior: linear-elastic, nonlinear hardening, and softening phases, in contrast to an almost linear behavior up to failure in case of unconfined UHPC. Moreover, the confinement effectiveness ratio was determined to be up to 1.06 and ultimate strain values up to 1.03% were observed for confined UHPC cylinders.
- For the large-scale columns tests, the main observed mode of failure for all tested UHPC columns was tensile rupture of the longitudinal rebars without concrete spalling, core damage, reinforcement exposure, or buckling as in a typical NSC column plastic hinge.
- In all of the tested UHPC columns, no cracks were observed until the columns reached 1% drift ratio. Concrete crushing in compression was ultimately observed at large drift ratios but without leading to any significant spalling or loss of the concrete section.
- The UHPC column with Grade 60 rebars showed an adequate ductile behavior with the displacement and curvature ductility found to be 8.4 and 15.4, respectively. These values are comparable to well-designed conventional reinforced concrete seismic columns in high seismic areas.
- The initial flexural stiffness of the UHPC columns was determined from the tests and found to be in the range of 0.6 to 0.7 times the product of the Elastic Young's modulus and the gross moment of inertia. Moreover, all columns showed a drop of almost 50% of the initial stiffness values after exposed to 2% drift ratio.

- In all of the tested UHPC columns, the measured strains in the transverse reinforcement within the plastic hinge region were found to be smaller than 0.1% which indicates insignificant activation of the confinement in the UHPC columns under the combined 5% axial and lateral cyclic loading.
- Overall, the use of UHPC of compressive strength that is almost 6 times that of NSC in addition to superior tensile behavior that results from using 2% steel fibers can lead to an 80% increase in the lateral load capacity and 11% increase in drift or displacement capacity.
- Using Gr 100 HSS rebars instead of Gr 60 rebars with the same longitudinal reinforcement ratio can lead to a 25% increase in the lateral load capacity. This increase when combined with the effect of using UHPC instead of NSC can result in more than double the capacity, which sets the stage for new design opportunities for compact bridge columns.
- The use of HSS can result in a significant decrease (about 23%) in the drift capacity of the UHPC columns when compared to Grade 60 steel. This might be considered an adverse effect only if the current existing ductility design approach is adopted for seismic columns. However, based on the observed major strength increase, new design approaches should be considered for UHPC columns that might deviate from the current ductility-based designs.
- Decreasing the transverse reinforcement ratio by half in the UHPC columns resulted in only 4% decrease in the lateral load capacity and 8% decrease in the maximum drift ratio. This confirms that confinement effects in UHPC columns under combined axial and bending might not be as pronounced as the cases of pure axial or applications of high axial loads.
- Reducing the longitudinal reinforcement ratio of a UHPC column by 35% when Gr 100 HSS was used resulted in about 15.5% decrease in the lateral load capacity and 11% decrease in the maximum drift ratio. However, using a longitudinal reinforcement ratio of 1.53% of Gr 100 rebars will result in almost the same lateral load capacity of a column with 2.37% Gr 60 longitudinal reinforcement. The Gr 60 design will still have a larger drift capacity. Thus, rethinking the design process of UHPC columns to properly benefit from HSS and fully utilize the mechanical properties of UHPC is worth investigating for a new generation of bridge column designs.

## 7.2. Future Work

The results obtained from this study demonstrate that UHPC can be potentially combined with HSS to realize new bridge column designs that will be compact, i.e. lighter and well-suited for precast and ABC construction, and extremely durable for harsh environments. While this project provided important knowledge on fundamental structural and seismic behavior of UHPC columns, more research is needed to identify best design practices or new design philosophies for UHPC columns with both conventional Grade 60 and HSS of Grade 100 or so. The following research topics are recommended for future studies:

- Larger-scale UHPC columns need to be tested with larger number of rebars and less sensitivity to construction errors or rebars misalignment. For instance, when 6 rebars were used in this study, each rebar significantly contribute to the moment capacity and any misalignment led to asymmetric behavior and large drops in force and moment capacity due to rupture. With larger number of rebars and larger diameter UHPC columns, both strength and displacement/drift capacities can be better defined.
- If the obvious observation is that UHPC can lead to compact cross-sections, more experimental testing will be needed for slender UHPC columns to understand the elastic and

inelastic buckling behavior and identify the acceptable range of slenderness ratios for economic designs.

- A new design philosophy can be considered for seismic UHPC columns with focus on low-damage concepts. The current seismic design philosophy is based on ductility concepts when in fact, emerging technologies and seismic protective systems are promoting resilient and damage-free designs to allow for immediate operation of critical structure, e.g. bridges, after large earthquakes. Thus, more research is needed to determine the proper ductility or R factor for UHPC column that can strike a balance between low-damage and economic cross-sections.
- Experimental testing of large number of UHPC columns will not be very feasible. Thus, building on this project and similar studies to provide robust computational and analytical tools for modeling UHPC columns is needed. More research is needed to calibrate constitutive models for UHPC based on full structural components and to provide best modeling approaches.

## REFERENCES


1. Aarup, B., Jensen, L. R., ApS, H. C., & Ellegaard, P. (2005). Slender CRC columns. Nordic Concr Res, 34,80-97.
2. AASHTO. (2014). AASHTO guide specifications for LRFD seismic bridge design, Washington, DC.
3. Aghdasi, P., Heid, A.E. and Chao, S.-H., "Developing Ultra-High-Performance Fiber-Reinforced Concrete for Large-Scale Structural Applications", ACI Mater. J., Vol. 113, No. 5, 2016, pp. 559-570.
4. Ali, M. M., Singh, M., & Sheikh, A. H. (2016). Structural behaviour of UHPFRC short and slender columns subjected to axial and eccentric loads. In Mechanics of Structures and Materials XXIV (pp. 456-461). CRC Press.
5. Aoude, Hassan, Frederic P Dagenais, Russell P Burrell, and Murat Saatcioglu. 2015. "Behavior of Ultra-High Performance Fiber Reinforced Concrete Columns under Blast Loading." International Journal of Impact Engineering 80: 185–202.
6. Astarlioglu, S. and Krauthammer, T., "Response of normal-strength and ultra-high-performance fiber-reinforced concrete columns to idealized blast loads", Eng. Struct., No. 61, 2014, pp 1–12.
7. Astarlioglu, Serdar, and Ted Krauthammer. 2014. "Response of Normal-Strength and Ultra-High-Performance Fiber-Reinforced Concrete Columns to Idealized Blast Loads." Engineering Structures 61: 1–12.
8. ASTM C230/C230M. (1998). Standard specification for flow table for use in tests of hydraulic cement.
9. ASTM. (2009). "Standard specification for low-alloy steel deformed and plain bars for concrete reinforcement." A706/A706M-09b, West Conshohocken, PA.
10. Burkart, I., & Müller, H. S. (2008, March). Creep and shrinkage characteristics of ultra high strength concrete (UHPC). In Proceedings of the Second International Symposium on Ultra High Performance Concrete (pp. 469-476).
11. Caldwell, Tricia. 2011. "Plastic Hinge Behavior of Reinforced Concrete and Ultra High Performance Concrete Beam-Columns under Severe and Short Duration Dynamic Loads." University of Florida.
12. Chao, Shih-Ho & Venkatesh, Kaka & Palacios, Guillermo & Kim, Jinsup & Choi, Youngjae & Aghdasi, Parham & Nojavan, Alireze & Schultz, Arturo. (2016). Seismic Behavior of Ultra-High-Performance Fiber-Reinforced Concrete Moment Frame Members. 10.21838/uhpc.2016.44.
13. Chao, Shih-Ho et al. 2016. "Seismic Behavior of Ultra-High-Performance Fiber- Reinforced Concrete Moment Frame Members." In First International Interactive Symposium on UHPC, Iowa.
14. Davila, Ricardo S. 2007. "Recommendations for the Design of Ultra-High Performance Concrete Structures." Massachusetts Institute of Technology.

15. Dexin, Xiong. 2012. “Structural Behaviour of Concrete Filled Steel Tubes With High Strength Materials.” National University of Singapore.
16. El-Tawil, S., Alkaysi, M., Naaman, A. E., Hansen, W., & Liu, Z. (2016). Development, characterization and applications of a non-proprietary ultra-high performance concrete for highway bridges (No. RC-1637). Department of Civil and Environmental Engineering, University of Michigan.
17. Empelmann, Martin, Corinna Mueller, and Daniel Busse. 2016. “Compact Reinforced UHPC Columns with Circular Hollow Cross-Section.” BAUTECHNIK 93(6): 345–55.
18. Federal Emergency Management Agency (FEMA). (2007). FEMA 461: Interim Testing Protocols for Determining the Seismic Performance Characteristics of Structural and Nonstructural Components.
19. Feng, J.W., and P.Y. Yan. 2008. “Mechanical Behaviour of UHPC and UHPC Filled Steel Tubular Stub Columns.” In Proceedings of the Second International Symposium on Ultra High Performance Concrete, eds. E. Fehling and M. Schmidt. , 355–362.
20. French-Standard. 2016a. NF P18-470 Concrete — Ultra-High Performance Fibre-Reinforced Concrete — Specifications, Performance, Production and Conformity.
21. French-Standard. 2016b. NF P18-710 National Addition to Eurocode 2 — Design of Concrete Structures: Specific Rules for Ultra-High Performance Fibre-Reinforced Concrete (UHPFRC).
22. Girgin, Zehra Canan, and Konuralp Girgin. 2015. “A Design-Oriented Combined Model (7 MPa to 190 MPa) for FRP-Confined Circular Short Columns.” POLYMERS 7(10): 1905–17.
23. Gowripalan, N., and Ian R Gilbert. 2000. “Design Guidelines for Ductal Prestressed Concrete Beams.” The University of New South Wales.
24. Graybeal, B. A. (2006). Material property characterization of ultra-high performance concrete (No. FHWA-HRT-06-103).
25. Graybeal, B. A. (2007). Compressive behavior of ultra-high-performance fiber-reinforced concrete. ACI materials journal, 104(2), 146.
26. Graybeal, B. A. (2010). Behavior of field-cast ultra-high performance concrete bridge deck connections under cyclic and static structural loading (No. FHWA-HRT-11-023). United States. Federal Highway Administration.
27. Graybeal, B. A. and Baby, F., “Development of Direct Tension Test Method for Ultra-High-Performance Fiber-Reinforced Concrete”, ACI Mater. J., Vol. 110, No. 2, 2013, pp. 177-186.
28. Graybeal, B. A., “Design and Construction of Field-Cast UHPC Connections”, FHWA, U.S. Department of Transportation, Report No. FHWA-HRT-14- 084, 2014.
29. Graybeal, B., & Tanesi, J. (2007). Durability of an ultrahigh-performance concrete. Journal of materials in civil engineering, 19(10), 848-854.
30. Guler, Soner, Alperen Çopur, and Metin Aydogan. 2013. “Axial Capacity and Ductility of Circular UHPC-Filled Steel Tube Columns.” Magazine of Concrete Research 65(15): 898–905. https://doi.org/10.1680/macr.12.00211.

31. Guler, Soner, Alperen Copur, and Metin Aydogan. 2013. “Nonlinear Finite Element Modeling of FRP-Wrapped UHPC Columns.” Computers and Concrete 12(4): 413–29.

32. Guler, Soner. 2014. “Axial Behavior of FRP-Wrapped Circular Ultra-High Performance Concrete Specimens.” Structural Engineering and Mechanics 50(6): 709–22.

33. Haber, Z. B., De la Varga, I., Graybeal, B. A., Nakashoji, B. and El-Helou, R., “Properties and behavior of UHPC-class materials”, FHWA, U.S. Department of Transportation, Report No. FHWA-HRT-18-036, 2018.

34. Hassan, A.M.T., Jones, S.W. and Mahmud, G.H., “Experimental test methods to determine the uniaxial tensile and compressive behaviour of ultra high performance fibre reinforced concrete (UHPFRC)”, Constr. Build. Mater., Vol. 37, 2012, pp. 874–882.

35. Heimann, Martin, Holger Schmidt, Ngoc Linh Tran, and Carl-Alexander Graubner. 2013. “Reliability of Highly Stressed UHPC-Columns.” Beton- Und Stahlbetonbau 108(1): 2–12.

36. Hoang, An Le, and Ekkehard Fehling. 2017a. “A Review and Analysis of Circular UHPC Filled Steel Tube Columns under Axial Loading.” STRUCTURAL ENGINEERING AND MECHANICS 62(4): 417–30.

37. Hoang, An Le, and Ekkehard Fehling. 2017b. “Analysis of Circular Steel Tube Confined UHPC Stub Columns.” Steel and Composite Structures 23(6): 669–82.

38. Hoang, An Le, and Ekkehard Fehling. 2017c. “Numerical Analysis of Circular Steel Tube Confined UHPC Stub Columns.” Computers and Concrete 19(3): 263–73.

39. Hosinieh, M. M., Aoude, H., Cook, W. D., & Mitchell, D. (2015). Behavior of ultra-high performance fiber reinforced concrete columns under pure axial loading. Engineering Structures, 99, 388-401.

40. Hosinieh, Milad Mohammadi, Hassan Aoude, William D Cook, and Denis Mitchell. 2015. “Behavior of Ultra-High Performance Fiber Reinforced Concrete Columns under Pure Axial Loading.” Engineering Structures 99: 388–401. http://www.sciencedirect.com/science/article/pii/S0141029615003260.

41. Hudoba, Igor, and Jan Mikus. 2013. “The Application of UHSC For Load-Bearing Composite Elements and Structures.” in concrete and concrete structures 2013 - 6th international conference, slovakia, procedia engineering, ed. j bujnak, j and vican. amsterdam, netherlands: elsevier science bv, 212–17.

42. Hung, C. C., & Hu, F. Y. (2018). Behavior of high-strength concrete slender columns strengthened with steel fibers under concentric axial loading. Construction and Building Materials, 175, 422-433.

43. Hung, C. C., Hu, F. Y., & Yen, C. H. (2018). Behavior of slender UHPC columns under eccentric loading. Engineering Structures, 174, 701-711.

44. Ichikawa, Shota et al. 2016. “Seismic-Resistant Bridge Columns with Ultrahigh-Performance Concrete Segments.” Journal of Bridge Engineering 21(9).

45. Illich, Guenther, Nguyen Viet Tue, and Bernhard Freytag. 2014. “Slender Prestressed Columns Made of UHPC - Experimental Investigation and Verification.” Beton- Und Stahlbetonbau 109(8): 534–43.

46. Joe, C. D., & Moustafa, M. A. (2016). Cost and Ecological Feasibility of Using UHPC in Bridge Piers. In First International Interactive Symposium on UHPC (pp. 18-20).

47. Kimura, Hideki, Yuji Ishikawa, Atsushi Kambayashi, and Hiroto Takatsu. 2007. "Seismic Behavior of 200MPa Ultra-High-Strength Steel-Fiber Reinforced Concrete Columns under Varying Axial Load." ACT 5(2): 193–200.

48. Lafarge Canada Inc. "Field-Cast Joint Fill Solutions for Precast Deck Panel Bridges." Ductal JS1000 Product Data Sheet. Accessed August 2017. http://www.ductal-lafarge.com/JS1000_2015.pdf.

49. Le Hoang, An, and Ekkehard Fehling. 2016. "Finite Element Analysis of Circular Steel Tube Confined UHPC Stub Columns." in 1st international conference on uhpc materials and structures, rilem proceedings, ed. d shi, c and wang. 157 rue des blains, 92220 bagneux, france: r i l e m publications, 95–99.

50. Li, Jun, Chengqing Wu, Hong Hao, and Yu Su. 2015. "Investigation of Ultra-High Performance Concrete Under Static and Blast Loads." INTERNATIONAL JOURNAL OF PROTECTIVE STRUCTURES 6(2, SI): 217–35.

51. Li, Jun, Chengqing Wu, Hong Hao, and Zhongxian Liu. 2017. "Post-Blast Capacity of Ultra-High Performance Concrete Columns." Engineering Structures 134: 289–302. http://www.sciencedirect.com/science/article/pii/S0141029616317308.

52. Li, Xiuling, Juan Wang, Yi Bao, and Genda Chen. 2017. "Cyclic Behavior of Damaged Reinforced Concrete Columns Repaired with High-Performance Fiber-Reinforced Cementitious Composite." Engineering Structures 136: 26–35. http://www.sciencedirect.com/science/article/pii/S014102961730041X.

53. Liew, J Y Richard, and D X Xiong. 2012. "Ultra-High Strength Concrete Filled Composite Columns for Multi-Storey Building Construction." Advances in Structural Engineering 15(9): 1487–1503. http://dx.doi.org/10.1260/1369-4332.15.9.1487.

54. Liew, J.Y.R., M.X. Xiong, and D.X. Xiong. 2014. "Design of High Strength Concrete Filled Tubular Columns for Tall Buildings." International Journal of High-Rise Building 3(3): 215–21.

55. Mander, J.B., Priestley, M.J.N. and Park, R., "Observed Stress-Strain Behavior of Confined Concrete", J. Struct. Eng., Vol. 114, No. 8, 1988, pp. 1827–1849.

56. Marchand, P., Baby, F., Khadour, A., Battesti, T., Rivillon, P., Quiertant, M., ... & Toutlemonde, F. (2016). Bond behaviour of reinforcing bars in UHPFRC. Materials and structures, 49(5), 1979-1995.

57. Markowski, Jan, Ludger Lohaus. 2017. "Uhpc Sandwich Structures with Composite Coating under Compressive Load." In International Symposium on Experimental Methods and Numerical Simulation In Engineering Sciences (Exnum 2016), Acta Polytechnica Ctu Proceedings, Ed. P Kytyr, D And Zlamal. Zikova 4, Prague 6 166 35, Czech Republic: Czech Technical Univ Prague, 38–42.

58. Massicotte, Bruno, Marc-André. Dagenais, and Fabien. Lagier. 2013. "Performance of UHPFRC Jackets for the Seismic Strengthening of Bridge Piers." In RILEM-Fib-AFGC

International Symposium on Ultra-High Performance Fibre-Reinforced, Marseille, France, 89–98.

59. Maten, R.N. ter. 2011. “Ultra High Performance Concrete in Large Span Shell Structures.” Delft University of Technology.
60. MS, Ridha. 2017. “Axial-Flexural Interaction of Square FRP Tube Columns In-Filled with Ultra-High Performance Concrete.” Polymer science 3(1). http://polymerscience.imedpub.com/axialflexural-interaction-of-square-frptube-columns-infilled-with-ultrahighperformance-concrete.php?aid=19334 (August 14, 2017).
61. Parham Aghdasi and Shih-Ho Chao, Ashley E Heid. 2016. “Developing Ultra-High-Performance Fiber-Reinforced Concrete for Large-Scale Structural Applications.” Materials Journal 113(5).
62. Popa, Mircea, Zoltan Kiss, Horia Constantinescu, and Geanina Bolca. 2016. “Case Study: Designing a 40 Storey High Office Building Using Two Variants, with Regular Concrete Columns and with Compound Ultra-High Performance Concrete Columns and Regular Concrete Columns.” Procedia Technology 22: 40–47. http://www.sciencedirect.com/science/article/pii/S2212017316000086.
63. Redaelli, D., Spasojevic, A., & Muttoni, A. (2017). Experimental and numerical study on the use of high-strength and ultra-high-performance fibre-reinforced concrete in columns. Special Publication, 310, 193-202.
64. Russell P. Burrell, Hassan Aoude and Murat Saatcioglu. “Blast Behaviour of Ultra High Strength CRC Columns.” Special Publication 293.
65. Saleem, M. A., Mirmiran, A., Xia, J., & Mackie, K. (2012). Development length of high-strength steel rebar in ultrahigh performance concrete. Journal of Materials in Civil Engineering, 25(8), 991-998.
66. Schmidt, Holger, and Martin Heimann. 2011. “Probabilistic Modelling of HSC and UHPC slender columns in high-rise buildings.” in applications of statistics and probability in civil engineering, ed. k faber, mh and kohler, j and nishijima. 6000 broken sound parkway nw, ste 300, boca raton, fl 33487-2742 usa: crc press-taylor & francis group, 1169–74.
67. Shafieifar, M., Farzad, M. and Azizinamini, A., “Experimental and numerical study on mechanical properties of Ultra High Performance Concrete (UHPC)”, Constr. Build. Mater. Vol. 156, 2017, pp. 402–411.
68. Shin, Hyun-Oh, Kyung-Hwan Min, and Denis Mitchell. 2017. “Confinement of Ultra-High-Performance Fiber Reinforced Concrete Columns.” Composite Structures 176: 124–42. http://www.sciencedirect.com/science/article/pii/S0263822316308170.
69. Sugano, Shunsuke, Hideki Kimura, and Kazuyoshi Shirai. 2007. “Study of New RC Structures Using Ultra-High-Strength Fiber-Reinforced Concrete (UFC)—the Challenge of Applying 200MPa UFC to Earthquake Resistant Building Structures.” J Adv Concr Technol 5(2): 133–147.
70. Tazarv, M., and M. Saiid Saiidi. 2014. Next generation of bridge columns for accelerated bridge construction in high seismic zones. Technical Rep. No. CA14-2176. Reno, NV: Univ. of Nevada.

71. Tue, Ngyen Viet, Holger Schneider, Gert Simsch, and Detlef Schmidt. 2004. “Bearing Capacity of Stub Columns Made of NSC, HSC and UHPC Confined by a Steel Tube.” In International Symposium on Ultra High Performance Concrete, , 339–50.

72. Uchida, Yuichi, Junichiro Niwa, Yoshihiro Tanaka, and and Makoto Katagiri. 2006. “Outlines of ‘Recommendations for Design and Construction of Ultra High Strength Fiber Reinforced Concrete Structures’ by JSCE.” In International RILEM Workshop on High Performance Fiber Reinforced Cementitious Composites in Structural Applications, eds. G. Fischer Li and V. C. , 343–51.

73. Verger-Leboeuf, S., Charron, J. P., & Massicotte, B. (2017). Design and Behavior of UHPFRC Field-Cast Transverse Connections between Precast Bridge Deck Elements. Journal of Bridge Engineering, 22(7), 04017031.

74. W. Xiangguo, Y. Qun, Z. Xinyu, Z. Wenzhong, H. Sangmook. 2013. “Uniaxial Compressive Strength of Durable Hybrid Pier with UHPCC Permanent Form.” In RILEM-Fib-AFGC International Symposium on Ultra-High Performance Fibre-Reinforced, , 207 – 216.

75. Wang, Zhen, Jingquan Wang, Tongxu Liu, and Fan Zhang. 2016. “Modeling Seismic Performance of High-Strength Steel-Ultra-High-Performance Concrete Piers with Modified Kent-Park Model Using Fiber Elements.” ADVANCES IN MECHANICAL ENGINEERING 8(2).

76. Wille, K., El-Tawil, S. A. and Naaman E., “Properties of strain hardening ultra high performance fiber reinforced concrete (UHP-FRC) under direct tensile loading”, Cem. Concr. Compos. Vol. 48, 2014, pp. 53–66.

77. Xu, Juechun et al. 2016. “Behaviour of Ultra High Performance Fibre Reinforced Concrete Columns Subjected to Blast Loading.” Engineering Structures 118: 97–107. http://www.sciencedirect.com/science/article/pii/S0141029616300839.

78. Yang, X., Zohrevand, P. and Mirmiran, A., “Behavior of Ultrahigh-Performance Concrete Confined by Steel”, J. Mater. Civ. Eng. Vol. 28, No. 10, 2016.

79. Yuan, J., & Graybeal, B. (2015). Bond of Reinforcement in Ultra-High-Performance Concrete. ACI Structural Journal, 112(6).

80. Zehfuss, Jochen, and Matthias Siemon. 2015. “Numerical Analysis of Fire Exposed Ultra-High Performance Concrete (UHPC) Columns.” BAUTECHNIK 92(5): 335–45.

81. Zhang, Fangrui et al. 2016. “Experimental Study of CFDST Columns Infilled with UHPC under Close-Range Blast Loading.” INTERNATIONAL JOURNAL OF IMPACT ENGINEERING 93: 184–95.

82. Zhang, Fangrui, Chengqing Wu, Xiao-Ling Zhao, and Zhong-Xian Li. 2017. “Numerical Derivation of Pressure-Impulse Diagrams for Square UHPCFDST Columns.” Thin-Walled Structures 115: 188–95. http://www.sciencedirect.com/science/article/pii/S0263823116303111.

83. Zhang, Fangrui, Chengqing Wu, Zhong-Xian Li, and Xiao-Ling Zhao. 2015. “Residual Axial Capacity of CFDST Columns Infilled with UHPFRC after Close-Range Blast Loading.” Thin-Walled Structures 96: 314–27.

84. Zohrevand, P., and Mirmiran, A. “Behavior of ultrahigh-performance concrete confined by fiber-reinforced polymers”. Journal of materials in civil engineering, Vol. 23, No. 12, 2011, pp. 1727-1734.

85. Zohrevand, Pedram, and Amir Mirmiran. 2012. “Cyclic Behavior of Hybrid Columns Made of Ultra High Performance Concrete and Fiber Reinforced Polymers.” Journal of Composites for Construction 16(1): 91–99. http://dx.doi.org/10.1061/(ASCE)CC.1943-5614.0000234.

86. Zohrevand, Pedram, and Amir Mirmiran. 2013a. “Effect of Column Parameters on Cyclic Behavior of Ultra-High-Performance Concrete-Filled Fiber-Reinforced Polymer Tubes.” ACI Struct. J. 110: 823.

87. Zohrevand, Pedram, and Amir Mirmiran. 2013b. “Seismic Response of Ultra-High Performance Concrete-Filled FRP Tube Columns.” Journal of Earthquake Engineering 17(1): 155–70. http://dx.doi.org/10.1080/13632469.2012.713560.

88. Zohrevand, Pedram. 2012. “Novel Hybrid Columns Made of Ultra-High Performance Concrete and Fiber Reinforced Polymers.” Florida International University.